STARS

2007

Helical Packing Regulates Structural Transitions In Bax

Nuska Tschammer
University of Central Florida

Showcase of Text, Archives, Research & Scholarship

HELICAL PACKING REGULATES STRUCTURAL TRANSITIONS IN BAX

by

NUSKA TSCHAMMER
B.S. University of Maribor, Slovenia, 1998
M.S. University of Maribor, Slovenia, 2002

A dissertation submitted in partial fulfillment of the requirements
for the degree of Doctor of Philosophy in Biomolecular Sciences
in the Burnett School of Biomedical Sciences
in the College of Medicine
at the University of Central Florida
Orlando, Florida

Fall Term
2007

Major Professor: Annette R. Khaled

ABSTRACT

Apoptosis is essential for development and the maintenance of cellular homeostasis and is frequently dysregulated in disease states. Proteins of the BCL-2 family are key modulators of this process and are thus ideal therapeutic targets. In response to diverse apoptotic stimuli, the pro-apoptotic member of BCL-2 family, BAX, redistributes from the cytosol to the mitochondria or endoplasmic reticulum and primes cells for death. The structural changes that enable this lethal protein to transition from a cytosolic form to a membrane-bound form remain poorly understood. Elucidating this process is a necessary step in the development of BAX as a novel therapeutic target for the treatment of cancer, as well as autoimmune and neurodegenerative disorders.

A three-part study, utilizing computational modeling and biological assays, was used to examine how BAX, and similar proteins, transition to membranes. The first part tested the hypothesis that the C-terminal α9 helix regulates the distribution and activity of BAX by functioning as a "molecular switch" to trigger conformational changes that enable the protein to redistribute from the cytosol to mitochondrial membrane. Computational analysis, tested in biological assays, revealed a new finding: that the α9 helix can dock into a hydrophobic groove of BAX in two opposite directions – in a self-associated, forward orientation and a previously, unknown reverse orientation that enables dimerization and apoptosis. Peptides, made to mimic the α9-helix, were able to induce the mitochondrial translocation of BAX, but not when key residues in the hydrophobic groove were mutated. Such findings indicate that the α9 helix of BAX can function as a "molecular switch" to mediate occupancy of the hydrophobic groove and regulate the membrane-binding activity of BAX. This new discovery contributes to the

understanding of how BAX functions during apoptosis and can lead to the design of new therapeutic approaches based on manipulating the occupancy of the hydrophobic groove.

The second and third parts of the study used computational modeling to examine how the helical stability of proteins relates to their ability to functionally transition. Analysis of BAX, as a prototypical transitioning protein, revealed that it has a broad variation in the distribution of its helical interaction energy. This observation led to the hypothesis tested, that proteins which undergo 3D structural transitions during execution of their function have broad variations in the distribution of their helical interaction energies. The result of this study, after examination of a large group of all-alpha proteins, was the development of a novel, predictive computational method, based on measuring helical interactions energies, which can be used to identify new proteins that undergo structural transitioning in the execution of their function. When this method was used to examine transitioning in other members the BCL-2 family, a strong agreement with the published experimental findings resulted. Further, it was revealed that the binding of a ligand, such as a small peptide, to a protein can have significant stabilizing or destabilizing influences that impact upon the activation and function of the protein. This computational analysis thus contributes to a better understanding of the function and regulation of the BCL-2 family members and also offers the means by which peptide mimics that modulate protein activity can be designed for testing in therapeutic endeavors.

V ljubeč spomin moji sestri in dedku

In loving memory of my sister and grandfather

Monika Kropivšek, 1980-2001

Alojz Perša, 1929-2006

ACKNOWLEDGMENTS

TABLE OF CONTENTS

LIST OF FIGURES

LIST OF TABLES

LIST OF ACRONYMS/ABBREVATIONS

AVE	Average
BAX	BCL-2 associated protein
BCL-2	B-cell lymphoma 2 protein
BH	BCL-2 homology
BIM	Bcl-2-like protein 11
BSA	Bovine serum albumin
CHAPS	3-[(3-Cholamidopropyl)-dimethylammonio]}-1-propanesulfonate
DMA	Dimethyl acetamide
DMSO	Dimethyl sulfoxide
DNA	Deoxyribonucleic acid
dsRNA	Double stranded RNA
DSS	Disuccinimidyl suberate
EBI	European Bioinformatics Institute
EBV	Epstein Barr virus
EGFP	Enhanced green fluorescent protein
ER	Endoplasmatic reticulum
EYFP	Enhanced yellow fluorescent protein
FACS	Fluorescence-activated cell sorter
FBS	Fetal bovine serum
HA	Hemaglutinin
HPLC	High Performance Liquid Chromatography

HRP	Horseradish peroxidase
HSP60	Heat shock protein 60
IL-3	Interleukin 3
IL-7	Interleukin 7
KSHV	Kaposi's sarcoma-associated virus
MM3	Molecular mechanics 3
MOM	Mitochondrial outer membrane
NHE	Na^+/H^+ exchange factor
NMR	Nuclear magnetic resonance
PBS	Phosphate Buffer Solution
PCR	Polymer chain reaction
pRNA	Packing RNA
PVDF	Polyvinylidene difluoride
RISC	RNA induced silencing complex
RNA	Ribonucleic acid
SD	Standard deviation
SDS-PAGE	Sodium dodecyl sulfate polyacrylamide gel electrophoresis
siRNA	Short interfering RNA
3D	Three dimensional

1 GENERAL INTRODUCTION

1.1 Introduction

Apoptosis is a form of cell death by which a programmed series of events leads to the cell's demise without initiating the release of intracellular contents that could provoke an inflammatory response (Nelson, White 2004). A multi-cellular organism typically eliminates unnecessary or damaged cells through the process of apoptosis (Borner 2003;Cory et al. 2003;Nelson, White 2004). Malfunctions in the regulation of apoptosis characterize a range of human diseases, including cancer, neurodegenerative, cardiovascular and autoimmune disorders (Cory et al. 2003;Gross et al. 1999). Diseases caused by excessive cell death, such as myocardial and cerebral ischemia, are two of three leading causes of death in the developed world (Letai 2005). Cancer, the third leading causing of death in the developed world, is also caused in part by the defects in the cell death process. It is therefore of great importance that the process of apoptosis be studied in order to develop novel regimens for therapeutic intervention.

The apoptotic pathway can be initiated by different mechanisms. A physiological relevant pathway involves the release of apoptotic factors from mitochondria. Modulators of mitochondria function and integrity are those proteins found in the BCL-2 (B Cell Lymphoma) family. The founder of the BCL-2 family, BCL-2, is a proto-oncogene whose activity is deregulated in a majority of patients with follicular lymphoma (Borner 2003;Gross et al. 1999;Lipford et al. 1987). Other BCL-2 family members include the anti-apoptotic proteins, BCL-XL, and the pro-apoptotic protein, BAX. Murine models of myocardial and cerebral ischemia demonstrated that BAX loss-of function mutations or overexpression of BCL-2 could attenuate apoptosis and reduced infracts size (Letai 2005). In contrast, transgenic mice

1

overexpressing BCL-2 developed leukemia (Borner 2003;Gross et al. 1999). These examples illustrate the importance of the BCL-2 family member in the regulation of apoptosis in disease models, and suggest that BCL-2 family members are valid therapeutic targets.

1.2 BCL-2 Family of Proteins

Apoptosis is triggered by a range of physiological and pathological death signals. The best characterized pathways that lead to apoptotic cell death involve the activation of cysteine proteases of the caspase family that cleave substrates after aspartate residues (Earnshaw et al. 1999). These enzymes are divided into two groups: (1) the initiator caspases (caspases 2, 8-10, 12), and the effector caspases (caspases 3, 6, 7) (Earnshaw et al. 1999). An initiator caspase acts at an early point in the apoptotic signaling pathway. After autoproteolysis of the initiator caspases active dimers are forms which activate effector caspases through proteolitic cleavage and thus enhances the apoptotic signal (Earnshaw et al. 1999). Effector caspases than cleave the substrates which lead to the break-down of the cell into apoptotic bodies and subsequent phagocytosis (Utz, Anderson 2000). The initiator caspases are in mammals activated by at least two pathways: (1) the death-receptor pathway, and (2) the mitochondrial (BCL-2 family) pathway. The death-receptor pathway is initiated by extracellular death-inducing ligands of the TNF superfamily (Krammer 2000;Locksley et al. 2001). The mitochondrial pathway involving BCL-2 family proteins is mostly triggered by growth factors and cytokines withdrawal, irradiation, viruses, bacteria and chemotherapeutic drug (Borner 2003;Gross et al. 1999). Various BCL-2 family members serve as sensors of the death stimuli, other target mitochondrial outer membrane to release apoptogenic factors (e.g. cytochrome c, Smac/DIABLO, Htr2A/Omi)

2

involved in the formation of apoptosome in mammalian cells (Borner 2003;Bouillet, Strasser 2002;Gross et al. 1999).

Members of the BCL-2 family are crucial regulators of the mitochondrial apoptotic pathway. The founding member of this family, BCL-2, was initially cloned from the breakpoint of the t(14;18) chromosomal translocation in human B-cell lymphoma (Gross et al. 1999;Lipford et al. 1987).   Today this family is comprised of over 30 proteins, sharing one or more BCL-2 homology (BH) domains. Based on their function in apoptosis, the family is divided into two groups: (1) anti-apoptotic proteins like BCL-2 and BCL-XL which possess three to four BH domains, (2) pro-apoptotic proteins like BAX and BAK, which possess three to four BH domains and mediators like BIM that possess only one BH domain (BH3-only proteins) (Borner 2003;Bouillet, Strasser 2002;Cory et al. 2003;Gross et al. 1999) (Table 1).

In the absence of apoptotic stimuli, a significant fraction of pro- and anti- apoptotic BCL-2 members sequester to separate subcellular compartments. Anti-apoptotic members like BCL-2 and BCL-XL are largely found membrane-bound in mitochondrial outer membrane (MOM), endoplasmic reticulum (ER) or nuclear membrane (Borner 2003;Bouillet, Strasser 2002;Gross et al. 1999). Pro-apoptotic members like BAX localize to cytosol or like BIM to cytoskeleton (Borner 2003;Bouillet, Strasser 2002;Gross et al. 1999).   Upon induction of a death signal, significant subcellular rearrangement of various family members takes place indicative of their ability to transition.   Pro-apoptotic proteins, like BAX, translocate to membranes, especially MOM, where they are thought to cause destabilization of the MOM and induce release of the apoptogenic factors from the mitochondria (Table 1).

3

Table 1: Summary of the most prominent mammalian BCL-2 family members.

BCL-2 family member	Function	BH homologies	Localization in healthy cells	Localization in apoptotic cells
BCL-2	Anti-apoptotic	BH1-BH4	MOM-, ER-, nuclear envelope inserted	MOM-, ER-, nuclear envelope inserted
BCL-XL	Anti-apoptotic	BH1-BH4	Cytosolic, loosely MOM-attached	MOM-inserted
BCL-W	Anti-apoptotic	BH1-BH4	MOM – loosely attached	MOM-inserted
MCL-1	Anti-apoptotic	BH1-BH4	MOM-, ER-, nuclear envelope inserted	MOM-, ER-, nuclear envelope inserted
BAX	Pro-apoptotic	BH1-BH3	Cytosolic, ER-, MOM-loosely attached	MOM-inserted, ER-inserted(?)
BAK	Pro-apoptotic	BH1-BH3	MOM-, ER- inserted	MOM-inserted, ER-inserted
BID	BH3-only	BH3	Cytosolic	MOM
BAD	BH3-only	BH3	Cytosolic	MOM
BIM	BH3-only	BH3	DLC1-associated	MOM-inserted(?)

Analysis of sequence homology among BCL-2 family proteins demonstrated that the family members posses low sequence homology, mostly limited to the BH regions. Mutagenesis studies of the BH1, BH2 and BH3 domains imply that these domains strongly influence homo- and hetero-dimerization of these proteins (Borner 2003;Gross et al. 1999). Prevailing dogma states that the BH3 domain is responsible for mediating interactions between anti-apoptotic and pro-apoptotic proteins and between BAX-like pro-apoptotic and BH3-only proteins (Borner 2003;Gross et al. 1999;Simonen et al. 1997). The sequence comparison among the BH3 domains of most prominent BCL-2 family proteins is presented in Table 2.

Table 2: The sequences of BH3 domains of most prominent BCL-2 family proteins.
The strictly conserved residues of BH3 domains are in italic.

BCL-2 family member	Function	BH3 domain sequence
BCL-2	Anti-apoptotic	*V*HLT*LRQ*A*GDD*F*SR*R
BCL-XL	Anti-apoptotic	*VK*Q*ALRE*A*GDEFE*L*R*
BAX	Pro-apoptotic	LSEC*L*RRI*GDE*LDSN
BAK	Pro-apoptotic	VGRQ*LALIGD*DINRR
BID	BH3-only	IARH*LAQIGDE*MDHN
BAD	BH3-only	YGRE*LRRMSDE*FEGS
BIM	BH3-only	IAQE*LRRIGDE*FNET

Some studies indicate that the BH3 domain has the ability to promote apoptosis (Bouillet, Strasser 2002;Kuwana et al. 2005;Putcha et al. 2001;Simonen et al. 1997). This opinion was strengthened by subsequent studies which used peptides derived from the BH3 domain of pro-apoptotic BCL-2 family members that bound to anti-apoptotic BCL-XL (Liu et al. 2003;Petros et al. 2004;Petros et al. 2000;Sattler et al. 1997). Expression of small peptide derive from the BH3 sequence of BAK was sufficient to induce apoptosis (Cosulich et al. 1997), small synthetic peptides derived from BH3 domains of the BH3-only proteins can suppress the anti-apoptotic BCL-2 family members (Dharap et al. 2003;Minko et al. 2003;Shangary, Johnson 2002).

In addition to the BH domains, many of the BCL-2 family members process a C-terminal hydrophobic domain, which is predicted to be responsible for membrane localization. Intriguingly enough, subcellular localization differs between the anti-apoptotic and pro-apoptotic proteins, and changes in the subcellular localization of these proteins upon apoptotic stimulus are characteristic of the early stages of apoptosis (Table 1). BCL-2 is predominantly anchored in the outer mitochondrial membrane and this membrane localization plays a key role in the ability of

BCL-2 to modulate mitochondrial membrane integrity (Borner 2003;Gross et al. 1999). The release of apoptogenic factors is inhibited by BCL-2 and BCL-XL. Pro-apoptotic BAX resides in the cytosol of healthy cells and translocates to mitochondria upon apoptotic stimulus (Annis et al. 2005;Borner 2003;Gross et al. 1999). The release of the apoptogenic factors is enhanced by membrane-bound BAX.

BH3-only proteins play a significant role in mediating a life or death decision. There is increasing evidence in the literature that these proteins are apoptotic-stimulus specific and cell-type specific. BIM, for example, is required for induction of apoptosis in lymphocytes upon cytokine withdrawal (Bouillet, Strasser 2002;Dijkers et al. 2000), stimulation of autoreactive antigen receptors, or treatment with taxol (Bouillet, Strasser 2002;Puthalakath et al. 1999). Current dogma states that BH3-only proteins directly activate BAX-like proteins to trigger the mitochondrial membrane disruption and consequently apoptosis (Bouillet, Strasser 2002). However, for many of these proteins including BIM, no direct binding to BAX was observed. An alternative model suggests that BIM and related proteins initiate apoptosis by binding of the anti-apoptotic proteins like BCL-2 and changing their conformation to enable the dimerization of BAX and the disruption of the mitochondrial membrane (Borner 2003).

1.3 Structure and function of BAX

The structure of BAX was determined in 2000 (Suzuki et al. 2000). BAX consists of nine α helices with eight amphipathic α helices clustered around one central hydrophobic α helix (α5) (Figure 1, 2). The overall fold of BAX closely resembles the fold of C-terminally truncated BCL-2 and BCL-XL. Helices 2, 3, and 4 form a hydrophobic groove. A portion of the C-

terminal region of BAX forms the helix α9 that binds within a hydrophobic groove, covering the

hydrophobic residues of the groove and burying its own hydrophobic residues.
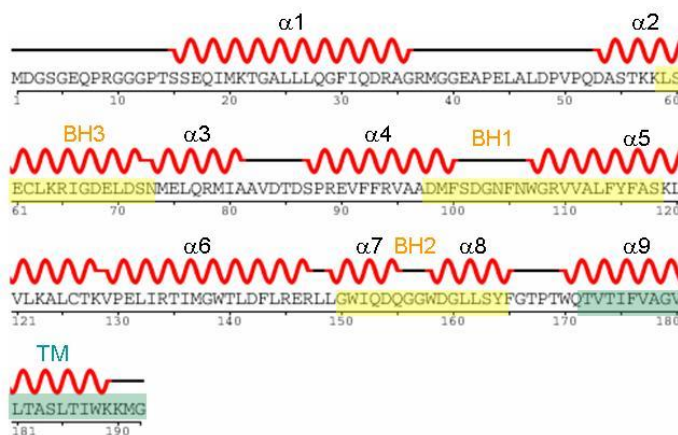
Figure 1: The amino acid sequence of BAX with indicated secondary structure, BH domains and transmembrane domain.
Complete amino acid sequence of BAX is shown in this figure. Alpha helices are in red, BH domains in yellow and transmembrane domain in green.

This may be important for increasing the solubility of the protein and contributes to the

fact that BAX exists predominantly in the cytosol before apoptosis induction. Helix α9 is

positioned in the hydrophobic pocket in a manner similar to the way the BH3 peptide of another

BCL-2 family member, BAK, is positioned in the hydrophobic groove of BCL-XL(Sattler et al.

1997). In essence, the directional sense of the peptide is opposite to that of the self-associated C-

terminal helix of BAX.
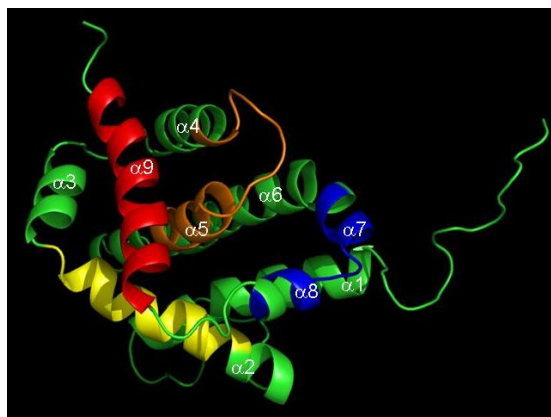
Figure 2: Ribbon representation of BAX structure.
The helices are numbered from 1-9, BH1 colored orange, BH2 blue, BH3 yellow, and α9 red.

In previous studies, Khaled et al. reported that a rapid increase in intracellular pH, associated with cytokine withdrawal in lymphocytes, triggered that translocation of BAX to mitochondria(Khaled et al. 1999). This concept led to the hypothesis that BAX undergoes conformational changes at pH 7.8 or higher. However, NMR studies obtained by Suzuki at al. did not report any conformational changes at high pH (Suzuki et al. 2000). Instead, they reported that BAX underwent conformational changes upon detergent treatment, which induced complex formation. This conformational changes exposed hidden epitopes that upon exposure were detectable by antibodies (Annis et al. 2005;Cartron et al. 2004;del Mar et al. 2001;Khaled et al. 1999). Conformational changes in BAX resulted in complex formation upon detergent treatment or in presence of lipids (Antonsson et al. 2000;Antonsson et al. 2001;Hsu, Youle 1998;Hsu, Youle 1997).

1.4 Molecular Modeling

"Molecular modeling is the science and art of studying molecular structure and function though model building and computation" (Schlick 2006). Molecular modeling begins with the refinement of the experimental data obtained by X-ray crystallography and NMR, and continues with the *ab initio* and semi-empirical quantum mechanics and empirical mechanics, molecular dynamics, structure/activity relationships and databases (Hinchliffe 2006;Machida 2007;Schlick 2006). Molecular modeling plays an important role in predicting structural and functional properties of increasing number of identified and characterized proteins. In my work I used empirical (molecular) mechanics approach.

Molecular mechanics is known also under terms force-field or potential energy method (Allinger 1976). An underlying principle in molecular mechanics is that cumulative physical forces can be used to describe molecular geometries and energies. The spatial conformation eventually obtained is then a normal adjustment of geometry to minimize the total internal energy. Molecules are considered as a collection of masses centered at the nuclei (atoms) connected by springs (bonds) (Hinchliffe 2006;Machida 2007;Schlick 2006). Molecular mechanics involves assembly of a potential energy, a function of atomic positions. Entropic contributions are either neglected or approximated (Machida 2007;Schlick 2006). Several versions force fields are commonly used. Molecular mechanics 2/3/4 is often used for small molecular systems (Allinger 1976;Lii, Allinger 1998b) , CHARMM (Brooks et al. 1983) package is preferred by protein modelers, AMBER (Case et al. 2005) is often used by nucleic acid modelers.

1.5 Thesis Objectives

Despite its critical importance in the apoptotic process, the mechanisms by which BAX is activated are still poorly defined. Research to date has revealed that BAX resides in the cytosol of healthy cells and upon apoptotic insults translocates to the membranes of organelles, principally the mitochondria and the endoplasmic reticulum (Borner 2003;Bouillet, Strasser 2002;Gross et al. 1999). Some progress has been made identifying possible proteins that could interact with BAX and mediate its membrane-binding activity. What is not known, however, is the actual means by which the apoptotic activity of BAX is triggered – what initiates the change from a cytosolic-form to a membrane-bound form. Lack of this information represents an important medical problem because, without an understanding of the conformational and physiological triggers that regulate the activation of BAX, the therapeutic potential of manipulating this protein in disease states cannot be fully developed. Current studies in the use of therapeutic apoptosis, which focus on the inhibition of cell death through manipulating BCL-2 family members, are in the early stages (Letai 2005).

The first objective of the work presented herein was to characterize the "molecular switch" which mediates the activation of BAX and identify possible physiological triggers that could "flip the switch". Based on published data and my preliminary observations, I developed the hypothesis that the subcellular distribution of BAX was governed by its C-terminal domain, the $\alpha 9$ helix. Published findings suggested that this domain functioned solely as a membrane anchor. Based on my initial findings, I proposed to examine a different function: the $\alpha 9$ helix operates as a "molecular switch" in response to apoptotic stimuli, inducing conformational changes that enable subsequent membrane integration. To validate this hypothesis, I employed

diverse methods of cell biology and computational modeling to demonstrate that basic residues in the α9 helix interact with residues in the α2 helix and hinge, which form part of a prominent hydrophobic groove, to mediate the subcellular localization of BAX. Using peptide mimics of the C-terminal α9 helix, I showed that occupancy of the hydrophobic groove by the α9 helix mediates the translocation of BAX from cytosol to mitochondria. To explore possible physiological triggers that could regulate the membrane-binding activity of the α9 helix, I observed that a transient raise in intracellular pH facilitated the movement of BAX to mitochondrial membrane, suggesting that the lipid bilayer of mitochondria could be a pH-responsive component. In total, these findings have significant implications for the development of novel therapeutic molecules for the modulation of apoptosis in drug development.

Second objective of the work presented herein was to develop a computational method to identify proteins, like BAX, capable of undergoing structural transitioning. To date, no such methodology is available for this purpose. Based on the computational analysis of helical packing energies in BAX, I developed the hypothesis that proteins which undergo significant conformational changes will have a broader distribution in their helical packing energies compared to less dynamic or static proteins. To test this hypothesis, multiple groups of proteins were analyzed by molecular mechanics 3 (MM3) and methods of computational analysis were developed to enable the prediction of which proteins which undergo conformational changes. These predications can be used to identify transitional proteins as well as transitional regions within proteins, indicating where changes are most likely to occur. I used this computational tool to examine multiple members of the BCL-2 family and was able to correlate their propensity to transition, as indicated by variations in helical packing energy, to their function. This work

contributes to the field of proteomics by providing a novel parameter by which transitional proteins can be identified for subsequent biological testing.

2 STRUCTURAL TRANSITIONS THAT MEDIATE THE MEMBRANE-ASSOCIATION ACTIVITY OF BAX ARE DEPENDENT ON ITS C-TERMINAL α-9 HELIX

2.1 Introduction

The pro-apoptotic member of BCL-2 family BAX is proposed to be the main executor of the mitochondria, causing a perforation of mitochondrial outer membrane and release of apoptogenic factors (Borner 2003;Cory et al. 2003;Degenhardt et al. 2002;Gross et al. 1999). This cytosolic protein translocates to mitochondrial membrane upon apoptotic stimuli (Antonsson et al. 2001;Nechushtan et al. 2001). The structural changes involved in the transition from inactive cytosolic form to an active membrane bound form are not completely understood. Structural studies suggested that BAX undergoes conformational changes as it translocates to membranes. The portion of a hydrophobic C-terminal region of BAX forms α9 helix. The helix α9 helix must disengage from the hydrophobic groove and the α2 helix must rotate to expose the BH3 domain for dimerization (Suzuki et al. 2000). However, that these are physiological events occurring during apoptosis has yet to be proven. Nor has conclusive evidence demonstrated how such conformational changes are accomplished. Diverse findings proposed regulatory interactions with BH3-only proteins such as BID (Ruffolo et al. 2000), BIM (Marani et al. 2002) or PUMA (Zhu et al. 2004), other proteins such as ACS (Ohtsuka et al. 2004), clusterin (Zhang et al. 2005) or Ku70 (Yoshida et al. 2004), and signaling proteins such as p53 (Chipuk et al. 2004), AKT (Gardai et al. 2004), JNK (Tsuruta et al. 2004), 14-3-3 (Nomura et al. 2003) or GSK-3 (Linseman et al. 2004) with BAX. In contrast to direct intervention by an accessory protein, Khaled et al. first reported that the activation of BAX coincided with a rise in

intracellular pH (Khaled et al. 1999), suggesting that BAX assumed a membrane-binding conformation in response to cytosolic alkalinization.

Several research reports suggested that the α9 helix is a transmembrane region essential for membrane binding (Nechushtan et al. 1999;Schinzel et al. 2004), while others maintain that it is either a regulatory domain (Arokium et al. 2004) or dispensable for apoptotic activity (Tremblais et al. 1999). Hence, how the α9 helix regulates the activity of BAX remains unclear. Likewise, the role of the hydrophobic groove also remains speculative – though it incorporates the critical BH3 domain. To better understand the function of these domains, I used computational modeling and targeted mutagenesis to demonstrate that the C-terminal α9 helix and the hydrophobic groove of BAX are both necessary for membrane association. I observed that, in the presence of endogenous BAX, the α9 helix could confer membrane-binding capacity to a cytosolic protein. To explain this, I propose that the α9 helix associates in reverse orientation with the hydrophobic pocket of adjacent BAX molecules, enabling dimerization and the release of additional membrane-binding domains that facilitate the insertion of BAX into mitochondrial membranes. Intracellular alkalinization may facilitate this process by altering mitochondrial membrane dynamics.

2.2 Material and Methods

2.2.1 Cell Lines and Reagents

The Flp-In T-REx-293 cell line (Invitrogen) was derived from 293 human embryonic kidney cells(Graham et al. 1977) that stably expressed the lacZ-Zeocin fusion gene and the Tet repressor. The 293 cell line was maintained in D-MEM (high glucose), 10% FBS (tetracycline-reduced) and 2 mM L-glutamine and 1% Pen-Strep. The HCT116 BAX$^{-/-}$ and BAX$^{+/+}$ colorectal cancer cell lines (from Dr. Bert Vogelstein, John Hopkins University) were maintained in McCoys 5A media, 10% FBS and 1% Pen-Strep. Staurosporine, Z-Vad-FMK (Calbiochem), nigericin (Molecular Probes), and dimethylamiloride (DMA) (Sigma) were prepared as stock solutions in DMSO or ethanol.

Peptides: The C-terminal peptide of wild-type BAX (Ac-VTIFVAGVLTASLTIWKKMG-NH2) and the BAX-leucine (BAX-LL) mutant peptide, (Ac-VTIFVAGVLTASLTIWLLMG-NH2) were synthesized by Biopeptide Co., (San Diego, CA) and were > 90% pure as confirmed by HPLC. The HPLC-purified, BIM BH3 peptide, DNRPEIWIAQELRRIGDEFNAYYAR, was donated by Dr. Douglas Green, St. Jude Children's Research Hospital. Peptides were resuspended in DMSO at a stock concentration of 10mM.

2.2.2 Plasmids, Mutagenesis and Transfection

For inducible expression of BAX wild-type (WT) and mutant proteins, I employed the Flp-In T-REx System (Invitrogen). BAX WT and mutant genes were cloned into the expression vector, pcDNA5/FRT/TO. This expression vector undergoes recombinase-mediated DNA

recombination at the Flp Recombination Target (FRT) site when co-expressed with the pOG44 plasmid that constitutively expresses the Flp recombinase. BAX constructs were amplified from the template, pEGFP-BAX (from Dr. Richard Youle, NINDS, NIH) with PCR, digested with EcoRV and cloned into pcDNA5/ FRT/TO expression vector.

All constructs were confirmed by sequencing. The pOG44 plasmid and the pcDNA5/FRT/TO vectors were cotransfected into the Flp-In T-REx 293 cell line, at a ratio of 9:1 with the Fugene 6 transfection reagent (Roche) following manufacturer's protocol. Stable Flp-In T-REx expression cell lines were then selected for blasticidin resistance (10 μg/ml), hygromycin resistance (100 μg/ml) and zeocin sensitivity (200 μg/ml). BAX expression was induced by the addition of tetracycline (1 μg/ml).

For transient, constitutive expression of BAX in HCT116 cells, pcDNA5/FRT/TO vectors, containing the BAX WT and mutant genes, were transfected using the TransIT-LT1 transfection reagent (Mirus) following manufacturer's protocol. In the absence of the Tet repressor, gene expression from pcDNA5/FRT/TO is constitutive. HCT116 cells were examined 24-48 hours after transfection for apoptosis by microscopy as described below.

PCR-directed mutagenesis of BAX was performed using HA-tagged primer sets, with mutations incorporated within the primer sequences (Table 2). To generate EGFP-BAX-CT, EGFP fused with the C-terminus of BAX was created by PCR from the template pEGFP (Clontech), and the PCR insert was cloned into pcDNA5/FRT/TO as previously described. HCT116 cells were transiently transfected using TransIT-LT1 reagent and cells assayed for EGFP expression 24-48 hours later.

Table 3: The list of BAX mutants and primers

BAX mutant	Forward Primer	Reverse Primer
BAX-KK	5'-GGATCACTCTCGGCCTG GACACCATGGGGATGTACCCATACG ATGTTCCAGATTACGCTGACGGGTCC GGGGAGCAG-3'	5'-CGTCGACTGCAGAATTCT CAGCCCATCTTCTTCCAGATGGTGAG CGAGG-3'
BAX-ΔNT (1-19)	5'-CCGGGGAGCAGCCCCATA TGTACCCATACGATGTTCCAGATTAC GCTATGAAGACAGGGGCCCTTTTGC-3	5'-CGTCGACTGCAGAATTCT CAGCCCATCTTCTTCCAGATGGTGAG CGAGG-3'
BAX-ΔCT (173-192)	5'-GGATCACTCTCGGCCTG GACACCATGGGGATGTACCCATACG ATGTTCCAGATTACGCTGACGGGTCC GGGGAGCAG-3'	5'-CGTCGACTGCAGAATTCT CAGGTCTGCCACGTGGGCGTCCCAA AG-3'
BAX-LL	5'-GGATCACTCTCGGCCTG GACACCATGGGGATGTACCCATACG ATGTTCCAGATTACGCTGACGGGTCC GGGGAGCAG-3'	5'-CGTCGACTG CAGAATTCTC AGCCCATGAGGAGCCAGATGGTGAG CGAGG-3'
BAX-DD	5'-GGATCACTCTCGGCCTG GACACCATGGGGATGTACCCATACG ATGTTCCAGATTACGCTGACGGGTCC GGGGAGCAG-3'	5'-CGTCGACTGCAGAATTCTC AGCCCATGTCGTCCCAGATGGTGAG CGAGG-3'
BAX-EE	5'-GGATCACTCTCGGCCTG GACACCATGGGGATGTACCCATACG ATGTTCCAGATTACGCTGACGGGTCC GGGGAGCAG-3'	5'-CGTCGACTGCAGAATTCTC AGCCCATCTCCTCCCAGATGGTGAG CGAGG-3'
BAX-RR	5'-GGATCACTCTCGGCCTG GACACCATGGGGATGTACCCATACG ATGTTCCAGATTACGCTGACGGGTCC GGGGAGCAG-3'	5'CGTCGATCTCAGCCCATTCGTCGCC AGATGGTGAGCGAGG-3'
BAX-QQ	5'-GGATCACTCTCGGCCTG GACACCATGGGGATGTACCCATACG ATGTTCCAGATTACGCTGACGGGTCC GGGGAGCAG-3'	5'-CGTCGACTGCAGAATTC TCAGCCCATCTGCTGCCAGATGGTG AGCGAGG-3'
BAX-KMGK	5'-GGATCACTCTCGGCCTG GACACCATGGGGATGTACCCATACG ATGTTCCAGATTACGCTGACGGGTCC GGGGAGCAG-3'	5'CGTCGACTGCAGAATTCTC ACTTCCCCATCTTCCAGATGGTGAGC GAGG-3
BAX-LK	5'-GGATCACTCTCGGCCTG GACACCATGGGGATGTACCCATACG ATGTTCCAGATTACGCTGACGGGTCC GGGGAGCAG-3'	5'-CGTCGACTGCAGAATTCTC AGCCCATCTTGAGCCAGATGGTGAG CGAGG-3'
BAX-KL	5'-GGATCACTCTCGGCCTG GACACCATGGGGATGTACCCATACG ATGTTCCAGATTACGCTGACGGGTCC GGGGAGCAG-3'	5'-CGTCGACTGCAGAATTCTC AGCCCATGAGCTTCCAGATGGTGAG CGAGG-3'
BAX-EK	5'-GGATCACTCTCGGCCTG GACACCATGGGGATGTACCCATACG ATGTTCCAGATTACGCTGACGGGTCC GGGGAGCAG-3'	5'-CGTCGACTGCAGAATTCTC AGCCCATCTTCTCCCAGATGGTGAGC GAGG-3'

BAX mutant	Forward Primer	Reverse Primer
BAX-KE	5'-GGATCACTCTCGGCCTG GACACCATGGGGATGTACCCATACG ATGTTCCAGATTACGCTGACGGGTCC GGGGAGCAG-3'	5'-CGTCGACT GCAGAATTCTC AGCCCATCTCCTTCCAGATGGTGAGC GAGG-3'
EGFP-BAX-CT	5'-GGATCACTCTCGGCCTGG ACGAGGATATCGTCGCCACCATGGT GAGCAAG-3	5'-TGCAGATATCTCAGCCCAT CTTCTTCCAGATGGTGAGCGAGGCG GTGAGCACTCCCGCCACAAAGATGG TCACGGTCTGCCACGTGGGGTTATCT AGATC-3'
BAX-ΔCT E69W	5'-CTCAAGCGCATCGGGGACTGGCT GGACAGTAACATGGAG-3'	5'-CTCCATGTTACTGTCCAGCCAGT CCCCGATGCGCTTGAG-3'
BAX-ΔCT E69R	5'-CTCAAGCGCATCGGGGACAAGC TGGACAGTAACATGGAG-3'	5'-CTCCATGTTACTGTCCAGCGGGT CCCCGATGCGCTTGAG-3'

2.2.3 Mitochondrial Translocation Assays, Crosslinking, Co-immunoprecipitation and Immunoblotting

BAX expression was induced in 293 cells by addition of 1 μg/ml tetracycline. EGFP-BAX-CT or BAX-ΔCT was constitutively expressed in HCT116 cells. After 48 hours of induction or expression, 293 or HCT116 cells were harvested and mitochondrial and cytosolic protein lysates were prepared using a mitochondrial extraction kit with minor modifications (Pierce). Briefly, 2×10^7 cells were lysed using the mild detergent method. This method is highly reproducible and does not induce conformational changes that lead to mitochondrial translocation of BAX. The final mitochondrial pellet was washed in 1M NaCl to remove any proteins peripherally associated with mitochondria. Mitochondrial and cytosolic protein lysates were loaded on 12% SDS-PAGE gels (Invitrogen), transferred to PVDF membranes and immunoblotted. For detection of HA-tagged BAX, an anti-HA mouse monoclonal antibody was used (16B12, Covance). For detection of endogenous BAX (N-20 Santa Cruz), prohibitin (Ab-2, Fitzgerald) and p38 MAPK (C20, Santa Cruz), rabbit polyclonal antibodies were used. For detection of EGFP (A.v. antibody, Clontech) a mouse polyclonal antibody was used. Appropriate

secondary rabbit or mouse antibodies crosslinked to horse radish peroxidase (HRP) (Cell Signaling) were used for detection. Enhanced chemo-luminescence (Pierce) was used for visualization following the manufacturer's protocol.

Crosslinking of BAX$^{-/-}$ HCT116 cells, co-transfected with BAX-ΔCT and EGFP-BAX-CT was performed using the crosslinking agent, disuccinimidyl suberate (DSS), following manufacturer's protocol. Forty-eight hours after transfection, whole HCT116 cells, after washing and resuspending in PBS, were treated for 30 minutes on ice with 10 mM DSS. The reaction was quenched with 10 mM Tris, pH 7.4 and 100 mM glycine. Cells were then lysed in mitochondrial isolation buffer (Pierce) as described above, and the cytosolic and mitochondrial protein fractions were combined and 2% CHAPS was added. Protein lysates were immunoprecipitated with an antibody specific for an internal BAX epitope (BAX Ab-4, Calbiochem) and analyzed on a 12% SDS-PAGE gel. Proteins were immunoblotted and detected with antibodies for EGFP as previously described.

To examine the direct effect of apoptotic mitochondria on the translocation of BAX, mitochondria were isolated from 2 x 10^7 BAX$^{-/-}$ HCT116 cells using the mitochondrial extraction kit (Pierce). To isolate EGFP-BAX-CT or BAX cytosolic proteins, these were expressed in HCT116 cells for 48 hours and cytosolic fractions were isolated from 10^7 cells using the mitochondrial extraction kit (Pierce). To determine whether EGFP-BAX-CT could translocate to apoptotic mitochondria, BAX$^{-/-}$ HCT116 cells were treated for 1 hour with 1 μM staurosporine or pH fixed at 7.2 or 7.8 for 20 minutes with 5 μM nigericin in a high K$^+$ HEPES buffer (25 mM Hepes, 145 mM KCl, 0.8 mM MgCl$_2$, 1.8mM CaCl$_2$, 5.5 mM glucose). Control, apoptotic or alkaline mitochondria were isolated using the mitochondrial extraction kit (Pierce). Cytosolic-derived EGFP-BAX-CT from HCT116 cells was incubated for 30 minutes with mitochondria at

19

37° C in a volume of 100 μl. Mitochondria were then washed 3 times in isotonic buffer (mitochondrial extraction kit). The final mitochondrial pellet was washed in 1 M NaCl to remove peripherally associated proteins. Mitochondrial protein lysates were prepared, resolved by SDS-PAGE and immunoblotted for BAX and prohibitin.

To assess the effect of the BAX and BIM peptides on the mitochondrial translocation of BAX, cytosolic endogenous BAX or constitutively expressed BAX-ΔCT were isolated from 10^7 HCT116 cells using the mitochondrial extraction kit (Pierce) and incubated with the peptides (5-25 μM) in a volume of 100 μl for 30 minutes. The cytosol/peptide mixture was then incubated for 30 minutes with neutral or alkaline mitochondria prepared as described above from 2 x 10^7 BAX$^{-/-}$ HCT116 cells. Mitochondria were then washed, resolved by SDS-PAGE and immunoblotted for BAX and prohibitin as previously described.

2.2.4 Triton X-114 Phase Partitioning

The hydrophobicity of BAX-KK and BAX-LL was examined by Triton X-114 phase partitioning (Brusca, Radolf 1994;Pryde 1998). Briefly, cytosolic extracts prepared in isotonic buffers were treated with 2% (vol%vol) Triton X-114 (Sigma), and the hydrophobic detergent phase was partitioned by incubation at 37°C followed by high-speed centrifugation. Bax was immunoprecipitated from the detergent phase and analyzed by immunoblot, as previously described.

2.2.5 pH Assays

The EGFP mutant, EYFP, exhibits pH dependent fluorescence in the pH range 6-8 (Hanson et al. 2002;Wachter et al. 1998). The fluorescence emission (527 nm peak) and excitation (514 nm peak) of EYFP decreases with decreasing pH. HCT116 cells were transfected with EYFP using TransIT-LT1 reagent (Mirus) and cells were assayed for EYFP expression 48 hours later. To induce alkalinization, EYFP-expressing cells were treated for 30 minutes to 1 hour with 1 μM staurosporine and changes in EYFP fluorescence were determined by flow cytometry   (BD-FACSCalibur; excitation 488 nm, emissions filtered through a 525 nm band pass (green fluorescence). Dead cells were excluded by forward and side scatter gating. A pH calibration curve was generated by incubation of EYFP-expressing cells for 30 minutes in a high K^+ Hepes buffer (described above) at different pH values from 6.8 to 8.0 in the presence of the ionophore nigericin (5 μM).   Cells were immediately assayed by flow cytometry (FACSCalibur; Becton, Dickinson and Company).

2.2.6 Confocal Microscopy

HCT116 cells were grown on coverslips coated with 200 μg/ml poly-L-lysine (Sigma) and transfected with the EGFP-BAX-CT using the Mirus LT-1 reagent according to the manufacturer's protocol. After 48 hours, apoptosis was induced with staurosporine (1 μM) or the cells were exposed to different pH conditions using nigericin and high K^+ buffers as described above. Cells were rinsed with PBS, fixed and permeabilized with ice cold methanol for 10 min at -20^0C. Cells were blocked with 1% BSA in PBS for 1 hour and stained with a primary

antibody HSP60 (H-300, Santa Cruz) for 45 min followed by secondary anti-rabbit IgG-Texas Red (Santa Cruz) for 30 min. After a final rinse, coverslips were mounted with Gel/Mount (Biomeda). The images were acquired by LSM 510 NLO, Carl Zeiss.

2.2.7 Computational Docking

The structure of BAX (PDB ID: 1F16) was obtained from the RCSB Protein Data Bank (http://www.rcsb.org/pdb). The primary sequences of BCL-2 proteins were obtained from UniProtKB (http://ca.expasy.org/uniprot). The BAX NMR encompasses 20 models. In order to determine the best representative from all models, the program NMRClust (Kelley et al. 1996a;Kelley et al. 1997) was used to cluster the structures. The best representative of the cluster (as determined by the most structures and the smallest RSMD for the cluster) was structure number 6. This structure was used in all calculations and computational manipulations.

Computational site directed mutagenesis was performed by substituting individual residues of BAX α9 helix with alanine using BioMed Cache 6.1.10 program (Fujitsu America, Inc., Sunnyvale, CA) as the graphical user interface. MM3 force field calculations were performed using parameters as described (Allinger et al. 1989b;Allinger et al. 1989a;Lii, Allinger 1989;Lii, Allinger 1994;Lii, Allinger 1998a). Calculations were performed *in vacuo*, disregarding an explicit water/membrane environment. The energy of each molecule was calculated until convergence (energy minimization) was reached. Energy terms included Van der Waals, electrostatics and hydrogen bonding interactions. All atoms in the structure were locked; except protons and side chains within a distance of 5Å from the mutation site. A conjugated gradient was used to locate the energy minimum. Van der Waals interactions between atoms separated by

more than 9.0Å were excluded. Optimization continued until the energy change was less than 0.001 kcal/mol. The estimated interaction energy (IE) was determined through separate calculations of the energy of the BAX structure prior the mutation (E_1), and the energy of the BAX structure after single site mutation (E_2), followed by the difference between these terms ($IE = E_2 - E_1$).

The peptides used in computational modeling and docking were peptides derived from BCL-XL (UniProtKB ID: Q07817), BCL-2 (P10415), BAD (Q92934), BIM (O43521), BAK (Q16611) and BAX (Q07812). All peptides used in the calculations were 20 amino acids in length. BCL-XL BH3 peptide incorporated residues 82-101 (UniProt sequence numbering), BCL-2 BH3 residues 89-108, BAD BH3 residues 107-116, BAX BH3 residues 54-73, BIM BH3 residues 146-165, and BAK BH3 residues 70-89. C-terminal peptides encompassed last 20 amino acids of the BCL-2, BCL-XL and BAX sequence.

The backbone of BAX α9 helix (residues 170-189) was used as a template on which peptides of BH3 domains and C-termini were built as alpha helices in BioMed Cache 6.1.10 program and their energy minimized using MM3 force field calculations under parameters described earlier. The atoms of the backbone were locked; atoms of side chains including protons were unlocked.

To perform receptor-ligand docking simulations, C-terminus of BAX (residues 170-192) was removed from the NMR structure to expose the hydrophobic groove. All the structures were submitted to the docking server GRAMM-X (Tovchigrechko, Vakser 2005a;Tovchigrechko, Vakser 2006a), where BAXΔ170-192 was assigned as a receptor and peptides as ligand. The server returned 10 different docking solutions for each receptor-ligand combination. The energy minimization was performed by MM3 force field calculation under parameters described earlier.

All atoms except protons were locked. The interaction energy (IE), was estimated through

separate determination of the energy of the complex ($E_{complex}$), the complex without the peptide

($E_{complex\ w/o\ peptide}$) and peptide alone ($E_{peptide}$), and by taking the difference between these terms

($IE=E_{complex}-(E_{complex\ w/o\ peptide}+E_{peptide})$). To determine the potential interaction energies for

different helical peptides with the hydrophobic pocket, the interaction energy obtained for each

peptide was compared with the interaction energy of BAX C-terminal peptide in the original

(forward) orientation within the pocket using the formula ($IE=IE_{peptide}-IE_{C\text{-}terminus\ BAX}$). The

graphic images were produced by DS Viewer Pro 5.0 (Accelrys Software Inc.).

2.3 Results

2.3.1 Lys189 and Lys190 in the C-terminal α9 helix modulate the intracellular localization of BAX.

The NMR structure of soluble, cytosolic-form of BAX shows that its C-terminal α9 helix

is partially buried in an internal hydrophobic pocket formed by helices 2, 3, 4 and 5(Suzuki et al.

2000). To serve as a potential transmembrane domain, the α9 helix must first disengage from the

hydrophobic pocket. Therefore, my first goal was to identify the residues within the α9 helix

that mediated the binding of the helix within the hydrophobic pocket. To begin this process, I

performed computational site-directed mutagenesis using the NMR structure of BAX as the

template. For this analysis, I chose the last twenty amino acids of the α9 helix. Each individual

amino acid was replaced with alanine and the effects on the interaction energy were determined.

Replacement of most of the amino acids throughout the C-terminus with alanine did not

significantly change the interaction energy of the residue within the helix (Figure 3). In contrast,

24

the mutation of lysine 189 resulted in dramatically altered interaction energy, primarily through a change in hydrogen bond energetics. This held true regardless of the orientation of the α9 helix within the groove. Though this simulation did not conclusively rule out a role for other residues within the α9 helix in the regulation of the activity of BAX, it does suggest that mutation of Lys189 could potentially destabilize the binding of the α9 helix with the charged residues on the margin of the hydrophobic pocket. Thus, lysine 189 might function as a loose anchor of the α9 helix through weak hydrogen bond interactions with acidic or polar residues within the hydrophobic pocket. The C-terminus of BAX contains two lysine residues back-to-back, lysine 189 and lysine 190, a unique feature among BCL-2 family members. My next step was to experimentally test the conclusion determined by computational analysis.
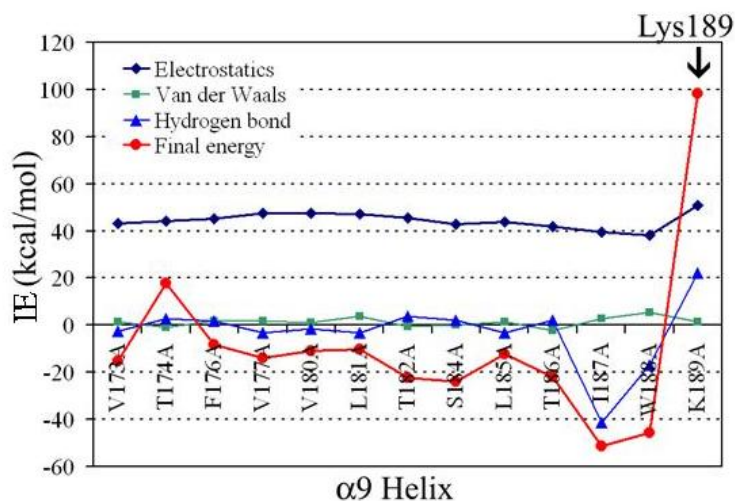
Figure 3: Summary of the computational mutagenesis of Lys189.
Computational site-directed mutagenesis was performed using the BioMed Cache 6.1.10 suite. Individual residues of the BAX α9 helix (amino acids 172-189) were substituted one at the time with the alanine. The resulting interaction energies (IE) were determined. Substitution of Lys189 for alanine could potentially destabilize the interaction of C-terminal α9 helix with the charged or polar residues on the margin of the hydrophobic pocket. IE = E_2-E_1, IE – the interaction energy, E_1 – the energy of BAX before mutation, E_2 – the energy of BAX after the mutation

To experimentally test the computational predictions, a series of mutagenesis experiments were performed targeting lysine 189 and 190 in the C-terminus of BAX. To circumvent the spontaneous apoptosis caused by the toxicity of the wild-type BAX (Annis et al. 2005;Antonsson et al. 2001;Borner 2003;Gross et al. 1999) and its construct, I applied two different strategies for expression in mammalian cells. I engineered (1) HA-tagged-BAX mutants for the tetracycline inducible expression in a 293 cell line, which did not cause spontaneous apoptosis during short term induction, and (2) HA-tagged-BAX mutants which were co-expressed with EGFP as a marker in a BAX$^{-/-}$ HCT116 cell line and the absence of EGFP^{+} cells was used as a measure of spontaneous apoptosis by microscopic inspection. I included the wild-type and N- or C-terminal truncated BAX mutants as controls along with the BAX Lys189/190 mutants. The 293 cells inducibly expressing wild-type BAX (BAX-KK) displayed a typical partitioning between cytosol and mitochondria. N-terminal truncated BAX mutant (BAX-ΔNT), lacking residues 1-19, was largely localized in mitochondria. C-terminal truncated BAX (BAX-ΔCT), lacking residues 173-192, was cytosolic (Figure 4). The remaining immunoblots demonstrating the results achieved for other C-terminal BAX mutants are not shown since this work was performed by other lab technical personnel. For purposes of discussion, the complete results for the C-terminal mutagenesis study are summarized in Table 4.
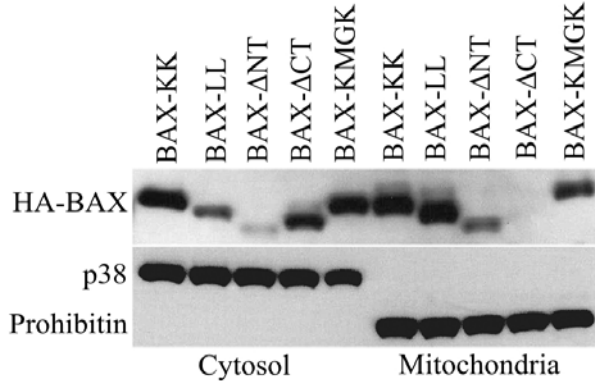
Figure 4: Expression of HA-tagged BAX mutants in 293 cells.
HA-tagged BAX mutants were inducibly expressed in 293 cells using the Flp-In T-Rex expression system. After 24 hours of induction with tetracycline, cells were lysed and mitochondrial and cytosolic lysates prepared. The presence of HA-BAX was assayed by immunoblotting with an anti-HA antibody. As controls for loading and subcellular fractionation, p38 MAPK was blotted for cytosolic content and Prohibitin was blotted for mitochondrial content. Note that loss of the two charged lysines altered the migration pattern of BAX-LL in SDS-PAGE gels. The mitochondrial translocation of other BAX mutants is summarized in Table 2.

Table 4: Summary of BAX mutagenesis in 293 cells.

Mutant	Mutations of the C-terminus	Primary Localization
BAX-KK	None	Cyto/mito
BAX-ΔCT	Δ173-192	Cyto
BAX-ΔNT	Δ1-19	Mito
BAX-LL	K189L, K190L	Mito
BAX-DD	K189D, K190D	Cyto
BAX-EE	K189E, K190	Cyto
BAX-RR	K189R, K190R	Mito
BAX-QQ	K189Q, K190Q	Cyto/mito
BAX-KMGK	K190M, M191G, G192K	Cyto/mito
BAX-KMG	ΔK190	Cyto/mito
BAX-MGK	ΔK189, K190M, M191G, G192K	Cyto
BAX-LK	K189L	Cyto/mito
BAX-KL	K190L	Mito
BAX-EK	K189E	Cyto
BAX-KE	K190E	Cyto/mito

The ability of BAX C-terminal mutant constructs to induce apoptosis was tested in the

absence of endogenous BAX by co-expressing EGFP, as a marker, with BAX mutants in the

27

BAX$^{-/-}$ HCT116 cells. The extent of spontaneous apoptosis was estimated by the loss of EGFP$^+$ cells through fluorescent microscopic analysis. This was the best available method to document apoptosis, since low transfection efficiency (about 40%) and constitutive expression of the apoptotic forms of BAX caused rapid cell death within hours of expression, making other apoptotic assays (i.e. annexin staining, PI exclusion) difficult to perform. Overexpression of BAX-KK and BAX-ΔNT resulted in a massive spontaneous apoptosis, documented by a significant loss of green fluorescent, EGFP$^+$ cells (Figure 5), and BAX-ΔCT remained exclusively cytosolic and did not induce apoptosis as evident from the presence of EGFP$^+$ cells (Figure 5). These results agree with most other published reports (del Mar et al. 2001;Nechushtan et al. 1999;Suzuki et al. 2000) and demonstrate that an intact C-terminus of BAX mediates the membrane docking step and subsequent apoptosis, while the N-terminus promotes cytosolic retention In the absence of the last 20 amino acids of the C-terminus, encompassing the α9 helix, BAX cannot translocate to mitochondrial membranes or cause apoptosis in mammalian cells.
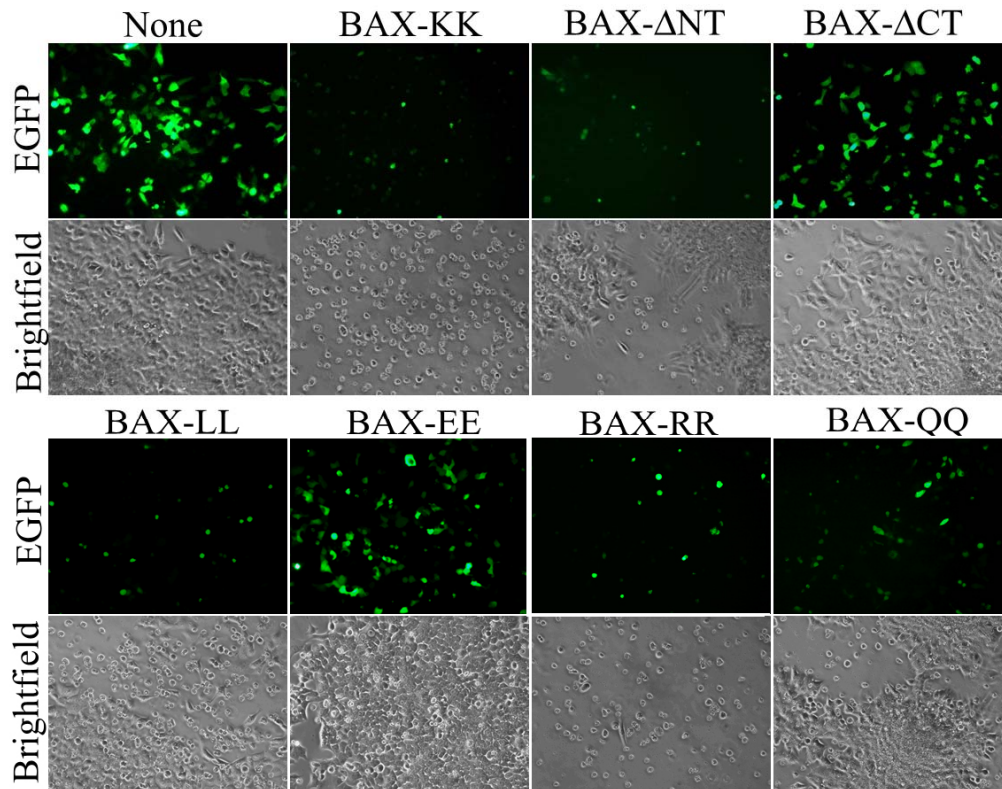
Figure 5: Co-expression of HA-tagged BAX mutants with EGFP in BAX$^{-/-}$ HCT116 cells.

HA-tagged BAX mutants were constitutively co-expressed with EGFP in BAX$^{-/-}$ HCT116 cells. After 48 hours, HCT116 cells were microscopically observed for loss of EGFP$^+$ cells, indicative of apoptosis induced by co-expression of BAX mutants. Images shown were acquired at 40X magnification.

Subsequent mutagenesis of lysine 189 and 190 emphasized the importance of a positive charge at the sites. Substitution of lysine 189 and 190 with a negatively charged residues, aspartate or glutamate, resulted in complete cytosolic retention of BAX (BAX-DD, BAX-EE, BAX-EK) in 293 cells, and no cell death was observed in BAX$^{-/-}$ HCT 116 cells (Figure 5, Table 4). When lysine 189 and 190 were replaced with positively charged arginine (BAX-RR), mitochondrial targeting and cell death resulted (Figure 5, Table 3). The mutation of lysine 189

29

and 190 into glutamine caused predominantly a cytosolic distribution of BAX-QQ and intermediate toxicity as compared to BAX-KK and BAX-RR (Figure 5, Table 4). I consistently found that the loss of lysine 189 confined BAX to cytosol (BAX-EK, BAX-MGK), while loss of lysine 190 did not have the same effect (BAX-KE, BAX-KMG, BAX-KMGK) (Figure 5, Table 4). These results suggest that the lysine 189 is an essential mediator of BAX subcellular distribution. I derive the conclusion from the mutagenesis studies that the presence of a positively charged residue at position 189 is necessary for the mitochondrial membrane targeting of BAX and the induction of spontaneous cell death, while a polar or negatively charged residue at this position confines BAX to the cytosol and prevents apoptosis.

Mutations that replaced lysine 189 and/or 190 with hydrophobic leucines resulted in spontaneous mitochondrial targeting (BAX-LL; Figure 4) and subsequent apoptosis (BAX-LL, BAX-KL; Figure 5, Table 4). The reason for this was that increasing the hydrophobic content of the C-terminus of BAX enhanced its membrane docking properties. Further experimental evaluation of this mutant demonstrated that it partitioned into the detergent phase of preparations treated with Triton-114, indicative of increased hydrophobic content (Figure 6A). Immunoprecipitation with an N-terminal and C-terminal specific BAX antibodies (Figure 6B) and protease digestion (Figure 6C) further suggested that BAX-LL assumes a more relaxed confirmation caused by the increased hydrophobicity of the C-terminal α9 helix and subsequent membrane binding. Increased pH also enhanced protease digestion as previously shown by Khaled et al. (Figure 6C). The effect of pH changes on BAX will be further examined in a later section. It should be noted that by substituting lysines in the C-terminus and increasing the hydrophobicity of this domain, the membrane binding of BAX was artificially induced in a manner that may not be physiological as will be further discussed. These findings do suggest,

however, that manipulation of the C-terminus altered the membrane-binding activity of BAX, indicating its important role in this process, and an examination of how this could be achieved was my next step.

A.

	KK	KK	LL	LL
HA-BAX—	D	A	D	A

B.

Mutant	KK		LL		KK		LL	
IP N-term	+	-	+	-	+	-	+	-
IP C-term	-	+	-	+	-	+	-	+

HA-BAX—

Cytosol   Mitochondria

C.

Prot. K	0	10	10	10
pH	7.0	7.0	7.5	8.0
KK				
LL				
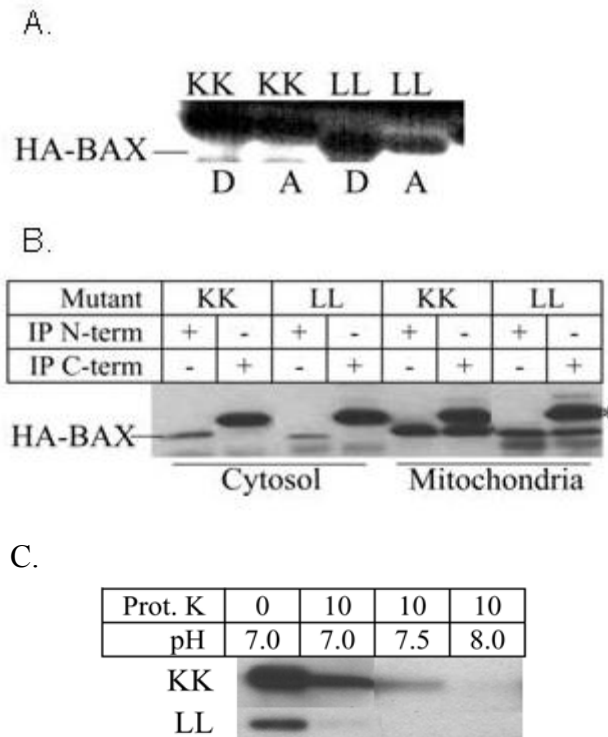
Figure 6: The BAX-LL mutant exhibits characteristics of an unfolded hydrophobic protein.
(A) Mitochondrial protein lysates were prepared from 293 cells induced to express either BAX-KK (wild-type) or BAX-LL (leucine mutant). Lysates were treated with Triton-X-100 to separate proteins into those that partitioned into an aqueous phase (A) and those that partitioned into a detergent phase (D). Proteins were assayed by SDS-PAGE and immunoblotted for the HA-tagged BAX protein using an anti-HA antibody (Covance). Compared to BAX-KK, more BAX-LL partitioned into the detergent (D) phase. (B) Cytosolic or mitochondrial protein lysates were prepared from 293 cells induced to express either BAX-KK (wild-type) or BAX-LL (leucine mutant). Lysates were immunoprecipitated with an N-terminal specific BAX antibody (N-20, Santa Cruz) or a C-terminal specific BAX antibody (ID3, Abcam). Immunoprecipitates were washed and assayed by SDS-PAGE and the HA-tagged BAX protein immunoblotted using an anti-HA antibody (Covance). The N-terminal epitope specific BAX antibody immunoprecipitated some cytosolic BAX but much more mitochondrial BAX, especially from cells expressing the BAX-LL mutant. In contrast the C-terminal epitope specific antibody did not immunoprecipitate cytosolic BAX, but could immunoprecipitate mitochondrial BAX from cells expressing either BAX-LL or BAX-KK. The * indicates non-specific bands. (C) Mitochondrial protein lysates were prepared from 293 cells induced to express either BAX-KK or BAX-LL. Lysates were treated with proteinase K, 0-10g/ml, in isotonic buffers at pH 7, 7.5 or 7.8. The BAX-LL mutant was more sensitive to protease digestion than BAX-KK at neutral pH, while both BAX proteins were digested at alkaline pH. This suggests that the BAX-LL mutant is more unfolded than the wild type protein and that alkaline pH further unfolds the protein.

2.3.2 The C-terminal α9 helix of BAX directs EGFP to apoptotic mitochondria

The previous studies demonstrated that Lys189/190 critically regulated the subcellular partitioning of BAX – positive charge at the positions 189/190 directing BAX to mitochondria, negative or polar charge retaining BAX in the cytosol. I next determined whether the C-terminus alone is able to direct a cytosolic protein to mitochondria. To test this, I engineered a fusion protein EGFP-BAX-CT by attaching the C-terminus of BAX (25 amino acids) to EGFP and evaluating its subcellular distribution in non-apoptotic and apoptotic cells. In my initial experiments, I fused only the last 20 amino acids of BAX to EGFP and did not achieve results of any significance. A possible explanation is that when the C-terminus of BAX is directly attached to a protein it requires the presence of a putative hinge region (Schinzel et al. 2004), containing a proline, in order to provide the flexibility required for protein:protein interactions. Also I did not express full length, wild-type BAX in this context since recall that the constitutive expression of BAX-KK is extremely toxic, hence the reason for using the fusion protein to study the C-terminus of BAX.

Using confocal microscopy, I visually inspected the distribution of EGFP-BAX-CT (green fluorescence) in BAX$^{+/+}$ HCT116 cells for either a diffuse staining pattern, suggestive of cytosolic localization, or a punctate staining, suggestive of membrane binding, upon induction of apoptosis by staurosporine (Figure 7B). Staurosporine was chosen as the lethal insult since it is a well-recognized method of inducing rapid apoptosis (Kuwana et al. 2005). I did not observe that the addition of the C-terminal of BAX to EGFP resulted in significant spontaneous membrane binding in non-apoptotic cells as had been previously reported (Schinzel et al. 2004). In healthy cells there were only minor differences in the staining patterns between cells

expressing cytosolic EGFP and EGFP-BAX-CT, with the latter showing more membrane association (Figure 7B). The drastic difference in the staining patterns between cells expressing cytosolic EGFP and EGFP-BAX-CT occurred upon induction of apoptosis by staurosporine. A distinctive punctate staining pattern, hallmark of membrane binding, was observed in apoptotic cells expressing EGFP-BAX-CT. This staining pattern significantly overlaid (yellow fluorescence) with the mitochondrial marker, HSP60 (red fluorescence), demonstrating that fusion of the last 25 amino acids of BAX to EGFP conferred membrane binding to EGFP, but preferentially in apoptotic cells. It was evident from these findings that the apoptotic environment promotes the translocation of EGFP-BAX-CT from the cytosol to the mitochondrial membrane. EGFP-BAX-CT thus mimicked the apoptotic behavior of BAX.

The mitochondrial co-localization studies were confirmed by immunoblotting mitochondria for EGFP. I obtained mitochondrial fractions from healthy or apoptotic mitochondria of BAX$^{-/-}$ HCT116 cells. Apoptosis was induced by staurosporine. Another set of HCT 116 cells, BAX$^{+/+}$ and BAX$^{-/-}$, was transfected with EGFP-BAX-CT. I extracted cytosolic fractions from the cells. In the final step I incubated the healthy or apoptotic mitochondria with the cytosol containing EGFP-BAX-CT. Analysis by immunoblotting showed that more EGFP-BAX-CT inserted into apoptotic mitochondria compared to healthy mitochondria (Figure 7A). The ratio of EGFP/prohibitin increased two-fold (BAX$^{-/-}$ HCT116 cells) and four-fold (BAX$^{+/+}$ HCT116 cells) in apoptotic cells, indicating that endogenous BAX contributed significantly to the translocation of the EGFP-BAX-CT. Note that EGFP-BAX-CT itself was not exposed to the apoptotic environment; hence the translocation of EGFP-BAX-CT to mitochondria had to be caused by the apoptotic mitochondria. The results also suggest while the last 25 residues of BAX

can confer mitochondrial targeting to EGFP, this is greatly enhanced in the presence of endogenous BAX.
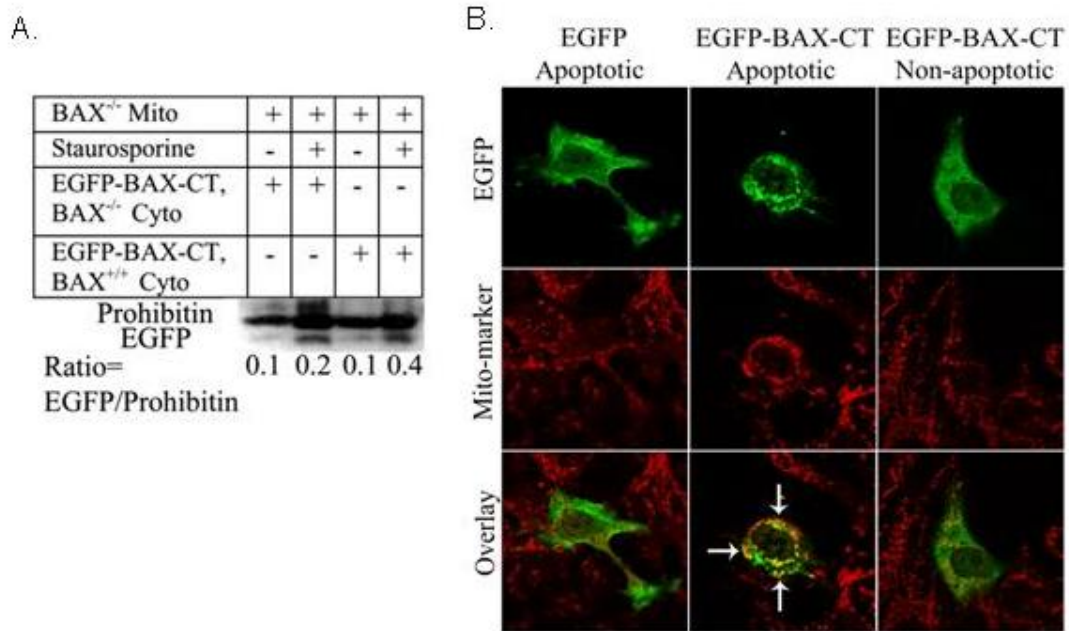
Figure 7: EGFP tagged with C-terminus of BAX confers mitochondrial membrane-binding properties in apoptotic cells.

(A) BAX$^{-/-}$ HCT116 cells were treated with or without 1 μM staurosporine for 1 hour and mitochondria harvested. Another set of BAX$^{-/-}$ or BAX$^{+/+}$ HCT116 cells were transfected with EGFP-BAX-CT and, after 48 hours, cells were lysed and the cytosol was incubated with non-apoptotic or apoptotic mitochondria in a test tube for 20 min. Mitochondria were than washed several times with 1M NaCl to remove peripherally associated proteins. Mitochondrial protein content was analyzed by SDS-PAGE and immunoblotted with an anti-EGFP antibody and an anti-Prohibitin antibody as a mitochondrial loading control. (B) BAX$^{+/+}$ HCT116 cells were transfected with EGFP or EGFP-BAX-CT and cells assessed for EGFP expression (green) by confocal microscopy. Mitochondria were identifies by staining with anti-HSP60 antibody followed by a rhodamine-labeled (red) secondary antibody. Apoptosis was induced by treatment with 1μM staurosporine for 1 hour. Diffuse cytosolic staining pattern was observed in all non-apoptotic cells or cells expressing EGFP, while in apoptotic cells that expressed EGFP-BAX-CT a punctate staining pattern was detected that largely overlaid with mitochondria (indicated by arrows).

To confirm that endogenous BAX was contributing to the binding of EGFP-BAX-CT to mitochondria, we repeated the expression of EGFP-BAX-CT in BAX$^{-/-}$ cells and did not observe the same degree of mitochondrial translocation that was evident when EGFP-CT-BAX was expressed in BAX$^{+/+}$ cells   (Figure 8).

BAX $^{-/-}$

	EGFP Apoptotic	EGFP-CT BAX Apoptotic	EGFP-CT BAX Non-Apoptotic
EGFP			
Mito-marker			
Overlay			
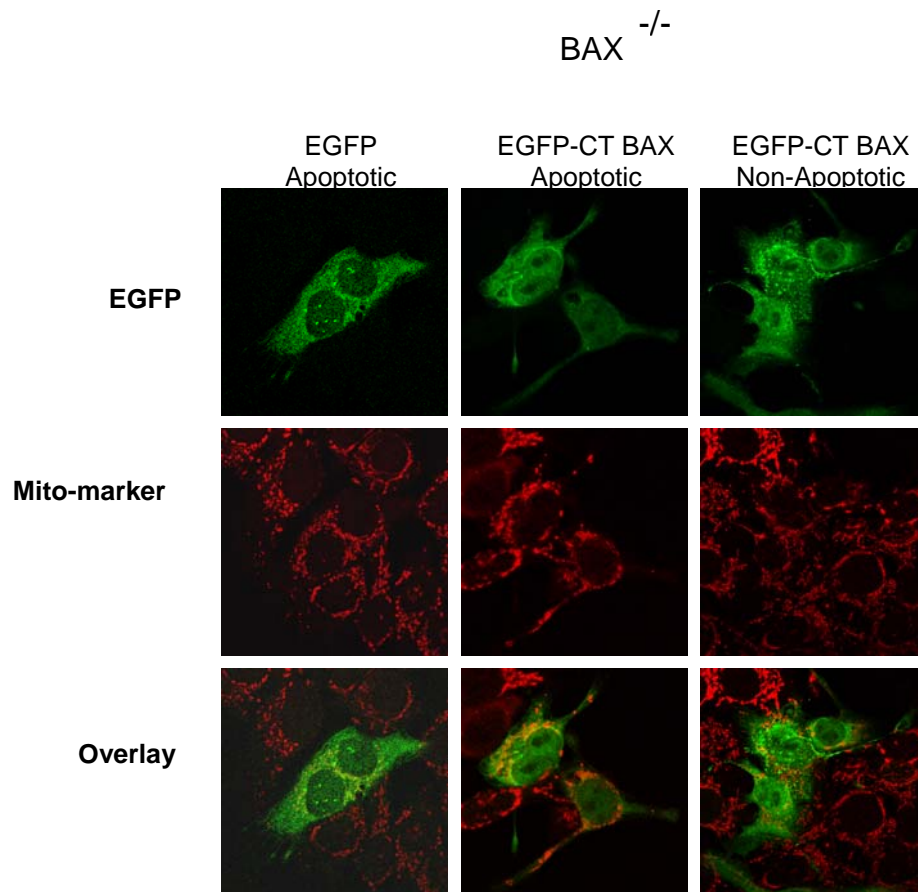
Figure 8: EGFP tagged with C-terminus of BAX does not confers mitochondrial membrane-binding properties in cells lacking endogenous BAX.

BAX$^{-/-}$ HCT116 cells were transfected with EGFP or EGFP-BAX-CT and cells assessed for EGFP expression (green) by confocal microscopy. Mitochondria were identifies by staining with anti-HSP60 antibody followed by a rhodamine-labeled (red) secondary antibody. Apoptosis was induced by treatment with 1μM staurosporine for 1 hour. Diffuse cytosolic staining pattern was observed in all non-apoptotic cells expressing EGFP or EGFP-BAX-CT. In apoptotic cells that expressed EGFP-BAX-CT a minimal mitochondrial overlay was detected (note lack of yellow overlay compared to Figure 6B).

These studies strongly indicated that the presence of endogenous BAX influenced the distribution of the fusion protein, EGFP-BAX-CT. To determine whether EGFP-BAX-CT could be in physical association with endogenous BAX, I performed a protein cross-linking experiment. I co-expressed the non-apoptotic form of BAX (BAX-ΔCT) with EGFP-BAX-CT in BAX$^{-/-}$ HCT116 cells (Figure 8). The intense band of cross-linked EGFP-BAX-CT heterodimers

at ≥64 kDa was more pronounced than the weak band of EGFP-BAX-CT monomers at 36 kDa. This indicated that almost all detectable EGFP-BAX-CT could be cross-linked and co-immunoprecipitated with BAX-ΔCT. Furthermore, this result strongly suggested that EGFP-BAX-CT and BAX-ΔCT were in physical association in heterodimeric complexes. This was not the case with EGFP and BAX-ΔCT (Figure 8). Note that this experiment was not performed in the presence of either constitutively expressed wild-type BAX, because of its toxicity, or non-apoptotic endogenous BAX, since it would not have undergone apoptotic conformational changes. The summary of my results suggests that the C-terminus of BAX attached to EGFP can bind to structural elements exposed in the C-terminal deleted form of BAX-ΔCT and form heterodimeric complexes that have the ability to integrate into the mitochondrial membrane.

BAX-ΔCT	-	+	+	-	+	+
EGFP	-	+	-	-	+	-
EGFP-BAX-CT	-	-	+	-	-	+
DSS (crosslinker)	-	-	-	+	+	+
IP-BAX antibody	+	+	+	+	+	+
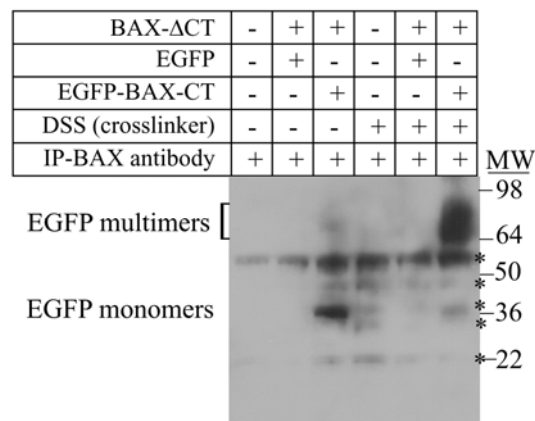
Figure 9: EGFP-BAX-CT forms heterodimers with BAX-ΔCT.
BAX^{-/-} HCT116 cells were transiently co-transfected with EGFP or EGFP-BAX-CT and BAXΔCT. After 24 hours, cells were treated with or without the crosslinker (DSS), lysed and combined cytosolic/mithochondrial proteins lysates prepared. Protein lysates were immunoprecipitated with BAX antibody (rabbit polyclonal, Ab-4), specific to an internal epitope. Immunoprecipitates were analyzed by SDS-PAGE and blotted for EGFP with anti-EGFP antibody (mouse monoclonal). EGFP-BAX-CT/BAXΔCT dimers (approximately 64 kDA) were detected in crosslinked samples from cells in which EGFP-BAX-CT and BAX-ΔCT were co-expressed. The* indicates non-specific bands, the most prominent being the heavy chain of immunoglobulins.

2.3.3 Intracellular Localization of BAX Controlled by α9 helix

Based on previous observations, I next wanted to examine the binding of the C-terminus of BAX to structural elements within BAX itself. Based on the NMR structure (Suzuki et al. 2000), I knew that the C-terminus of BAX, encompassing α9 helix, self-associates in forward directional orientation within the hydrophobic pocket. The association of the BH3 peptides derived from BH3-only proteins BIM (Liu et al. 2003), BAD (Petros et al. 2000) and BAK (Sattler et al. 1997) with BCL-XL deciphered by structural studies demonstrated that those peptides associate with the hydrophobic pocket of BCL-XL in a reversed directional orientation. Such findings suggest that occupation of the hydrophobic pocket plays a major role in the regulation of the intracellular distribution of BCL-2 family members. To explore this possibility, I used a computational approach, employing the docking web server GRAMM-X (Tovchigrechko, Vakser 2005b;Tovchigrechko, Vakser 2006b), in order to determine where on the surface of BAX would the α9 helix preferentially bind. The underlying concept for this approach was that BAX would be computationally treated like a receptor and the C-terminal α9 helix would be its ligand.

We submitted the C-terminus-truncated structure of BAX (based on the NMR structure (Suzuki et al. 2000)) and the structure of the C-terminal α9 helix for testing. By truncating the C-terminus, I mimicked a form of BAX with an unoccupied hydrophobic pocket, which could occur also upon exposure of the α9 helix during apoptosis. Figure 9A represents the overlay of 10 docking solutions resolved by GRAMM-X. It is evident from my results that the α9 helix of BAX fits predominantly within the hydrophobic pocket. This implies that the association of the α9 helix with the hydrophobic pocket is energetically the most favorable location for interaction.

37

In the next step I resolved the individual docking solutions. As shown in Figure 9B, the soluble, cytosolic form of BAX emerged. The α9 helix was bound into the hydrophobic pocket in the forward orientation, characteristic of the self-associated form, but surprisingly this forward orientation of binding was not the most energetically favorable docking solution. The reverse orientation of binding was the most energetically favorable (Figure 9C). In this reverse orientation lysine 189 of the α9 helix is in binding proximity to the acidic residue glutamate 69, a conserved site in the α2 helix, and asparagine 73, in the hinge between the α2 and α3 helices. Both these residues are found within the BH3 domain of BAX.
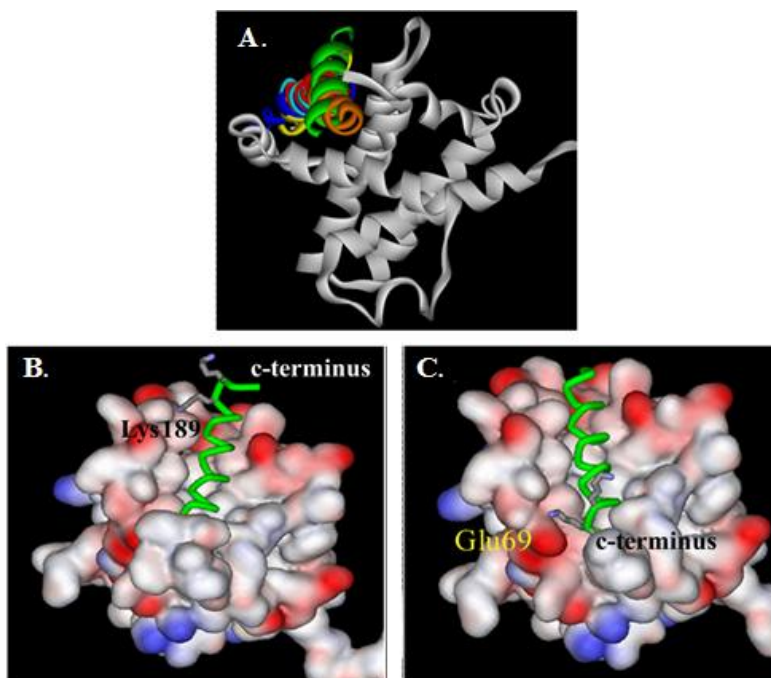
Figure 10: The helical C-terminus of BAX associates with the hydrophobic pocket of BAX in two orientations.

(A) Overlay of 10 docking solutions derived from the GRAMM-X docking software for the binding of the α9 helix on the surface of BAXΔCT. The α9 helix binds predominantly within the hydrophobic pocket formed by helices 2,3,4 and 5. (B) The forward binding model of the soluble form of BAX results when the hydrophobic pocket is occupied by its own C-terminal α9 helix – the helix is bound in the pocket in the forward orientation and Lys189 is solvent exposed. (C) The more energetically favorable reverse binding model results when the C-terminal α9 helix binds in reverse orientation in the hydrophobic pocket of BAX. In this orientation, the Lys189 is in binding proximity to Glu69, a conserved site and Asp73 (not shown) within the BH3 domain.

In order to establish the validity of the computational docking analysis, I compared the outcome of these findings with other potential binding partners of BAX. Using the same methods, I estimated the binding energies which resulted from interactions between the BH3 peptides of BIM, BAD, BAX and BAK with the hydrophobic pocket. A number of published findings support such interactions (Bouillet, Strasser 2002;Cosulich et al. 1997;Kuwana et al. 2005;Shangary, Johnson 2002;Simonen et al. 1997). The results of the computations are summarized in Table 4. Negative numbers indicate more favorable binding energies, while positive numbers indicate less favorable binding energies. The binding energies of different BH3 helices, which were docked in more energetically favorable reverse directional orientation, were compared to the α9 helix of BAX bound in the forward orientation that occurs during self-association. The results of computational docking suggested that most BH3 domains of the BCL-2 family members, including that of BAX itself, would not bind to the hydrophobic pocket of BAX because of the unfavorable interaction energy (Table 5), suggesting that BH3 interactions are not the primary mode through which these proteins could heterodimerize. The only exception was that of the BH3 domain of BCL-2 (Table 5) that I did observe could co-immunoprecipitate (not shown) and therefore interact with BAX. The interaction between BAX and BCL-2, but not for example the interaction between BAX and BAD or BAX and BIM, is also supported by findings in the literature (Kuwana et al. 2005;Shangary, Johnson 2002;Simonen et al. 1997).

Table 5: Analysis of BH3 peptides docked into the hydrophobic pocket of BAX.

IE represents the difference in the binding energy between the complex, where the peptide is docked in the reverse orientation, and the complex, where the C-terminal of BAX is docked in forward orientation: IE =IE$_{\text{peptide}}$-IE$_{\text{C-terminus BAX}}$.

Peptide	Sequence	IE (kcal/mol)
CT BAX-KK	VTIFVAGVLTASLTIWKKMG	-52.0
BAK BH3	QDASTKKLSECLKRIGDELD	420.8
BAX BH3	ASTKKLSECLKRIGDELDSN	707.2
BAD BH3	QRYGRELRRMSDEFVDSFKK	375.4
BIM BH3	IWIAQELRRIGDEFNAYYAR	267.1
BCL-XL BH3	PMAAVKQALREAGDEFELRY	259.0
BCL-2 BH3	VPPVVHLTLRQAGDDFSRRY	-7.7

I observed that BAX could not interact with another BAX molecule through its BH3 domains (Table 5). However, hypothetically, BCL-XL could interact with the hydrophobic pocket of BAX via its C-terminal end. Therefore, I used computational docking to evaluate the possibility that C-terminal helices, rather than BH3 domains, interacted with the hydrophobic groove. Additionally, I also examined how different BAX C-terminal Lys189/190 mutants bound in the reverse orientation within the hydrophobic pocket of BAX. Table 5 presents calculations derived from comparing the helical C-terminus of wild-type BAX, bound in the forward orientation to the hydrophobic pocket, to the binding of the α9 helices of BCL-XL, BCL-2 and a wild-type or C-terminal mutant of BAX bond in the more energetically favorable (negative ΔIE) reverse orientation. Note that the C-terminus of BCL-XL bound favorably within the hydrophobic pocket, and that his observation is supported by previously published data showing that BCL-XL can directly interact with BAX-ΔCT (Hsu et al. 1997).

Table 6: Analysis of C-terminal peptides docked into the hydrophobic pocket of BAX.
IE represents the difference in the binding energy between the complex, where the peptide is docked in the reverse orientation, and the complex, where the C-terminal of BAX is docked in forward orientation: IE =IE$_{peptide}$-IE$_{C-terminus\ BAX}$. * - See Table 2

Peptide	Sequence	ΔIE (kcal/mol)	Membrane Binding*
CT BAX-KK	VTIFVAGVLTASLTIWKKMG	-52.0	Yes
CT BCL-XL	FLTGMTVAGVVLLGSLFSRK	-134.0	Yes
CT BCL-2	LLSLALVGACITLGAYLGHK	53.6	Yes
CT BAX-DD	VTIFVAGVLTASLTIWDDMG	223.1	No
CT BAX-EE	VTIFVAGVLTASLTIWEEMG	103.3	No
CT BAX-QQ	VTIFVAGVLTASLTIWQQMG	11.8	No
CT BAX-RR	VTIFVAGVLTASLTIWRRMG	-75.1	Yes
CT BAX-LL	VTIFVAGVLTASLTIWLLMG	51.0	Yes

Those Lys 189/190 mutations (Table 6) which did not cause spontaneous apoptosis had unfavorable binding energies (positive ΔIE) within the hydrophobic pocket (negatively charged residues). While those Lys 189/190 mutations which did cause spontaneous apoptosis had favorable binding energies within the hydrophobic pocket (positively charged residues). The only exception was a leucine 189/190 mutant, which showed unfavorable energy of binding within the hydrophobic pocket (Table 6) but caused significant spontaneous apoptosis (Figure 5), likely due to the increase in the hydrophobic content achieved because of the replacement with leucines (Figure 7). The computational docking analysis suggested a mechanism that would explain the results of my mutagenesis studies (Table 4) and EGFP-BAX-CT expression studies (Figure 7). The binding of the α9 helix within the hydrophobic pocket seems to be modulated by lysine 189 and 190. *In the forward orientation, Lys 189 and 190 interact with the margin of the hydrophobic groove and are partially solvent exposed. In the reverse orientation, Lys 189 and 190 interact with multiple residues within the hydrophobic groove.* In this manner, Lys 189 and

190 may regulate the membrane-binding activity of BAX, disputing a sole role for the α9 helix as a transmembrane anchor.

2.3.4 Occupancy of the hydrophobic pocket by the α9 helix mediates the translocation of BAX to membranes.

We next wanted to determine whether the more energetically favorable binding of the α9 helix in the reverse orientation to the hydrophobic pocket caused the displacement of the α9 helix bound in forward orientation (as it occurs during self-association within BAX to retain the soluble, cytosolic form) in order to promote the mitochondrial association of the protein. To investigate this possibility, a peptide that incorporated last 20 residues of BAX (C-terminal α9 helix) was commercially synthesized. This peptide did not include the "hinge region" since it was not tethered to a protein (as in EGFP-CT-BAX) but was a free, soluble peptide. I isolated the cytosol containing endogenous BAX from BAX$^{+/+}$ HCT116 cells and added the BAX C-terminal peptide. After a short incubation, this mixture was added to the mitochondria enriched from BAX$^{-/-}$ HCT116 cells. Analysis of the samples by immunoblotting showed that under these cell-free conditions BAX integrated into mitochondrial membranes only when preincubated with the free BAX C-terminal peptide. In addition, I overexpressed BAX-ΔCT in BAX$^{-/-}$ HCT116 cells. Recall that this mutant does not induce spontaneous apoptosis (Figure 5) or translocates to the mitochondria (Table 3). When I incubated the cytosol of these cells with the BAX C-terminal peptide, BAX-ΔCT now associated strongly with the mitochondria despite the lack of its own α9 helix. These results implied that the truncated version of BAX had higher affinity toward to the BAX C-terminal peptide and that the BAX C-terminal peptide bound to the

hydrophobic pocket of BAX molecules in a manner that leads to the exposure of other membrane

binding domains (e.g. a transmembrane region formed by the α5, α6 helices as will be

discussed).

BAX peptide μM	-	25	-	-	25	-
BIM peptide, μM	-	-	25	-	-	25
Prohibitin						
BAX						

BAX BAX-ΔCT
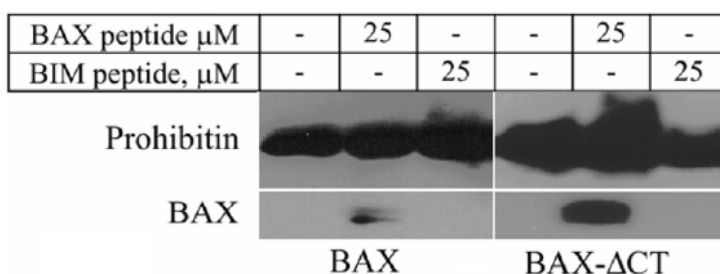
Figure 11: BAX C-terminal peptide, not BIM BH3 peptide, induces the translocation of
wild-type and C-terminally truncated BAX.
Cytosol (isolated in buffer at pH 7.0) was harvested from BAX^{-/-} HCT116 cells transfected with BAXΔCT.
The cytosol was incubated for 30 min with 25 μM of BAX α9 peptide (20-mer) or a BIM BH3 peptide (25-mer).
The cytosol was then incubated with mitochondria, isolated from BAX^{-/-} HCT116 cells (in buffer at pH 7.0) for 20
min, and mitochondria were washed several times with 1M NaCl to remove peripherally associated proteins.
Mitochondrial proteins content was analyzed by SDS-PAGE and immunoblotted with an anti-BAX antibody and an
anti-Prohibitin antibody as a mitochondrial loading control.

Having determined the effect of the BAX C-terminal peptide upon the membrane binding

of BAX, I next examined a BH3 peptide derived from BIM. Such BH3 peptides have been

routinely used in experiments with artificial lipid vesicles and isolated mitochondria to show the

effect of these peptides upon membrane insertion (Kuwana et al. 2005). Using the same

experiment as described earlier, I demonstrated that the BH3 peptide of BIM did not cause the

mitochondrial translocation of BAX or BAX-ΔCT (Figure 10). This observation coincided with

the results obtained by computational docking, which indicated that the BH3 peptide of BIM

does not interact with the hydrophobic pocket of BAX in an energetically favorable manner

(Table 6). Next, I wanted to test if the computational docking predictions also held true for the

BAX-LL mutant. This mutant is highly toxic, and it spontaneously translocated to the

mitochondrial membrane, causing apoptosis (Table 4, Figure 5).

BAX peptide μM	-	5	-	25	-
BAX-LL peptide, μM	-	-	5	-	25
Prohibitin					
BAX					

BAX-ΔCT
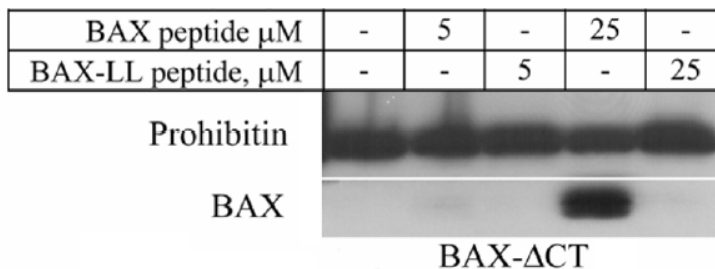
Figure 12: BAX-ΔCT does not insert into mitochondrial membrane upon addition of BAX-LL peptide.

Cytosol (isolated in buffer at pH 7.0) was harvested from BAX^{-/-} HCT116 cells transfected with BAX-ΔCT. The cytosol was incubated for 30 min with 25 μM of BAX α9 peptide (20-mer) or a BAX α9 peptide in which Lys189/190 were mutated to leucines (BAX-LL, 20-mer). The cytosol was then incubated with mitochondria, isolated from BAX^{-/-} HCT116 cells (in buffer at pH 7.0) for 20 min, and mitochondria were washed several times with 1M NaCl to remove peripherally associated proteins. Mitochondrial proteins content was analyzed by SDS-PAGE and immunoblotted with an anti-BAX antibody and an anti-Prohibitin antibody as a mitochondrial loading control.

The computational docking results implied that this mutant would not bind to the hydrophobic pocket due to unfavorable binding energy. I repeated the experiment described above, only this time I used a BAX C-terminal peptide in which lysine 189 and 190 were both replaced by leucines. Even in the case of the truncated version of BAX (BAX-ΔCT), the leucine mutant peptide did not cause the mitochondrial insertion of BAX-ΔCT. Hence, charged residues located at positions 189/190 are essential for the BAX C-terminal peptide to promote the mitochondrial integration of the protein. To explain our earlier results with BAX-LL (Figures 4, 5 and Table 4), recall that these involved expression of the full-length BAX mutant protein, enabling it to translocate to membranes because of the increased hydrophobicity of the C-terminus. But these results did not suggest that increased hydrophobicity was the physiological mechanism by which BAX normally moves to mitochondria.

44

Computational docking implied that binding of the α9 helix in reverse into the hydrophobic pocket occurs because of the presence of a positive charge at residue 69 (glutamate) within the BH3 domain, suggesting that Lys 189 and Glu 69 could interact. In addition, a residue in the hinge between the α2 and α3 helices, Asn73, could also interact with Lys 189. I performed computational site-directed mutagenesis of Glu 69 with different amino acids. A preliminary assumption would be that the mutation of Glu 69 into an amino acid with a positive charge (e.g., lysine) would "repel" the incoming α9 helix. Simply two positive positioned lysines back-to-back at the far end of its C-terminus could prevent any further conformational changes of BAX and thus inhibit its incorporation in the mitochondrial membrane and consequently apoptosis. However, computational mutagenesis suggested that the mutation of glutamate 69 to lysine or arginine would actually results in a stronger binding of the α9 helix within the hydrophobic pocket in the forward directional orientation as it occurs during the self-association (Table 5). This could prevent the release of the self-associated α9 helix to expose the hydrophobic groove. Mutation of Glu 69 to aspartate would make the BH3 domain more "BCL-2/BCL-XL like" (Table 7), resulting in the destabilization of the binding of α9 helix in the forward orientation and probably result in faster release of the self-associated α9 helix independent of apoptotic stimuli. Because of this information, I opted to mutate Glu69 in BAX-ΔCT and not in full-length BAX. The alternation of this conserved residue could affect the self-association of the C-terminus, creating a more toxic form of BAX or nonfunctional BAX. The results of the mutations Glu69Arg and Asn73Arg are presented in the Figure 13. The mitochondrial targeting mediated by BAX C-terminal peptide was impeded when Glu69 was exchanged for positively charged Arg. This impediment of the BAX peptide-induce

mitochondrial translocation was further increased upon double mutation, in which the conserved Glu69 was exchanged for positive Arg and Asn73 to Arg. These results significantly strengthen the conclusion that the reverse orientation of binding of α9 helix to the hydrophobic pocket regulates the mitochondrial integration of BAX and that this involves interactions between the charged residues, Lys 189/190, in the α9 helix, and Glu69/Asn73 within the hydrophobic pocket, confirming computational predictions.

Our computational and experimental results led us to the conclusion, that the C-terminus of BAX (encompassing α9 helix) might function as a membrane anchor, but more importantly, it is most essential for promoting the apoptosis by interacting in reverse orientation with the hydrophobic pocket of adjacent BAX molecule, forming dimers and inducing conformational changes that expose additional transmembrane domains, leading to mitochondrial integration.

Table 7: Summary of the computational mutations of conserved glutamate 69.
IE represents the difference in the binding energy between the α9 helix and the hydrophobic pocket after the mutation and before the mutation of Glu69. IE =E_2-E_1, IE – the interaction energy, E_1 – the energy before mutation, E_2 – the energy after mutation

| Mutation	Electrostatics (kcal/mol)	Hydrogen bond (kcal/mol)	Van der Waals (kcal/mol)	IE (kcal/mol)
E69A	388.5	-35.9	5.9	-95.2
E69R	*307.0*	*-37.1*	*17.3*	*-158.8*
E69N	379.2	-6.5	-0.4	-87.2
E69D	446.7	13.3	3.7	24.0
E69C	399.4	-35.8	6.8	-82.3
E69Q	364.4	-49.2	6.8	-143.5
E69G	391.7	-20.3	2.2	-80.9
E69H	390.7	-38.1	10.4	-57.1
E69I	386.4	-40.8	8.8	-103.0
E69L	389.3	-39.6	19.3	-78.5
E69K	307.5	-136.9	-2.3	-319.2
E69M	380.3	-41.2	6.5	116.5
E69F	396.6	-15.8	13.6	-47.3
E69P	655.9	-25.8	27.2	-16.8
E69S	401.1	-48.7	7.4	-99.8
E69T	399.5	-8.6	22.7	-12.2
E69W	*392.2*	*-2.4*	*14.8*	*-45.7*
E69Y	392.2	-2.4	14.8	-46.7
E69V	389.1	-35.8	7.8	-89.0
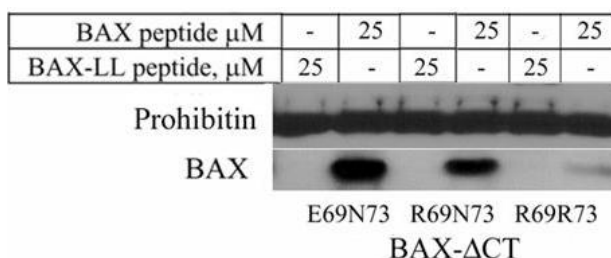
Figure 13: BAX-ΔCT R69R73 does not insert into mitochondrial membrane upon addition of BAX- peptide.
Cytosol (isolated in buffer at pH 7.0) was harvested from BAX^{-/-} HCT116 cells transfected with BAX-ΔCT E69N73, BAX-ΔCT R69N73 and BAX-ΔCT R69R73. The cytosol was incubated for 30 min with 25 μM of BAX α9 peptide (20-mer) or a mutant BAX α9 peptide in which Lys189/190 were mutated to leucines (BAX-LL, 20-mer). The cytosol was then incubated with mitochondria, isolated from BAX^{-/-} HCT116 cells (in buffer at pH 7.0) for 20 min, and mitochondria were washed several times with 1M NaCl to remove peripherally associated proteins. Mitochondrial proteins content was analyzed by SDS-PAGE and immunoblotted with an anti-BAX antibody and an anti-Prohibitin antibody as a mitochondrial loading control.

2.3.5 BAX responds on the changes in pH.

My results in the previous sections established that lysine 189 and 190 are important mediators of intracellular localization of BAX, promoting mitochondrial membrane binding. Based on these observations I wanted to study possible physiological processes that could be involved in facilitating the movement of BAX to membranes. Previous work by Khaled et al. demonstrated that changes in the intracellular pH are common features in the cytokine dependent cell lines (Khaled et al. 1999). Briefly, during death induced by cytokine withdrawal in an IL-7-dependent pro-T cell line (D1) or an IL-3-dependent pro-B cell line (FL5.12A), there was a transient rise of intracellular pH above 7.8 several hours after cytokine removal. This rise in pH coincided with the translocation of BAX to mitochondria.   Treatment with inhibitors of the sodium-hydrogen exchanger (NHE) or p38 MAP kinase inhibited alkalinization inhibited the alkalinization process, indicating that these proteins were involved in mediating the change in intracellular pH (Khaled et al. 1999). I observed that this same transient alkalinization also occurred in $BAX^{+/+}$ or $BAX^{-/-}$ HCT116 cells within 30 minutes to one hour of staurosporine treatment (Figure 13A). Intracellular pH changes were measured by detecting the pH-sensitive changes in EYFP fluorescence. Engineered mutants of EGFP that exhibit pH-dependent absorbance and fluorescence emission properties are commonly used for the measurement of pH changes within cells and cell organelles (Demaurex 2002;Llopis et al. 1998;Matsuyama et al. 2000;Wachter et al. 1998). Furthermore, Khaled et al. previously observed that BAX translocation to the mitochondria could be controlled by manipulating pH levels (Khaled et al. 1999). A similar experiment is shown in Figure 14B. The translocation of BAX was regulated by inducing or inhibiting alkalinization.   Intracellular pH in staurosporine-treated $BAX^{+/+}$

HCT116 cells was fixed at pH 7.2 with the ionophore, nigericin, in high K^+ buffers, preventing

the mitochondrial translocation of BAX. These results indicated that changes in cytosolic pH

could affect the movement of BAX to the mitochondria. I observed that the rise in pH could

induce the translocation of BAX and neutral pH could prevent it.
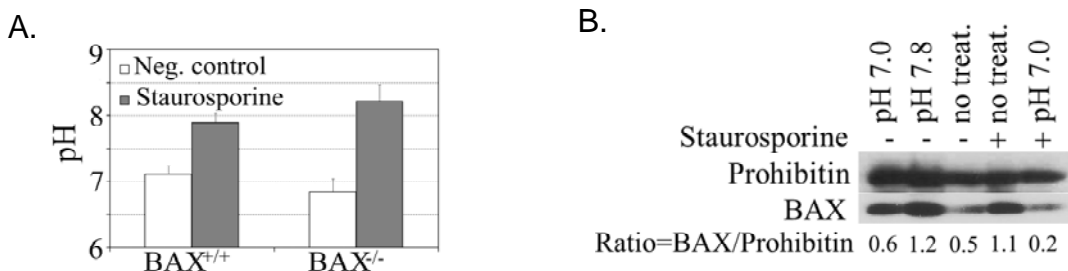
Figure 14: The intracellular distribution of BAX depends on pH.
(A) BAX-/- or BAX +/- HCT116 cells, expressing pH-sensitive deYFP vector, were treated for 1 hour with 1μM staurosporine and intracellular pH measures by detecting changes in the EYFP fluorsence by flow cytometry against a previously established calibration curve. Staurosporine treatment induced a transient alkalinization that is independent of the presence of BAX. (B) BAX+/+ HCT116 cells were cultured with or without 1μM staurosporine and permeabilized with 1 μM nigericin in a high K+ buffer at pH 7.2 or 7.8 for 30 min. Mitochondrial lysates were prepared and BAX and Prohibitin (mitochondrial loading control) assayed by immunoblotting. Alkaline pH induces the mitochondrial translocation of BAX, while neutral pH prevents it. The ratio of BAX to the control protein Prohibitin was determined by densitometer.

2.3.6 Alkalinization Alters Mitochondrial Physiology

BAX translocates to the mitochondrial membrane during apoptosis or upon exposure to

alkaline pH in healthy cells. The question is: how does alkaline pH mediate the translocation of

BAX to mitochondrial membranes? Alkalinization may disrupt weak hydrogen bond interaction

between the C-terminal lysine 189 in the α9 helix when it is bound in the forward orientation

within the hydrophobic pocket, leading to local conformational changes which destabilize the

helix, exposing the hydrophobic pocket. This could also be initiated by the presence of lipid

membranes (Yethon et al. 2003). My experiments performing targeted mutagenesis of lysine

189 and 190 could not mimic the subtle effects that intracellular alkaline pH could have on hydrogen bond interactions. However, the observation that an intact positive charge at position 189 was required for apoptotic activity (Table 5) indicated that a positive charge at the distal end of the C-terminus is required for the membrane association. Thus an alternative explanation is that alkalinization may have a more pronounced effect by disrupting membrane dynamics and facilitating the insertion of BAX. To explore this possibility, I designed experiments to determine whether the affinity of mitochondria toward BAX changed with pH.

Because previous experiments showed that intracellular pH rises within 30 minutes to 1 hour after the staurosporine treatment, I wanted to determine if EGFP-BAX-CT responded to mitochondrial changes caused differences in pH. A similar experiment was performed with apoptotic mitochondria and showed that apoptotic mitochondria attracted more BAX (Figure 7A). To examine pH-dependent effects, I used non-apoptotic mitochondria from $BAX^{-/-}$ HCT116 cells, which were exposed to conditions that equilibrated intracellular pH at 7.2 and 7.8. The equilibration of intracellular pH was achieved by exposing $BAX^{-/-}$ HCT116 cells to high K^+ buffer at pH 7.2 or 7.8 with the potassium ionophore, nigericin. The isolated mitochondria were then incubated with cytosol from $BAX^{+/+}$ HCT116 cells transfected with EGFP-BAX-CT. The results showed that EGFP-BAX-CT preferentially associated with mitochondria exposed to an alkaline environment (Figure 15).

To confirm this finding, I inspected the ability of EGFP-BAX-CT to associate with mitochondria in alkalinized cells in experiments similar to ones performed with staurosporine to induce apoptosis (Figure 8). As was shown in Figure 14A, alkalinization occurs as a result of staurosporine treatment. EGFP-BAX-CT was mostly diffused throughout the cytosol of $BAX^{+/+}$ HCT116 cells equilibrated at pH 7.2, while cells at pH 7.8, a pronounced punctuate pattern was

observed (Figure 15A). The staining overlaid with mitochondria marker HSP60, suggesting that the attachment of the last 25 amino acids of BAX C-terminus to EGFP conferred mitochondrial membrane binding upon intracellular alkalinization. In $BAX^{+/+}$ cells exposed to pH 7.2 as a control also indicated a small amount of mitochondrial overlay. This was expected because the C-terminus of BAX enabled some tagged EGFP to bind to mitochondria (Figure 16A). However, this process was significantly enhanced by alkalinization. These results, though preliminary, suggest that that during apoptosis, intracellular alkalinization is an important physiological event that alters the mitochondrial membrane and facilitates the movement of BAX. Whether this occurs by enabling the release of the self-associated α9 helix from the hydrophobic groove remains to be determined.

$BAX^{-/-}$ Mito	+	+
pH	7.2	7.8
EGFP-BAX-CT, $BAX^{+/+}$ Cyto	+	+
Prohibitin		
EGFP		
Ratio= EGFP/Prohibitin	0.3	1.6
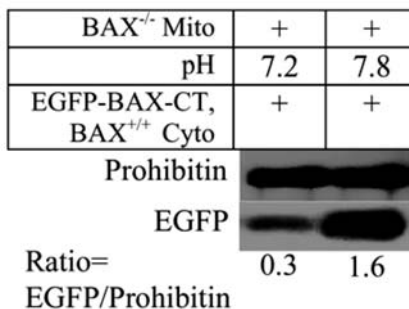
Figure 15: EGFP-BAX-CT preferentially associates with alkalinized mitochondria.
$BAX^{-/-}$ HCT116 cells were equilibrated to pH 7.2 or pH 7.8 by treatment with nigericin for 30 min and mitochondria harvested. Another set of $BAX^{+/+}$ HCT116 cells were transfected with EGFP-BAX-CT and, after 48 hours, cells were lysed and the cytosol harvested by high speed centrifugation. The EGFP-BAX-CT containing cytosol was incubated with neutral or alkaline mitochondria in a test tube for 20 min and than the mitochondria were washed several times with 1 M NaCl to remove peripherally associated proteins. Mitochondrial protein content was analyzed by SDS-PAGE and immunoblotted with an anti-EGFP antibody and an anti-Prohibitin antibody as a mitochondrial loading control.
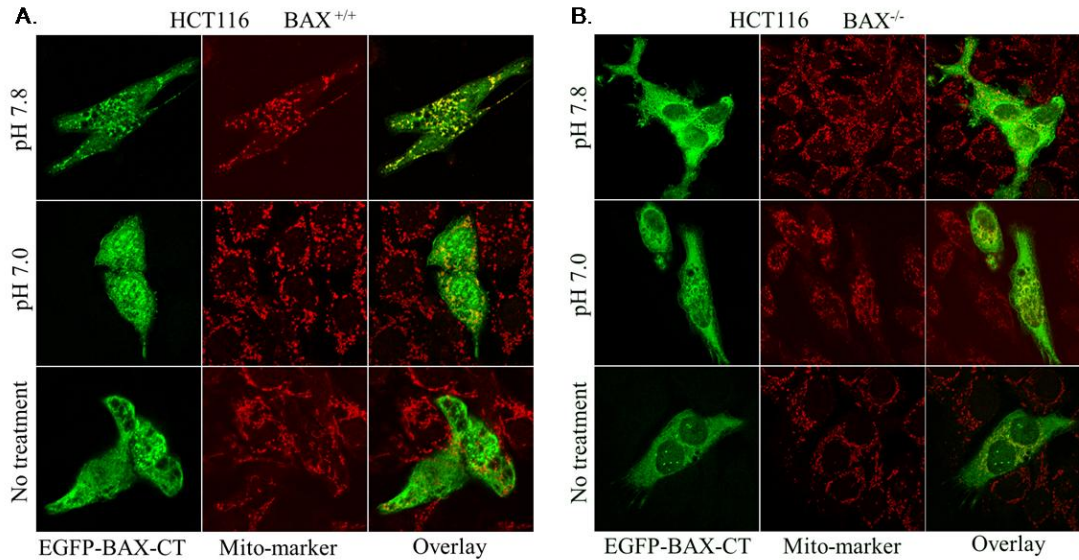
Figure 16: EGFP-BAX-CT displays different staining pattern in the presence than in the absence of endogenous BAX upon alkalinization.

BAX^{+/+} and BAX^{-/-} HCT116 cells were transfected with EGFP-BAX-CT and, after 48 hours, equilibrated to pH 7.2 or pH 7.8 by treatments with nigericin for 30 min. Cells were assessed for EGFP expression (green) by confocal microscopy. Mitochondria were identified by staining with anti-HSP60 antibody followed by a rhodamine-labeled (red) secondary antibody. A diffuse distribution of EGFP-BAX-CT was observed at pH 7.2, with increased aggregation EGFP-BAX-CT at pH 7.8 which substantially overlaid with mitochondria suggestion mitochondrial membrane binding. More EGFP-BAX-CT associated with alkalinized mitochondria in BAX^{+/+} cells than BAX^{-/-} cells.

2.4 Discussion

In response to an apoptotic signal, BAX translocates from the cytosol to the mitochondria. This translocation is thought to be connected with significant conformational changes and dimerization (Antonsson et al. 2000;Antonsson et al. 2001;Suzuki et al. 2000), but the mechanism is still poorly understood.

The C-terminal α9 helix of BAX is in literature mostly designated as putative transmembrane domain that anchors the protein in membranes (Annis et al. 2005;Antonsson et

al. 2000;Antonsson et al. 2001;del Mar et al. 2001) . In the absence of C-terminal α9 helix, BAX does not translocate to mitochondria (Annis et al. 2005;Antonsson et al. 2000;Antonsson et al. 2001). The α9 helix of cytosolic BAX is buried in the hydrophobic pocket as demonstrated by NMR (Suzuki et al. 2000). My computational mutations of the residues within α9 helix demonstrated that lysine 189/190 is an important residue that mediates the binding of the α9 helix with the hydrophobic pocket. Computational results confirmed the findings from mutagenesis and mitochondria translocation experiments, showing that the presence of two positive charges at the distal end of C-terminus is necessary for the appropriate subcellular distribution of BAX and its translocation to mitochondria during apoptosis. Additional computational docking results suggested that the C-terminal α9 helix of BAX is not necessarily a putative transmembrane domain as others have suggested. Computational docking predicted that the α9 helix would associate in a reversed direction within the hydrophobic pocket of adjacent BAX molecules that resulted in a more energetically favorable interaction. This is in comparison with the less energetically favorable forward orientation that occurs during self-association of the α9 helix within the hydrophobic pocket. The activation and predicted dimerization of BAX would thus be dependent on the occupancy of the hydrophobic pocket by the α9 helix and not by the BH3 domain as the prevailing dogma states. In support of this assumption, peptide mimics of the α9 helix caused the translocation of wild type BAX and, importantly, the translocation of C-terminally truncated BAX – BAX deficient of its putative transmembrane C-terminal domain. The same effect was not observed by adding the free BH3-only BIM peptide. The peptide-induced mitochondrial translocation of BAX C-terminal mutant was inhibited by the mutation of Glu69/Asn73, conserved residues in the hydrophobic pocket that are in binding proximity of

Lys189 when the α9 helix was bound in the reverse orientation. Mutations of residues in the C-terminus that abrogated the mitochondrial translocation of BAX further strengthened the hypothesis, which states that the C-terminal α9 helix is the crucial regulatory domain in BAX that is responsible for the translocation and induction of conformational changes, dimerization and/or mitochondrial membrane insertion.

The model proposed states that the C-terminal α9 helix of BAX is not putative transmembrane domain but is rather the mediator of membrane-binding conformational changes and dimer formation. In response to apoptotic stimuli, the forward-bound, self-associated α9 helix is released from the hydrophobic pocket. This enables the binding of the α9 helix from neighboring BAX molecules in the energetically more favorable reverse orientation within now exposed hydrophobic pocket. This results in the exposure of a novel transmembrane domain and the formation of dimers that permeabilize mitochondria and cause the release of the apoptogenic factors. The C-terminal α9 helix thus regulates the subcellular localization of BAX. My findings imply that the orientation and the type of peptide bound in the hydrophobic pocket of BAX direct the subcellular distribution of the protein, retaining the soluble form of BAX in the cytosol or inducing the lethal membrane-bound form.

The importance of the C-terminal helix in the regulation of BAX's apoptotic activity has parallels in the structural studies performed with the anti-apoptotic proteins, BCL-W and BCL-XL. Examination of the structure of BCL-W demonstrated that the C-terminal α9 helix of BCL-W is released during apoptosis by accommodating the BH3 domain of BIM (Denisov et al. 2003). The occupancy of the hydrophobic pocket is thought to regulate the pro-apoptotic activity of BCL-W (Hinds et al. 2003). Similarly, the intracellular distribution of BCL-XL is regulated

by the occupancy of the hydrophobic pocket by its C-terminal helix (Jeong et al. 2004). The exchange of the C-terminal helices between two adjacent BCL-XL molecules led to the formation of dimers and the cytosolic retention of BCL-XL, consequently modulating the anti-apoptotic activity of this protein.

The prevailing dogma states that the pro-apoptotic function of BAX is modulated though its interaction with BH3 domains of other BCL-2 family members (Borner 2003;Gross et al. 1999). This dogma was supported by studies which showed that BH3 peptides derived from BID or BIM triggered the pore forming abilities of BAX, leading to the permeabilization of lipid vesicles (Kuwana et al. 2005). Also, detergent treatment induced BAX-BIM association (Marani et al. 2002). Yet oligomeric complexes of BAX with BH3-only proteins have not been described (Wei et al. 2000), nor has BAX bound to BH3-only proteins been isolated from the apoptotic cells (Zhu et al. 2004). BAX was also able to translocate to the mitochondria of the cells deficient in the BH3-only proteins BIM and BAD, demonstrating that the redistribution of BAX occurs independently of these BH3-only protein (Ekert et al. 2006).

My study suggests that the activation of BAX is not necessarily mediated by interactions with BH3-only proteins, but rather by occupancy of the hydrophobic pocket with the C-terminal α9 helix – a process that can suppress or facilitate the exposure of additional membrane-binding domains. This finding resolves the controversy as to which domain(s) of BAX is required for membrane integration. The C-terminal with its α9 helix is necessary for BAX to associate with the mitochondria, since the deletion of this domain retained BAX in the cytosol. However, in the absence of a *directly* attached α9 helix, but in the presence of free peptide mimics of the α9 helix, I demonstrated that BAX-ΔCT could associate with mitochondria. Thus BAX could

contain other transmembrane domains. These domains may not be exposed unless the hydrophobic pocket is occupied by the α9 helix in the more favorable reverse orientation. The most likely candidates for the membrane-binding domain exposed by occupancy of the hydrophobic pocket are helices α5 and α6, which others have shown can form a hairpin (Garcia-Saez et al. 2005;Garcia-Saez et al. 2006). The peptides derived from the sequences of helices α5 and α6 could induce large-sized pores in artificial lipid vesicles (Garcia-Saez et al. 2006). A study of the topology of BAX demonstrated that helices α5 and α6, as well α9, insert into the mitochondrial membrane in a stepwise manner (Annis et al. 2005;Suzuki et al. 2000). The question remains how the binding of helix α9 in reverse orientation to the hydrophobic pocket promotes the exposure of helices α5 and α6. One could hypothesize that a release of self-associates helix α9 and docking of adjacent helix α9 induces enough stress to cause the deformation of the hydrophobic pocket and exposure of additional membrane spanning domains. NMR structure of BAX indicates that α5 is a central helix of soluble BAX, buried deeply within the protein (Suzuki et al. 2000). The exposure of this helix would thus require significant structural rearrangement.

The findings presented further suggested that Lys189/190 and conserved residues within BH3 domain, Glu69 and Asn73, were critical for the regulation of the subcellular localization of BAX. A basic amino acid was required at the position 189/190, at the distal end of helix α9, in order for BAX to associate with mitochondrial membranes and induce apoptosis. Attaching last 25 amino acids of BAX, which encompasses helix α9, to EGFP conferred mitochondrial targeting to a cytosolic protein, mimicking the behavior of BAX during apoptosis. Studies of the C-terminal domains of other BCL-2 family members demonstrated that a transmembrane domain

flanked by basic amino acids could function as a targeting signal for mitochondria (Antonsson et al. 2000), if this domain was long enough . I observed that the replacement of Lys189/190 with leucines generated very potent mutant that spontaneously interacted with mitochondria and induced apoptosis. These results indicated that by increasing the hydrophobicity of the helix α9, I could turn the helix α9 into a potent transmembrane domain. However, these findings also support the alternative function of helix α9 of BAX, where conserved acidic residue Glu69 plays important role. Computational docking suggested that Glu69 and Asn73 at the wedge of the hydrophobic pocket could interact with Lys189/190 in the helix α9, creating hydrogen bond interactions that anchor the helix α9 within the pocket. Results from our mutagenesis studies indicated that replacement with uncharged or acidic residues abolished this interaction, while replacement by basic residues sustained it. Likewise, I showed experimentally that replacement of Glu69 and Asn73 with basic residue abolished the capacity of free BAX C-terminal peptide to induce conformational changes needed for the membrane association of BAX, lacking its helix α9.

My results demonstrated that the C-terminal helix α9 is necessary for the regulation of the activity of BAX, not as membrane anchor, but rather by binding in reverse orientation to a hydrophobic pocket of adjacent BAX molecule to form membrane-binding dimers. Hence the self-association or binding of the helix α9 in the forward orientation is functionally different from binding in reverse; the former sequesters BAX in the cytosol while the latter promotes membrane binding and dimerization.

I speculate that the initial exposure of the hydrophobic pocket could occur during the transient alkalinization that occurs at the early stage of apoptosis. Khaled et al. previously

reported that apoptotic stimuli induced a transient alkalization of the cytosol in the cytokine dependent cell lines and caused the translocation of BAX (Khaled et al. 1999). Others have also shown that the translocation of BAX to the mitochondrial membrane is associated with cytosolic alkalization (Belaud-Rotureau et al. 2000;Kim et al. 2003;Lagadic-Gossmann et al. 2004;Tafani et al. 2002). I observed that HCT116 cells also alkalinized upon staurosporine treatment independent of the presence of BAX. By the manipulation of intracellular pH, I demonstrated that alkalinization could promote the mitochondrial localization of BAX as well as that of EGFP-BAX-CT. Maintaining a neutral pH in apoptotic cells prevented the movement of BAX to the mitochondria (Khaled et al. 1999).

Despite the fact that some physiological data support the motion that BAX is pH-responsive, there is no structural data available that demonstrates that significant conformation changes are triggered by an alkaline pH. An NMR study of BAX did not indicate any conformational changes between pH 6-8 (Suzuki et al. 2000). However, epitope-specific antibodies, which recognize buried epitopes only in the apoptotic cells, did recognize these same epitopes in cells with an alkaline cytosol (Cartron et al. 2004;Khaled et al. 1999). Alkaline conditions also caused increased sensitivity of BAX to protease digestion, suggesting that pH induces a more relaxed conformation and exposes hidden epitopes (Khaled et al. 1999). The important difference between later experiments and the NMR study is that the NMR information was acquired in the absence of lipids. Other results were derived in the presence of both BAX and mitochondria or lipid vesicles. This is an important piece of information because it is well documented that BAX undergoes conformational changes in the presence of lipids (Annis et al. 2005;Antonsson et al. 2000;Yethon et al. 2003). In support, I was able to demonstrate that the affinity of mitochondria for BAX changes upon alkalinization. Alkalinized mitochondria were

able to bind BAX as well EGFP-BAX-CT from the cytosol of non-apoptotic cells in a manner similar to that observed with apoptotic mitochondria. Intracellular pH, through its effects upon mitochondria, can be an important mediator of the conformational changes of BAX in the presence of lipids.

The influence of an alkaline pH on the mitochondrial membrane physiology remains speculative. A piece of supplementary data not shown was that the affinity of a free C-terminal BAX peptide to lipid vesicles increased with an alkaline pH, suggesting that lipids could be the pH sensitive component (Tschammer et al. 2007b). pH gradients across a lipid bilayer can affect the diffusion and distribution of individual lipids, sequester some lipids, and induce increased lipid bilayer assimetry (Hope, Cullis 1987). Increasing evidence exists that BAX can induce the rate of lipid diffusion across a bilayer and move the cardiolipin from the inner to the outer mitochondrial membrane (Epand et al. 2003). Recently, BAX was also found to mediate the fusion and fission of mitochondria (Karbowski et al. 2006;Karbowski et al. 2002).

My experiments demonstrated that the C-terminal α9 helix is necessary for the pro-apoptotic function of BAX, not as a membrane anchor, but as the domain which interacts with the hydrophobic groove of adjacent BAX molecules. This interaction can occur in two different orientations: (1) binding in the reverse directional orientation within the hydrophobic pocket of adjacent molecules, and (2) binding in the forward that occurs during self-association. The forward orientation inhibits the pro-apoptotic function of BAX by sequestering the protein in the cytosol, while the reverse orientation initiates conformational changes, mitochondrial membrane integration and subsequent apoptosis. This process seems to be enhanced by transient alkalinization of the cytosol, which increases the affinity of the mitochondrial membrane for BAX.

3 HELICAL INTERACTION ENERGY DISTRIBUTION IN TRANSITIONAL PROTEINS

3.1 Introduction

New developments in biotechnology resulted in an information explosion derived from numerous eukaryotic sequencing projects and the subsequent gains in post-genomic research, including novel structural studies and new discoveries in protein–protein interactions. One tool that plays an important role in predicting structural and functional properties of the increasing number of newly identified and characterized proteins is molecular modeling (Schlick 2006). Because modeling predictions are based on existing data, they must be refined whenever new and more detailed structures or relationships are available. Homology modeling (Rodriguez et al. 1998), threading techniques (Lu et al. 2003;McGuffin, Jones 2003), hidden Markov models (HMMs) (Eddy 1996;Karplus et al. 1998) and secondary structure prediction using neural networks (Lin et al. 2005) are only few examples of the structure-function predictions. A drawback with these systems is that most models consider proteins as static objects, despite the obvious fact that many proteins (e.g. signaling proteins) are highly dynamic and undergo significant conformational changes upon execution of their function. The structural dynamics of proteins can be thus depicted as a continuum with proteins characterized by very rigid structures at one end and highly dynamic proteins at the other end. The dynamic nature of proteins structure is important for many biological processes ranging from signaling events to enzymatic activity. Changes in the protein structure can occur locally, for example within the active site, where minute changes in the side chain position become complementary to the transition state (Keough et al. 2005), or globally, where unstructured proteins adopt a well-defined three

dimensional (3D) structure upon the formation of a protein complex (Demarest et al. 2002). Although critically necessary to elucidate protein function, a method for probing the ability of the protein to undergo transitions is not currently available.

The motivation for undergoing a computational examination of protein transitioning originated in my studies on the pro-apoptotic protein BAX (Chapter 2), which is known to undergo significant structural transitions in response to apoptotic stimuli. Analyzing the interaction energy forces at the interface of the helices within the all α-helical bundle of BAX, I sought to develop a measurable parameter that would describe the ability of such proteins to undergo transitions.

Using the 3D structure of BAX, I initially studied the helix interaction energies of the carboxyl-terminal region of BAX (known as the α9 helix) in an attempt to understand the role of this C-terminal region in the regulation of subcellular distribution of BAX and its apoptotic activity. We determined that the interaction of the α9 helix with an internal hydrophobic pocket could explain how BAX transitions from a soluble cytosolic protein to a membrane associated protein that appears to undergo dimerization as described in the findings presented in Chapter 2 (Tschammer et al. 2007b). However, the initiating events that enable interactions between the α9 helix and the hydrophobic pocket of BAX remained indefinable. In an attempt to elucidate the initiating events, we measured the helical interaction energies of all helices within the BAX to better understand the static packing arrangement of the helices across the entire 3D structure. Our results indicated that BAX displays significant variation in helical interaction energies (IEs) that may explain its ability to undergo structural transitions during apoptotic signaling events.

To test the hypothesis that a significant variation in helical interaction energies correlates with biological function, we randomly selected coordinate sets for proteins from the Protein Data

61

Bank (PDB) that were structurally similar to BAX to serve as controls in our calculations. These proteins were meant to weigh the level of variation of helical interaction energies within protein structures in the all alpha class. Our results demonstrated that a significant number of proteins involved in DNA binding, viral invasion, transcription regulation, and other cellular signaling events also have a significant variation in helical packing energies, while those proteins that are known not to be transitional do not share this property. These results indicate that a measure of propensity for transition may be afforded by analysis of the static structures based on the statistical distribution of helical interaction energies within a well defined 3D structure.

3.2 Material and Methods

3.2.1 Structures

The 3D structures of proteins were obtained from the RCSB Protein Data Bank (http://www.rcsb.org/pdb). The ensemble of coordinates representing the NMR structure of BAX (PDB ID: 1F16) (Suzuki et al. 2000) was grouped into a conformationally related subfamily using the NMRClust program (Kelley et al. 1996b). The most populated group was used for one set of calculations (based on the statistics of the program) and a statistically distinct group was used for another set of similar calculations. Based on the statistical deviation of helix packing energies between these groups, our control proteins were primarily chosen from structures determined by x-ray crystallography. When NMR structures were used, the most populated group (as determined by the NMRClust program) was used for the analysis. The selection criteria for our randomly chose set were as follows: a) under 300 amino acids in length, b) belonging to the all alpha class, c) containing similar number of helices (ranging from 3-16),

d) no co-factors such as ions or disulfides that might stabilize the proteins´s 3D fold, e) contained a single peptide chain, and f) determined by x-ray crystallography. These selection criteria were input into the PBD´s database search engine and resulted in 153 proteins that contained regions of beta-strands, disulfides, and stabilizing co-factors. Additionally, some coordinate sets were missing regions of the structure that prohibited their analysis. These were rejected from our test set and the resulting number of structures available for analysis was found to be 74. Our results as based on 53 (72%) of these available structures.

The graphic images were produced by PyMol v0.99 (DeLano Scientific, California).

3.2.2 Energy Calculations

In determining the level of calculations to perform a number of factors was considered. Although QM/MM methods have become popular due to their accuracy they are computationally expensive and are primarily used for active site analysis and reaction profiling (Cheng et al. 2005). Methods capable of simulating proteins side-chain flexibility using Monte Carlo minimization are also available (Meiler, Baker 2006) and molecular dynamics simulations have been shown to be reliable in evaluating protein-peptide interaction energies in dynamic systems (Bartels et al. 2005). However, this study deals with the direct measurements of static structures, achieving results on 53 independent coordinate sets that had an average of 8 helices each, which required calculations for the helix alone, the helix in complex with the protein, and the protein in the absence of the helix. Based on this criteria, the use of molecular mechanics (MM3) force files with directional hydrogen bonding potentials was chosen to evaluate the static interaction energy (Lii, Allinger 1998b). These values are presented as relative interaction energies due to the

understanding that calculations completed with different force files potential will result in different energy values. Calculations were performed *in vacuo*, disregarding an explicit water/membrane environment, which would result in substantially lower energy values due to entropic factors. Only the forces at the interface of each helix were considered in the calculations.

The calculations were performed using the BioMed Cache 6.1.10 program (Fujitsu America, Inc., Sunnyvale, CA) as the graphical user interface. MM3 force field calculations were performed using parameters as described in the literature. Separate energy calculations were performed for: (1) the entire protein (no helices removed), (2) the entire protein, but the investigated helix removed, and (3) the helix only. The energy of each molecule was calculated until convergence (energy minimization) was reached. Energy terms included Van der Waals, electrostatics and hydrogen bonding interactions. All atoms in the structure were locked, except protons were allowed to move during the calculations. This was done to ensure that no changes in the atomic positions (other than protons) or bond characteristics would occur during the calculations relative to the original coordinates in PDB file. A conjugated gradient was used to locate the energy minimum. Van der Waals interactions between atoms separated by more than 9.0 Å were excluded. The interaction energy (IE) was estimated through separate determinations of the energy of the complex ($E_{complex}$), complex without the investigated helix ($E_{complex\ w/o\ helix-n}$) and helix alone ($E_{helix-n}$), and by taking the difference between these terms ($IE=E_{complex}-(E_{complex\ w/o\ helix-n}+E_{helix-n})$). This difference in the relative energies terms provides the interaction energy ($IE_{helix-n}$) at the interface of each helix being investigated with respect to the entire structure using the MM3 potential.

3.2.3 Protons and Ionization States

Because the proton positions are not available in structures determined by x-ray crystallography, I edited each structure individually to ensure the proper location of hydrogen atoms. This required adjustment in ionization states for individual amino acids in each protein. The following guidelines were used for the setting of the ionizations states of the individual amino acids: (1) cysteines were protonated, (2) glutamate and aspartate side chains had the oxygen farthest from the backbone of the helix investigated assigned a formal negative (-1) charge, (3) lysine side chains had a formal positive (+1) charge on the terminal amine, (4) arginine side chains were assigned a positive (+1) charge on the nitrogen farthest from the backbone of the helix investigated, (5) the new N-termini (generated upon removal of the helix of the protein) for the both the protein (without the helix) and the helix itself was given a formal positive (+1) charge, and (6) the new C-termini was changed to an aldehyde functional group (no charge). For structures determined by NMR, the experimentally determined proton positions were used for energy minimization.

3.2.4 Statistical Analysis

The $IE_{helix-n}$ values for each helix were tabulated as shown in Table 7. The average (AVE) helical interaction energy values are shown and provide a measure of the overall stability of the helices within the protein structure. The standard deviation (SD) values are calculated to measure the statistical variation of all helices within the entire 3D structure. Because different molecular mechanics potential functions yield variable interactions energies based on the force fields

employed, I propose that the absolute value of the variation over the average (|SD/AVE|) provides a general statistical representation of the distribution of helical interaction energies that should be independent of the force field potential used for the calculations. Based on the distribution of |SD/AVE| values observed, it is apparent that proteins that are known to undergo transitions based on experimental evidence have larger |SD/AVE| value compared to those that do not undergo transitions. Although no formal cut-off value can be assigned based on the proteins used in this study, it is clear that the |SD/AVE| values can serve as a measure of the propensity for transition, which is similar to the Random Coil Index (RCI) (Berjanskii, Wishart 2005) and probabilistic scores (based on pair-wise energy profiles) (Dosztanyi et al. 2005) used to assign random coil regions and intrinsically unstructured proteins.

3.3. Results and Discussion

3.3.1. Variation of helical IE values within each structure

In an attempt to understand the transitional mechanism of BAX, I hypothesized that the propensity for transition has to be evident from the packing of the helices in 3D structure. The calculation of the interaction energy values at the interface (IE) for all the helices in the protein showed that the IE values were widely dispersed. Lacking a basis for comparison, I could not estimate whether this was common for most proteins or specific for BAX. In order to make an impartial evaluation, I randomly selected the proteins that were in the same structure class and had similar molecular properties. This randomly selected set provides values for 72% of the available proteins within the PDB that were comparable to BAX. After the analysis of IE values

and ranking of the proteins by |SD/AVE| values, the correlation between the dispersion of IE values and the property of the protein to undergo transition emerged. Proteins that undergo structural transitions have more dispersed IE values compared to the proteins which do not undergo structural transitions (Table 8, Figure 17).

The interaction energy values for all of the helices of protein phosphatase 5 (1A17) (Das et al. 1998), phospholipase-C (1AH7)(Hough et al. 1989), and retinoblastoma tumor suppressor (1AD6) (Kim, Cho 1997) were negative, representing favorable interaction energies. The average and standard deviation of the interaction energies established that the stability is evenly distributed across the entire structure. The ratio |SD/AVE| for all three of these proteins was found to be 0.65, 0.73, and 0.94 for protein phosphatase 5, phospholipase-C and retinoblastoma tumor suppressor, respectively (Table 9). In contrast, the IE values of BAX (1F16) (Tschammer et al. 2007a) are not evenly distributed across the 3D structure. The core helix of BAX helix 5 had an IE of -405,14 kcal/mol. The average IE value was -40.57 kcal/mol, indicating a favorable overall stability, but the ratio |SD/AVE| was 3.90, indicative of widely dispersed IE. These values demonstrated an uneven distribution of helical interaction forces within the stable 3D structure of BAX, which may elucidate its ability to undergo structural transitions related to its apoptotic activity.
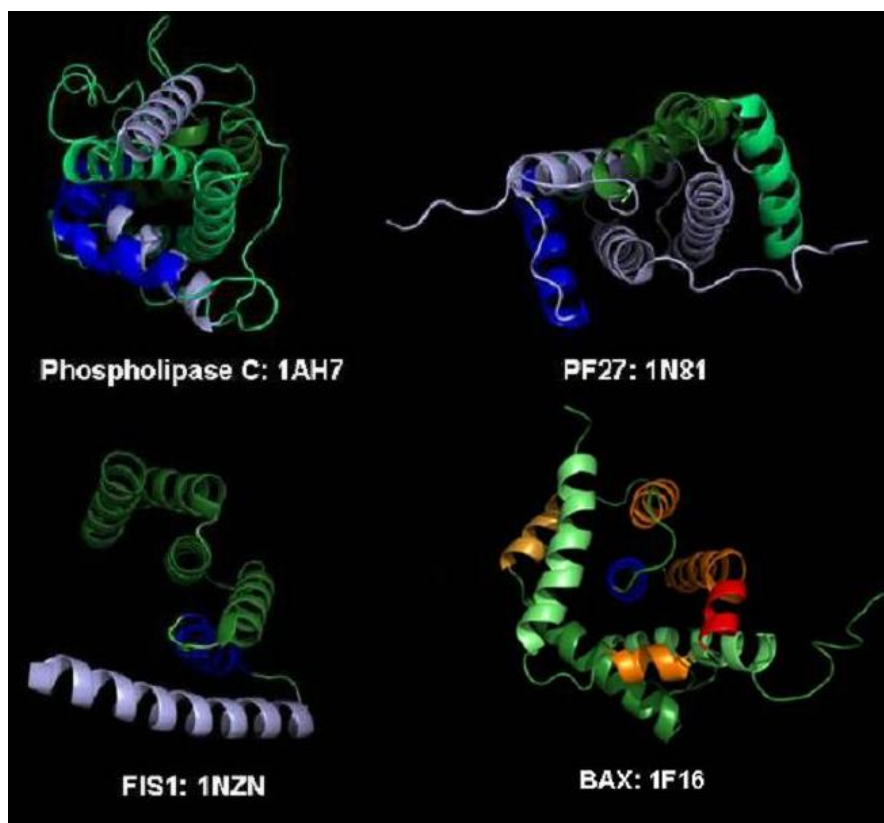
Figure 17: Non-transitional proteins have less variability in helical stability.

Ribbon diagrams of non-transitional proteins and BAX as the representative of transitional proteins. The color codes correspond to: blue – the most stable, green – stable, yellow – less stable, orange – unstable, red – very unstable. As shown in the figure, the topology of the helices within the structures is similar, but the distribution energies are not. Notably BAX has more unstable helices the structure compared to phospholipase C, PF27 and FIS1.

No correlation appeared to exist between the helix length (and the corresponding number of amino acids capable of interactions) and the interaction energy values (Table 9). As shown in Equation IE=$E_{complex}$-($E_{complex\ w/o\ helix-n}$ +$E_{helix-n}$), the numbers of atoms are the same (or corrected for) in comparing the bound helix compared to the helix alone and the protein without the helix present. My interpretation of these results is that the IE values represent a relative measure of the static interaction forces based on: a) the type of interactions (van der Waals, electrostatics, and hydrogen bonding) and b) the number of interactions that each helix is capable of making

within the protein structure. This indicates that the forces involved in stabilizing a 3D structure, or permitting a structural transition, are inherent to the forces involved at the interface and cannot be understood based on visual inspection of such properties as helix length and/or the number of helices within the structure.

Table 8: Statistical data on helix stabilities.
The entire set of randomly selected proteins (including BAX) used in this study sorted by |SD/AVE| in descending order. At the top of the list are proteins involved in apoptosis, cellular signaling, DNA binding and cellular toxicity which are known to undergo 3D structural transitions and at the bottom of the table are enzymes and other proteins that are not involved in such transitions. The BAX protein (model 20) shows the highest |SD/AVE| ratio and represents the statistical variation of helical interactions within the deposited NMR ensemble, while BAX (model 1) was from the most populated cluster of the ensemble (see METHODS). Proteins that are involved in membrane interactions are shown in *italic* and show moderate |SD/AVE| values that may reflect their mechanism of transition being controlled through significant hydrophobic contact during their structural transitions.

Protein Name	PDB ID	Physiological Role	AVE Helix Energy (kcal/mol)	SD Helix Energy (kcal/mol)	/SD/AVE/
BAX (NMR), model 20	1F16	Pro-apoptotic protein	-11.90	142.46	11.97
APAF-1 CARD	1C15	Apoptotic protease	10.98	102.81	9.44
Colicin E7 immunity protein	1CEI	Antibacterial protein	23.22	117.81	5.07
BAX (NMR), model 1	1F16	Pro-apoptotic protein	-40.57	158.09	3.90
DNA-binding domain of TRP repressor	3WRP	DNA binding protein	16.94	64.58	3.81
APAF-1 CARD domain	2YGS	Apoptotic protease	-28.23	74.90	2.65
Methyl-accepting chemotaxis protein II	1JMW	Signaling protein	-39.55	102.22	2.58
RGS-like domain from PDZ-Rho$_{GEF}$	1HTJ	Signaling protein	-51.29	127.58	2.49
RAD51	1B22	DNA binding protein	42.59	93.64	2.20
Engrailed homeodomain	1ENH	DNA binding protein	-75.30	161.05	2.14
Diphtheria toxin	*1DDT*	*Toxin*	*-84.65*	*166.43*	*1.97*
Actin-crosslinking domain	1AOA	Actin binding protein	-166.30	303.62	1.83
Phosphorelay signaling protein YPD1P	1C03	Signaling protein	-176.01	300.13	1.71
FAT domain of focal adhesion kinase	1K40	Transferase	-72.72	106.52	1.46
Tetracyclin repressor	1BJZ	Transcription regulation	-182.71	250.54	1.37
STAT-4 N-domain	1BGF	Transcription factor	-131.19	178.34	1.36
B562RIL, a redesigned four helix bundle	1M6T	Electron transfer	-124.17	163.59	1.32
Amphiphysin BAR domain	1URU	Endocytosis	-285.88	357.75	1.25
SMAC/DIABLO	1FEW	Apoptotic protein	213.09	262.03	1.23
YGFB	1IZM	Unknown function	414.86	491.59	1.18

Protein Name	PDB ID	Physiological Role	AVE Helix Energy (kcal/mol)	SD Helix Energy (kcal/mol)	/SD/AVE/
KAIA homolog	1V2Z	Circadian clock protein	-110.49	129.89	1.19
Apolipoprotein	*1AEP*	*Lipoprotein*	*-43.50*	*48.11*	*1.11*
Pore-formin domain of Colicin A	*1COL*	*Antibacterial protein*	*-126.01*	*139.42*	*1.11*
EPHB2	1F0M	Signaling protein	-91.86	97.07	1.06
Cyochrome C6	1CTJ	Electron transfer	109.89	112.02	1.02
RGS9 RGS domain	1FQI	Signaling protein	-176.33	174.23	0.99
Retinoblastma tumor suppressor	1AD6	Transcription regulation	-99.60	94.10	0.94
Myoglobin	1DWR	Oxygen transport	-150.58	139.98	0.93
Phosphate uptake regulator	1XWM	Unknown function	255.99	235.99	0.92
P115Rho$_{GEF}$ domain	1IAP	Signaling protein	-99.49	89.93	0.90
Histon HMFB from *M. fervidus*	1B6W	DNA binding protein	-128.78	114.10	0.89
Bovine cyclin A3	1VIN	Binding protein	-118.63	102.56	0.86
Ribosomal protein S15	1A32	Ribosomal protein	-227.578	191.697	0.84
Glutathione S-transferase	13GS	Catalysis of the conjugation of reduced glutathione	-213.85	178.00	0.83
Calponin homology domain from beta-spectrin	1BKR	Acting binding	-90.43	75.14	0.83
CALM-N N-terminal domain of clathrin	1HF8	Clathrin	-179.169	148.504	0.83
Endonuclease V	2END	Endonuclease	-266.10	210.00	0.79
Epsin N-terminal homology domain	1EYH	Cell lycle	130.13	100.41	0.77
Middle domain of EIF4GII	1HU3	Translation	-129.78	98.94	0.76
Phospholipase C	1AH7	Hydrolysis of phosphatidylcholine	-329.98	241.89	0.73
Interferon beta	1WU3	Cytokine	-124.56	123.89	0.71
Apolipoprotein E4	*1GS9*	*Lipoprotein*	*-200.75*	*143.94*	*0.72*
N-terminal fragment of NS1 protein	1AIL	RNA binding protein	-175.46	123.89	0.71
Hyperplastic disc protein	1I2T	Ligase	-133.62	90.02	0.67
Plasmodium falciparum gamete gene PF27	1N81	Unknown function	-228.95	148.64	0.65
Serine/threonine protein phosphatase 5	1A17	Skeletal muscle calcium binding protein	-227.24	147.27	0.65
BH domain from Graf	1F7C	Signaling protein	-101.77	64.31	0.63

Protein Name	PDB ID	Physiological Role	AVE Helix Energy (kcal/mol)	SD Helix Energy (kcal/mol)	|SD/AVE|
Human mitochondrial fission protein Fis-1	1NZN	Mitochondrial fission	-82.50	49.90	0.60
CRO protein	2CRO	Gene regulation	-132.33	71.99	0.54
Troponin	1A2X	Calcium-dependent regulator of muscle contraction	753.19	382.73	0.51
EPH receptor	1B0X	Transferase	-63.62	26.83	0.42
Sperm lysin	2LIS	Cell adhesion	-152.24	49.88	0.33

Table 9: Helical stability of three non-transitional proteins
Legend: AVE – average, SD – standard deviation

Helix Number	PP-5 Sequence	(1A17)) Helix Energy (kcal/mol)	Phospholipase C Sequence	(1AH7) Helix Energy (kcal/mol)	Retinoblastoma tumor suppressor Sequence	(1AD6) Helix Energy (kcal/mol)
1	22-40	-44.34	14-27	-147.49	384-390	-53.46
2	44-57	-71.50	35-52	-308.70	398-405	-59.11
3	62-74	-234.89	86-103	-221.21	412-434	-227.56
4	78-91	-149.35	106-122	-862.70	439-468	-281.28
5	96-108	-432.87	126-130	-254.66	474-477	-66.62
6	112-125	-369.85	141-148	-209.35	480-497	-83.43
7	130-164	-287.92	173-186	-463.81	516-520	-57.20
8			193-204	-41.08	525-538	-88.23
9			206-242	-460.79	544-559	20.46
AVE		-227.24		-329.98		-99.60
SD		147.27		241.89		94.10
|SD/AVE|		0.65		0.73		0.94

The distribution of IE values for the helices with the respect to the 3D structures of phospholipase-C, PF27 (Sharma et al. 2003), FIS1 (Karbowski et al. 2002), and BAX are graphically depicted in Figure 17. These structures demonstrate that IE of the helices varies independently of the topological arrangement within the 3D structure. This is a further indication that the number and types of interactions each helix is capable of making is the most important

factor in understanding the variation in IE. The green and blue colors represent regions of high stability (negative IE) and regions of orange and red colors represent regions of relative instability (positive IE). The C-terminal helix in BAX (α9, shown in light green) had a favorable IE (-76.71 kcal/mol) and is located next to two helices (#3 and #4) that are relatively unstable. Helix α9 seems to be critical for membrane localization though its interactions with the hydrophobic pocket (Tschammer et al. 2007b) and most likely plays a role in stabilizing or destabilizing other helices, enabling a structural transition to occur that facilitates mitochondrial membrane insertion or association with another BCL-2 related protein.

The complete set of randomly selected proteins (including BAX) used in this study is provided in Table 8. The BAX protein (model 20) is at the top of the list with a |SD/AVE| ratio of 11.97. This ratio was the highest in our study and appears to represent the statistical variation of helical interactions within the deposited NMR ensemble for the BAX protein. BAX (model 1) was from the most populated cluster of the ensemble (see Methods) and this structure had a value of 3.91. The value 11.97 was obtained with one set of coordinates that was part of the deposited ensemble, but did not cluster with model 1. For this reason, I used NMR structures sparingly in the study and when they were used, only the most populated cluster from the ensemble was used for IE calculations.

As shown in Table 8, the variation in IE values for proteins varies significantly even though these proteins are in the all alpha-class and have similar molecular properties. This distribution provided a basis for comparing the helical IE values within BAX, as well as other proteins in the all alpha-class. Because BAX is known to undergo a structural transition, and is near the top of the list, I interpret these results as a mean of measuring the propensity for the transition for proteins with stable 3D structures. However, as described later in the report, the

|SD/AVE| values may differ depending on the mechanism of transition and the involvement of other proteins, or membranes, which are involved in initiating the transition for each protein.

3.3.2. Statistical variation within the randomly selected set

Following the analysis of BAX and comparing the IE values of this protein to those that were randomly selected, I came to the understanding that the statistical variation in IE values may represent a measure of propensity for transition within proteins that have a defined 3D fold. When considering a protein that has a biological role in signaling, and undergoes a structural transition, the forces required to induce this transition (which may be afforded though binding another biological molecule or a membrane surface) must be stronger than those forces stabilizing the structure prior the transition. For this reason, I suggest that the statistical variation of IE represents regions within 3D structures that make these processes energetically favorable and yet allow a global stability within protein structure that enables the molecule to remain in a native state prior to transition.

The average value, standard deviation and absolute ratio |SD/AVE| for all the randomly selected proteins (Table 8) showed trends that appear to correlate with each protein´s physiological role. While BAX is near the top of the list, APAF-1 CARD (Caspase Recruitment Domain) protein also shows a high |SD/AVE| ratio. This protein consists of six tightly packed amphipatic alpha-helices. Its cellular role involves the activation of Caspase-9 though the homophilic CARD/CARD interaction. The |SD/AVE| ratio for this protein is 9.44. The structure of the protein has been determined in the unbound state (Zhou et al. 1999) and in complex with pro-domain of pro-caspase 9 (Qin et al. 1999) and shows a significant structural mobility upon

binding. Almost all the helices within the protein undergo some level of structural rearrangement upon ligand binding as demonstrated by the Cα trace (Figure 18). The protein undergoes the smallest conformational rearrangement in the segment of the helix α5 (amino acids 50-64). This segment had an IE of -190 kcal/mol and was the most stable helix in the structure. The segments represented by helix α3 (amino acids 23-31) and helix α4 (amino acids 37-46) had the most unfavorable IE (97.45 and 115.24 kcal/mol, respectively) and showed the most rearrangement upon ligand binding. These two helices are in direct contact with the CARD domain of procaspase-9, which may indicate that regions of relatively unfavorable IE find stability in binding their particular biological targets.

In addition to the analysis of the NMR structure of the APAF-1 CARD domain, a second structure of APAF-1 CARD domain obtained by X-ray crystallography was analyzed. The |SD/AVE| ratio for this from was 2.65. Although this ratio was considerably smaller that that of the NMR structure (9.44), it positioned this protein among the proteins that undergo structural transitions. Additionally, the helical segments of the two proteins (as given in the PBD header) are slightly different. The most stable segments (amino acids 50-64 (NMR) and 48-61 (X-ray) were consistent in both structures and the regions described above (that interact with the CARD domain of procaspase-9) appeared to be less stable due to higher IE. These results suggested that the IE values are not dependent on the method used for structure determination, the resolution, or the helical limits, because the most stable segments were similar in both structures.

The TRP repressor (3WRP) has a |SD/AVE| ratio of 3.81. The structure of this protein was determined by x-ray crystallography with a resolution of 1.8 Å (Orth et al. 1999). The authors of this study found different forms of the proteins fro different crystallization conditions and described this flexibility based on the TRP repressor´s ability to search for and adhere to its

different operator sites (Orth et al. 1999). Therefore, this protein has an intrinsic flexibility that had been well characterized and the |SD/AVE| ratio correlates well with these observations. The TRP repressor undergoes rearrangement upon DNA binding, which can be observed in the C_α trace of the bound (green) and unbound forms (red).The most stable region of this protein is found to be the region around 79-91 (helix 5) with an IE value of -90,48 kcal/mol. This helix is one of the helices that make direct contact with the DNA. The regions from 46-63 (helix 3) and 68-74 (helix 4) have IE of 61.24 and 88.27 kcal/mol, respectively, and are the least stable helices within the structure. These two helices are on the outside of the structure and may find stability by interacting with helix 5 (Figure 18). These two helices (along with helix 5) are found at the interface of the bound DNA with helix 5 bound in the major groove (Figure 18). This helix also overlays best in the C_α trace between the bound and unbound form, which may be interpreted as a further measure of the stability of this helix. Unlike the APAF-1 CARD protein, the TRP repressor uses regions of relative stable and unstable regions for DNA binding, but the regions with higher IE appear to be involved in both cases.
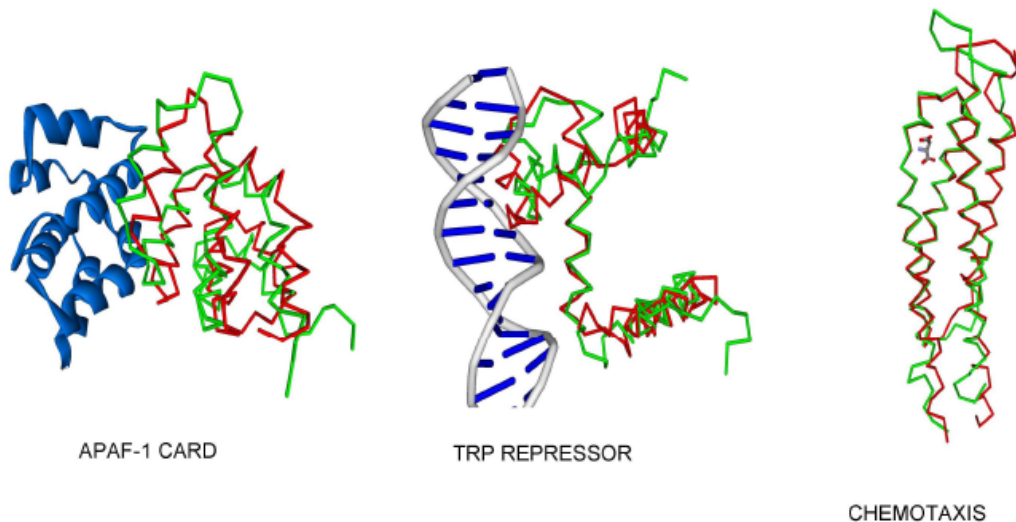
Figure 18: Structural changes for transitional proteins based on Cα overlays.

The green Cα trace represents the protein in the bound form and red traces represent the unbound form of the proteins. For the Trp-repressor, APAF-1 CARD, and chemotaxis proteins, their respective ligands (DNA, caspase-CARD domain, and aspartate) are shown to identify the regions of where interactions occur.

The ligand binding domain of the methyl-accepting chemotaxis protein II is also represented in the PDB in a bound and unbound form. The unbound form (Figure 18) shown in red is slightly different than the protein with bound aspartate (green). Although the changes in the helical positions (based on C_α traces) are not as dramatic as those found for the TRP repressor and the APAF-1 CARD domain, there are noticeable differences that can be observed in comparing the two forms. The region with most favorable IE within this protein are 87-110 (-140.08 kcal/mol) and 116-144 (-191.91 kcal/mol). These two helices are on the opposite face of the aspartate binding region. Amino acids 40-75 (41.89 kcal/mol), 145-152 (22.59 kcal/mol), and 153-175 (50.15 kcal/mol) which represent helices #2, 5 and 6 are on the interface where the aspartate molecule is bound and have the highest IE values. This protein has a |SD/AVE| ratio of 2.58, which is lower than the previously described proteins, but higher than most of the proteins

from the randomly selected list. This lower |SD/AVE| ratio appears to correlate with the smaller changes in the C_α traces compared to the previously described proteins. The APAF-1 CARD proteins shows the most dramatic change (Figure 17) and has the highest |SD/AVE| ratio (9.44), whereas the TRP repressor (3.81) and chemotaxis protein (2.58) have decreasing values that correlate with more fine changes in the bound and unbound forms as seen though the C_α traces.

As demonstrated by the data above, the larger |SD/AVE| ratio correlates with those proteins that are involved in protein-DNA and protein-protein interactions. Additionally, the statistical variation in |SD/AVE| ratio as a measure of propensity for transition is supported by changes in the structures when comparing the bound and unbound forms. However, as discussed below, the degree of statistical variation within a single structure may vary depending on the types of forces involved in initiating the transition.

3.3.3. IE distribution and protein function

A clear division of statistical variation within IE values would be a convenient mean of predicting propensity of the protein to undergo transition. The comparison of |SD/AVE| ratio of the proteins with the published experimental description of the proteins tendency to undergo transition yielded |SD/AVE| ratio distribution between 1.11 and 9.44, and for the proteins which do not undergo transition between 0.33 and 1.06. The approximate cut-off value could be around 1.1 with transitional proteins having |SD/AVE| ratio larger than 1.1 and non-transitional proteins ratio smaller than 1.1.

Proteins with the |SD/AVE| ratio of 1.1 or above have more unfavorable average IE values compared to those having |SD/AVE| ratio less than 1.1 (Table 8), although no correlation to function can be made based on average IE values alone. The non-transitional proteins show a slight correlation that provides a slope of -1.08 in the plot of standard deviation *vs* average IE value, while the transitional proteins appear to be more scattered and have varied average IE values, as well as higher standard deviations (Figure 19). For this reason, the |SD/AVE| ratio appears to be a better measure if propensity for transition than the average energy values alone. As shown in Figure 19, it appears to be a region where the correlation (based on non-transitional proteins) is lost. For example, proteins such as actin binding protein (1AOA, -166.30 kcal/mol), the phosphorelay signal transduction protein YPD1P (1C03, -176.01 kcal/mol), tetracycline repressor (1BJZ, -182.71 kcal/mol), and the BAR membrane curvature sensor protein (1URU, -285.88 kcal/mol) have all favorable IE, but have |SD/AVE| ratio above 1.2. This demonstrates a wider statistical distribution of helical interaction forces across the entire protein structure in a structure that appears to be very stable. Based on their functional classification, these types of proteins would be expected to have some flexibility within their 3D structures, but this is not apparent based on the average IE values and their stable 3D structures.
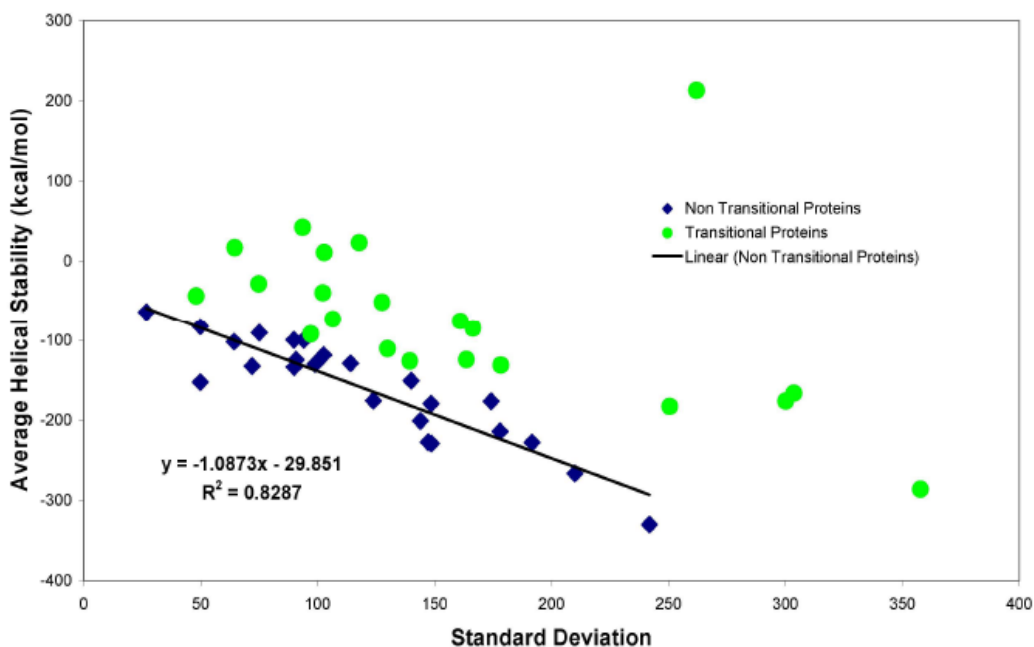
Figure 19: Graphical representation of the average IE values and standard deviations. The proteins that are known not to be involved in 3D structural transitions are shown with black diamonds and those known (or described in the literature) to undergo structural rearrangement are shown with green circles. While the non-transitional proteins have some correlation between their average IE values and deviations, the transitional proteins appear to be more scattered and have no correlation.

3.3.4. Proteins with unknown function

Many proteins in the current databases are annotated as "unknown function", because their structures were obtained prior to any biological studies being performed. While 3D structures are of values in many areas of research, the lack of biological information makes the choice of further characterization of these proteins difficult. Based on the results presented in this study, it may be possible to classify these unknown proteins based on their |SD/AVE| ratio to determine which proteins may be of interest because of their potential role in signaling and/or transition.

Three of the proteins in our randomly selected set are annotated as unknown function in the PDB. The first protein is a gametocyte protein essential for sexual development in *Plasmodium falciparum* (1N81) known as Pfg27. This proteins has been described as a RNA and SH3 domain binding protein capable of binding two SH3 domains simultaneously (Sharma et al. 2003). It has an average IE value of -228.95 kcal/mol and |SD/AVE| ratio of 0.65. Based on this structure and the described biological roles, this protein does not appear to be involved in 3D structural transitions related to its function.

The second protein of unknown function is annotated as a phosphate uptake regulator (1XWM) homologous with PhoU proteins that function as negative uptake regulators in *E.coli*. This protein has an average IE value of 255.99 kcal/mol with a |SD/AVE| ratio of 0.92. Based on these values, we might predict that the deviation within helical energy distribution for this protein may indicate a transition in the 3D structure being involved in the mechanism of controlling phosphate uptake, but biological data to support this is still pending. It has been shown that the PstSCAB transporter and PhoU may be regulated by a mechanism that may involve their interactions with each other as well as inorganic phosphate and the sensor proteins, PhoR (Steed, Wanner 1993). PhoU might use its lowered helical interaction energy to promote interactions with the transporter protein, other proteins in the phosphate uptake pathway, or possibly membrane lipids. However, this would require solid experimental evidence to support this mechanism, and based on the distribution of |SD/AVE| ratio in this study, this protein is clearly intermediate and one cannot determine the propensity of transition for this protein based on these values.

The third protein is HI0817 *Haemophilus influenzae* (1IZM) (Galkin et al. 2004). It has an average IE value of 414.86 kcal7mol with a |SD/AVE| ratio of 1.18. This protein is classified as a conserved hypothetical protein and homologous to a 24-member family that includes a brad number of human (12), bovine, insect and plant pathogens. Although the biological mechanism for this conserved pathogen is not known, I would predict based on these values (and those from other proteins in my test) that its biological mechanism is related in some way to the statistical distribution of interaction energies across the 3D structure. This would fit in the grouping of proteins with relatively high IE values and |SD/AVE| ratio such as those found for the 1AEP and 1COL structures that are involved in membrane associated protein transitions. However, experimental evidence is needed to support this proposed transition.

While further studies need to be completed to determine the biological function of unknown proteins before they are classified as transitional, I feel the statistical methods outlined in this report may provide insight for future studies on those proteins that are conserved across a number of species, yet have no clear biological role.

3.4. Conclusions

Biological signaling is often controlled by the binding events that are transient in nature involving random coil, molten globules, and proteins with stable 3D folds. While the classification and mechanisms of signaling for random coil and molten globule proteins can be understood based on their ability to undergo structural transitions, no measure of propensity for transition is available for stable proteins that are involved in signaling. With the idea of a "continuum of protein structure" being available to describe proteins involved in cellular

signaling comes the understanding that these types of transitions (and the mechanism by which they occur) should have some measurable parameter, even for proteins with stable 3D folds. For intrinsically disordered and random coil proteins, these parameters are found in the pair-wise indexing and random coil index, respectively. Although these parameters do not have statistical cut-off values that clearly classify proteins as completely random or completely unstructured, they do provide an indication of the degree of randomness and/or potential lack of 3D structure. Analysis of helical interaction energies, as described in this study, appears to provide a similar type of measurable parameter, with the difference being that static energies are used and the proteins that are being compared need to be in the same structural class and lack factors that stabilize the 3D fold.

Analysis of stable 3D structures using the method outlined in this study will be valuable in guiding experimental efforts to understand the transitional mechanisms of proteins. With an increasing number of proteins being discovered by structural genomics efforts (Stevens et al. 2001) (without experimental data such as 1IZM and 1XWM), parameters such as those examined in this study may provide information about those areas of least stability within a protein's 3D structure and identify the region(s) of contact for the biological molecules that are involved in the interaction(s). Although this study only addresses helical interaction energies in small proteins of the all alpha-class, it is possible to assume that other types of proteins, of varying structural complexity, will also have stability trends within their 3D structures that will assist in understanding their ability to control biological signaling events and as well as elucidate the mechanisms of transitioning that regulate their function.

4 ANALYSIS OF HELICAL INTERACTION ENERGIES TO PROBE THE STABILITY AND MECHANISMS OF STRUCTURAL TRANSITIONS IN THE BCL-2 PROTEIN FAMILY

4.1 Introduction

Three-dimensional (3D) protein transitions are important for a number of biological processes and signaling events ranging from host invasion to DNA binding and apoptosis (Hinds et al. 2003;Patel et al. 1990). These structural transitions may occur locally at flexible loop regions, or involve complex folding events like e.g. diphtheria toxin (Dumont, Richards 1988). Because these structural transitions are governed by the stability of a protein's localized domains and/or secondary structural elements, the analysis of the thermodynamic stability of these individual elements should provide insight into the mechanisms of the transitions. Such measurements should provide a mean of computational classification of those proteins that have a propensity for transition, as well as identify domains within the protein that are likely to be involved in the initiation of 3D structural changes. My previous study (Tschammer et al. 2007a) showed that this type of the parameter exists. Analysis of the static interaction energy (IE) for the helices within all-alpha class proteins indicated that the transitional proteins have wider distribution of IE, resulting in higher |SD/AVE| ratio compared to non-transitional proteins. BAX appeared to be the protein with one of the broadest IE distribution among the evaluated proteins.

BAX is a member of BCl-2 family of apoptotic regulators (Borner 2003;Cory et al. 2003). The BCL-2 family can be divided in two functional categories – those that mediate survival, such as BCL-XL and BCL-2, and those that mediate death, such as BAX, BID or BIM – based on the presence of one or more BCL-2 homology (BH) domains. Structural studies of

BCL-2 family members demonstrated that the members retain a similar folded structure despite their significant difference in the amino acid sequence (Petros et al. 2004). NMR or X-ray structures are available for six family members (BCL-XL (Muchmore et al. 1996), BCL-2 (Petros et al. 2001), KSHV-BCL-2 (Huang et al. 2002), BCL-W (Denisov et al. 2003), BAX (Suzuki et al. 2000) and BID (Chou et al. 1999;McDonnell et al. 1999). The solution structure of BAX showed that BAX is folded in a similar manner than other BCL-2 family members. Helices #2, #3, #4 and #5 form a hydrophobic pocket which is occupied by the C-terminal α9 helix (Suzuki et al. 2000). BCL-XL structure contains similar pocket which is occupied by the bound BH3 peptide mimics (Petros et al. 2004;Petros et al. 2000).

Based on my previous work in which I analyzed the mechanism of BAX activation (Tschammer et al. 2007b) and the variations in the helical stability in static structures of proteins (Tschammer et al. 2007a), I focused on the analysis of 3D structures of BCL-2 family members deposited in the Protein Data Bank (PBD)(Berman et al. 2000). The reason for studying the BCL-2 family proteins originates in their ability to undergo structural transitions during execution of their biological function (Borner 2003;Schlesinger et al. 1997;Zhang et al. 2004). Little is known how these structural transitions occur. Using methods of computational modeling, I analyzed different BCL-2 family members and found that these proteins have, similar as BAX, broad distribution of IE, although the force of interaction between various helices within each structure varied. This variations in the IE within each structure and the changes that occur upon peptide binding led to conclusion that these differences could reflect different transitional mechanisms and/or functions for members of the BCL-2 protein family.

4.2 Materials and Methods

4.2.1 Structures

The 3D structures of proteins were from the RCSB Protein Data Bank (http://www.rcsb.org/pdb). The representatives of BCL-2 family of proteins are: BAX (PDB ID 1F16) (Suzuki et al. 2000), BCL-W (1MK3) (Denisov et al. 2003), BCL-2, isoform 1 (1G5M) (Petros et al. 2001), BCL-XL X-ray structure (1R2D) (Muchmore et al. 1996), BCL-XL NMR structure (1MAZ) (Muchmore et al. 1996), human BID (2BID) (Chou et al. 1999), mouse BID(1DDB) (McDonnell et al. 1999) and CED9 (1OHU) (Woo et al. 2003). BHRF1 protein from Epstein-Barr Virus (EBV) (1Q59) (Huang et al. 2003) and BCL-2 homolog from Kaposi´s sarcoma-associated herpes virus (1K3K) (Huang et al. 2002) are the representatives of viral BCL-2 homologs. Coordinates of BCL-XL in complex with the peptides were as follows: BAD (1G5J) (Petros et al. 2000), BAK (1BXL) (Sattler et al. 1997) and BIM (1PQ1) (Liu et al. 2003). The coordinates for CED) in complex with the EGL-1 peptide were PDB ID code 1TY4 (Yan et al. 2004).

The graphic images were produced by PyMol v0.99 (DeLano Scientific, California).

4.2.2 Energy Calculations

In determining the level of calculations to perform a number of factors was considered. Although QM/MM methods have become popular due to their accuracy they are computationally expensive and are primarily used for active site analysis and reaction profiling (Cheng et al. 2005). Methods capable of simulating proteins side-chain flexibility using Monte Carlo

minimization are also available (Meiler, Baker 2006) and molecular dynamics simulations have been shown to be reliable in evaluating protein-peptide interaction energies in dynamic systems (Bartels et al. 2005). However, this study deals with the direct measurements of static structures, achieving results on 53 independent coordinate sets that had an average of 8 helices each, which required calculations for the helix alone, the helix in complex with the protein, and the protein in the absence of the helix. Based on this criteria, the use of molecular mechanics (MM3) force files with directional hydrogen bonding potentials was chosen to evaluate the static interaction energy (Lii, Allinger 1998b). These values are presented as relative interaction energies due to the understanding that calculations completed with different force files potential will result in different energy values. Calculations were performed *in vacuo*, disregarding an explicit water/membrane environment, which would result in substantially lower energy values due to entropic factors. Only the forces at the interface of each helix were considered in the calculations.

The calculations were performed using the BioMed Cache 6.1.10 program (Fujitsu America, Inc., Sunnyvale, CA) as the graphical user interface. MM3 force field calculations were performed using parameters as described in the literature. Separate energy calculations were performed for: (1) the entire protein (no helices removed), (2) the entire protein, but the investigated helix removed, and (3) the helix only. The energy of each molecule was calculated until convergence (energy minimization) was reached. Energy terms included Van der Waals, electrostatics and hydrogen bonding interactions. All atoms in the structure were locked, except protons were allowed to move during the calculations. This was done to ensure that no changes in the atomic positions (other than protons) or bond characteristics would occur during the calculations relative to the original coordinates in PDB file. A conjugated gradient was used to

locate the energy minimum. Van der Waals interactions between atoms separated by more than 9.0 Å were excluded. The interaction energy (IE) was estimated through separate determinations of the energy of the complex ($E_{complex}$), complex without the investigated helix ($E_{complex\ w/o\ helix-n}$) and helix alone ($E_{helix-n}$), and by taking the difference between these terms ($IE = E_{complex} - (E_{complex\ w/o\ helix-n} + E_{helix-n})$). This difference in the relative energies terms provides the interaction energy ($IE_{helix-n}$) at the interface of each helix being investigated with respect to the entire structure using the MM3 potential.

4.2.3 Protons and Ionization States

Because the proton positions are not available in structures determined by x-ray crystallography, I edited each structure individually to ensure the proper location of hydrogen atoms. This required adjustment in ionization states for individual amino acids in each protein. The following guidelines were used for the setting of the ionizations states of the individual amino acids: (1) cysteines were protonated, (2) glutamate and aspartate side chains had the oxygen farthest from the backbone of the helix investigated assigned a formal negative (-1) charge, (3) lysine side chains had a formal positive (+1) charge on the terminal amine, (4) arginine side chains were assigned a positive (+1) charge on the nitrogen farthest from the backbone of the helix investigated, (5) the new N-termini (generated upon removal of the helix of the protein) for the both the protein (without the helix) and the helix itself was given a formal positive (+1) charge, and (6) the new C-temini was changed to an aldehyde functional group (no charge). For structures determined by NMR, the experimentally determined proton positions were used for energy minimization.

4.2.4 Statistical Analysis

The $IE_{helix-n}$ values for each helix were tabulated as shown in Table 8. The average (AVE) helical interaction energy values are shown and provide a measure of the overall stability of the helices within the protein structure. The standard deviation (SD) values were calculated to measure the statistical variation of all helices within the entire 3D structure. The structures were ranked in terms of their |SD/AVE| ratio to provide a measure of the propensity for transition as described in Chapter 2. As shown in Table 8, significant changes in the |SD/AVE| ratios were found when BCL-2 family members are in the complex with various peptides.

4.2.5 Changes in the secondary structure

The CED9 and BCL-XL proteins in this study were analyzed with and without small peptides bound. In some cases changes in the secondary structure have occurred upon peptide binding. In order to represent the interaction energies accurately, two sets of calculations were completed. The first set used the same atoms for bound and free forms, irrespective of any change in the secondary structure. The helical boundaries for CED9 and BCL-XL proteins (without any bound peptide) were determined by the information in the PDB header. These same atoms were then used for calculations for the bound form even if these atoms were no longer in a helical conformation. This allowed direct comparison of the energies for the free and bound forms using the same number of atoms in each calculation. Any change in the number (or type) of atoms used would change the relative interaction energy values, and make the two sets of values difficult to compare accurately. This set of values was designated as "Set 1". In a second

set of calculations, the interaction energies for the CED9 and BCL-XL complexes were calculated with the helix boundaries taken directly from the PDB header. This allowed comparison of any changes in helical interaction energy (IE) relative to the resulting changes in the secondary structure. The data comprised "Set 2" in the tables. Specifically, the following changes in the two structures occurred upon peptide binding (based on PDB secondary structure annotation): (1) BCL-XL residues 103-106 are in a helix in the bound form, but form a beta-turn in the free form, and (2) CED9 residues 141-144 form a beta-turn in the absence of the peptide, but form a helix in the presence of the peptide.

4.3 Results

My previous analysis of the helical interaction energies (IEs) in the all alpha-class proteins that are known to undergo structural transitions demonstrated a broad distribution of IEs within the structure (Tschammer et al. 2007a). Within the randomly chosen set of proteins which were used in the mentioned study, BAX was estimated to have one of the broadest IE distributions of all the proteins analyzed. Based on this observation and the fact that BCL-2 family proteins employ structural transitions to regulate apoptotic events, I analyzed the IEs for those BCL-2 family proteins for which structural information is available in free and bound form with the intention to detect the changes in the IE distribution which occur upon ligand binding.

4.3.1 Helix Stability and Packing of BCL-2 Family Members

The common feature of the known structures of the BCL-2 family members is so-called core region of the protein represented by at least one helix. The other helices are arranged around this core set and form α-helical bundle (Figure 20). Despite the overall similarity in the fold of BCL-2 family members (Petros et al. 2004), I detected significant differences in the helix stability and helical packing among different members (Table 10).

All of the BCL-2 family proteins analyzed in this study had |SD/AVE|values that were greater than 1.1 when the protein was not in the complex with a peptide/ligand (Table 10). The |SD/AVE| ratios ranged form 1.17 for BHRF1 (a viral BCL-2 homolog) to as high as 11.97 for BAX (Model 20). The BAX structure with the |SD/AVE| ratio of 11.97 was derived from the least clustered coordinate set obtained from the NMR ensemble of structures deposited in the PBD (see 4.2 Material and Methods). The most populated cluster resulted in a |SD/AVE| value of 3.9 (BAX, Model 1). Even with this variability in |SD/AVE| ratio for different members of NMR ensemble, BAX showed a significant distribution of IE within its 3D structure. The BCL-XL structure (as determined by NMR) had a |SD/AVE| ratio of 4.38 and the structure determine by X-ray crystallography 4.24. These results demonstrated that structures determined by NMR (using the most populated group of structures within the ensemble) and X-ray crystallography have comparable |SD/AVE| ratio and that the IEs are not dependent on the method of the structure determination.
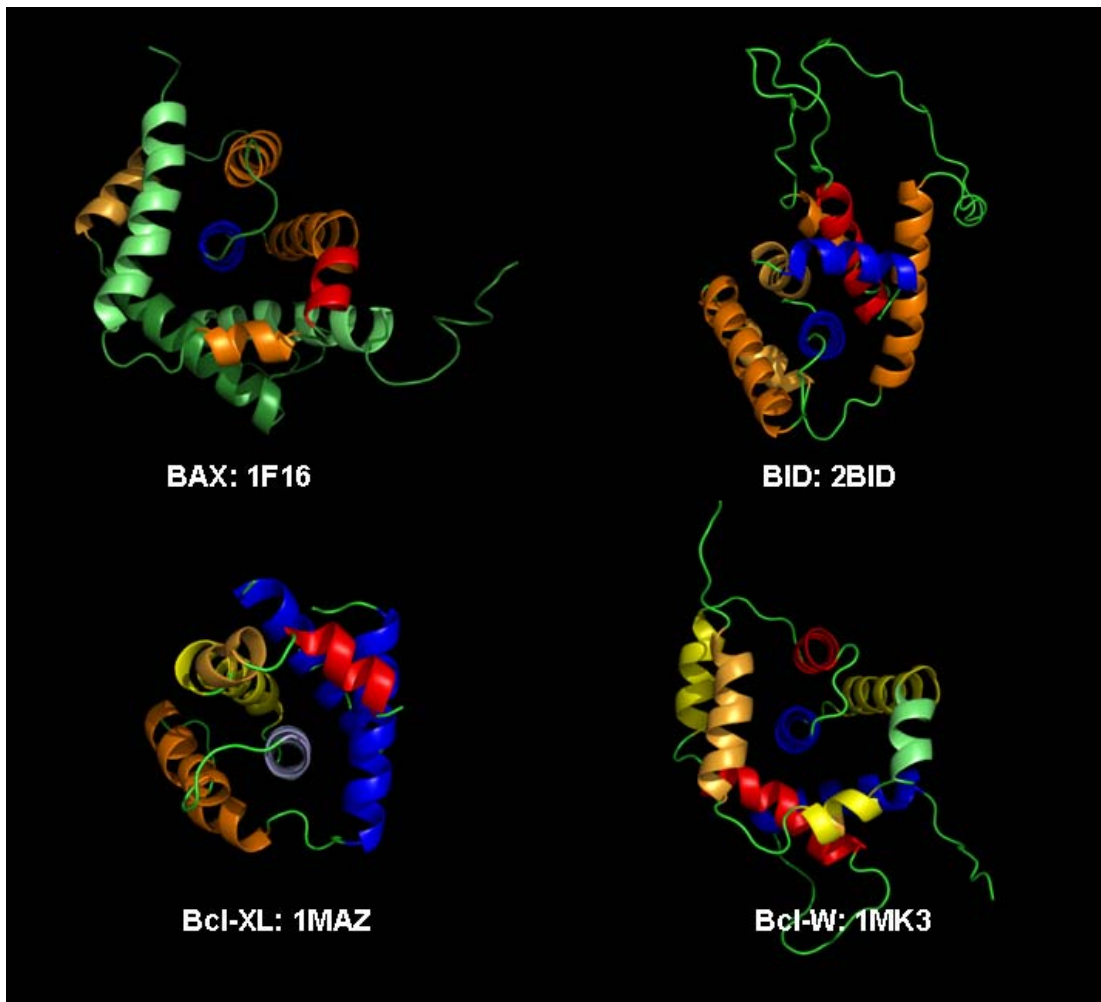
Figure 20: BCL-2 family proteins have stabile central helix.

Ribbon diagrams of protein belonging to the BCL-2 family color coded by stability. The color codes correspond to: blue – the most stable, green – stable, yellow – less stable, orange – unstable, red – very unstable. As shown in the figure, the topology of the helices within the structures is similar, but the distribution energies are not. Notably BAX has more unstable helices on the outer edge of the structure compared to BCL-W, BCL-XL, and BID. I interpret these variations as potential differences in the mechanism of transition for each structure, which is governed by each protein's distribution of helical interaction energy values and overall stability.

The differences observed in the helical stability and packing of BCL-2 family proteins mirrors their unique pro- or anti-apoptotic function. The BCL-2 family members with multiple conserved BH domains, BAX, BCL-W, BCL-XL, BCL-2 and BCL-2 homolog of Kaposi's sarcoma virus, demonstrated distinctive pattern in the helical stability and the helical packing

with only one core helix relatively stable (α5, the energy value in the range from -400 in BAX to 10 kcal/mol in BCL-2; Table 11). CED9 has two relatively stable helices (α5, α6) that form a similar stable core (-280 to 380 kcal/mol). The central stable core helix (or helices in CED9) is the main component of the hydrophobic groove, which is an essential structural and functional element among anti- and pro-apoptotic BCL-2 family members (Petros et al. 2004).

Table 10: Statistical data on helix stabilities for BCL-2 family proteins.

Standard deviation (SD), average (AVE), and |SD/AVE| values for the BCL-2 protein family investigated in this study. Values are sorted and ranked by |SD/AVE| value. Protein Data Bank (PDB) codes for the atomic coordinates are also included. This distribution represents the variation in helical interaction energies for the various BCL-2 protein family members and demonstrates their broad distribution of energies that may enable structural transitions to occur.

Protein Name	PDB ID	Physiological Role	AVE Helix Energy (kcal/mol)	SD Helix Energy (kcal/mol)	|SD/AVE|
BAX, Model 20	1F16	Apoptosis regulator	-11.90	142.46	12.0
BCL-XL	1MAZ	Apoptosis regulator	-46.75	204.69	4.4
BCL-XL	1R2D	Apoptosis regulator	-61.26	259.98	4.2
BAX, Model 1	1F16	Apoptosis regulator	-40.57	158.09	3.9
Human BID, Model 15	2BID	Apoptosis regulator	66.83	238.63	3.6
BCL-2 homolog from KSHV	1K3K	Viral protein	-28.99	85.12	2.9
BCL-W, Model 1	1MK3	Apoptosis regulator	25.15	72.14	2.9
BCL-2, Isoform 1	1G5M	Apoptosis regulator	46.95	133.93	2.9
Human BID, Model 1	2BID	Apoptosis regulator	100.14	259.49	2.6
Mouse BID, Model 1	1DDB	Apoptosis regulator	118.13	179.90	1.5
Mouse BID, Model 10	1DDB	Apoptosis regulator	125.99	184.24	1.5
BCL-W, Model 10	1MK3	Apoptosis regulator	60.88	86.95	1.4
CED-9	1OHU	Apoptosis regulator	-157.48	190.35	1.2
BHRF1	1Q59	Viral protein	210.73	247.39	1.2

BAX, BCL-W, BCL-XL, BCL-2 and the BCL-2 homolog of Kaposi's sarcoma-associated virus further separate into two subgroups. The first subgroup, represented by BAX, BCL-W and BCL-2 homolog of Kaposi's sarcoma-associated virus, does not have the peripheral helices more stable than the core helix α5. The second subgroup, represented by BCL-XL and

BCL-2, has peripheral helices more stable than the core helix α5. The helices α1 and α2 have energy values between -340 to -100 kcal/mol, compared to the range from -230 to 10 kcal/mol for the core α5 (Tables 11, 15). This difference most likely originates in their structural difference compared to other BCL-2 family members. Both BCL-2 and BCL-XL have a long, highly dynamic unstructured loop between helices α1 and α2. The dynamic nature of this region caused a lack of any structural information between the residues 28 and 81. Likewise, the 3D structure of BCL-2 was noticeably altered by the replacement of the putative flexible loop region with the same region from BCL-XL. This long and unstructured loop between the helices α1 and α2 is thought to be the main site of proteins posttranslational modifications, including phosphorylation and cleavage by caspases (Petros et al. 2004). The increased stability of helices α1 and α2 could thus serve as an anchor for the highly flexible loop and contribute to the stability of the BCL-2 and BCL-XL structure.

Human and mouse BID and BHRF1 (BCL-2 homolog from Epstein-Barr virus) displayed a distinctive pattern of the helical packing that differed significantly from the BAX, BCL-W, BCL-2 and BCL-XL. Their primary structures have low sequence homology with other BCL-2 family members (Petros et al. 2004) and have only one conserved BH domain (BH3 in BID, BH2 in BHRF1). Overall, the 3D structures of BID and BHRF1 displayed only 1-2 relatively stable helices. The pronounced hydrophobic groove and the long flexible loop between α1 and α2 similar to those in BCL-XL and BCl-2 are absent in BID and BHRF1. Furthermore, BID lacks of C-terminal transmembrane domain while BHRF1 has it. The differences in the 3D structures and helical packing pattern indicated that different mechanisms govern the activity of BID and BHRF1 compared to anti-apoptotic BCL-2 or BCL-XL and pro-apoptotic BAX.

Table 11: Helical stability of BCL-2, BCL-W and BAX.

Data for the helical IE values of individual helices for the representatives of BCL-2 family proteins demonstrating the patterns of stability observed within the various structures. Helix numbering, amino acids in each helix, and the length of each helix is indicated. This data is comparable to Figure ?, where the distribution of interaction energies in each structure varies for different members of the BCL-2 family. We interpret these differences as an indication of potentially different mechanisms of transition for each member of the BCL-2 family.

Helix Number	BAX (1F16) Sequence	Helix Energy (kcal/mol)	BCL-2 (1G5M) Sequence	Helix Energy (kcal/mol)	BCL-W (1MK3) Sequence	Helix Energy (kcal/mol)
1	15-36	-58.66	10-25	-168.85	8-23	-65.22
2	53-72	-132.36	92-109	-98.40	40-56	132.80
3	73-81	31.02	113-118	149.96	58-70	32.24
4	87-100	55.02	122-138	27.85	74-87	124.11
5	107-128	-405.14	143-164	10.10	92-112	-71.19
6	129-147	27.08	166-184	158.81	114-132	30.47
7	149-155	104.78	184-193	68.78	133-141	-15.26
8	158-165	89.82	194-203	227.33	142-148	6.25
9	170-189	-76.71			154-168	52.19
AVE		-40.57		46.95		25.15
SD		158.09		133.93		72.14
|SD/AVE|		3.90		2.85		2.87

4.3.2 Homology and Topology

When comparing the helical packing energies of the proteins within one family like BCL-2 family, the question of homology as a function of energy distribution became obvious. One would expect a similar distribution of helical interaction energies in the case of two related proteins which share significant sequence homology. The BCL-2 family proteins are all involved in the regulation of apoptosis and have roughly similar folds, but their sequence homology is quite low and does not correlate with the helical interaction energy distribution. A standard BLAST search (NCBI BLAST, http://www.ncbi.nlm.nih.gov/BLAST) and hidden Markov models (HMM) (Soding et al. 2005) were used to weigh similarities in both the overall sequence and the individual helices themselves.

The standard statistical parameters for the BLAST analysis include percent identity (ID), percent positives (P), and percent gaps (G) along the homologous number of amino acids. The sequence of BAX was the base for the analysis. BCL-2 and BCL-XL had the highest homology aligning to 152 and 147 amino acids (Table 11). The statistics for these alignments were 28% ID, 50% (P), and 7% (G) for BCL-2 and 25% (ID), 45% (P) and 10% (G) for BCL-XL. BCL-W and hBID had to some extent better percentage statistics than BCL-XL, but only aligned with 132 and 129 amino acids. This homology analysis that represents the comparison of the BAX sequences with the other BCL-2 family members enclosed in this study confirmed low homologies, and demonstrated that the variation of IE distribution within each structure has no correlation with the homology.

Table 12: BLAST sequence search of BCL-2 family members

NCBI BLAST was used to search and obtain the statistics from the sequence alignment of the BCL-2 family members against BAX. Standard BLAST statistics is tabulated; ID – percent identity, P – percent positives, G- percent gaps.

Protein	No. of amino acids aligned	ID (%)	P (%)	G(%)
hBCL-2	152	28	50	7
hBCL-XL	147	25	45	10
hBCL-W	132	28	47	12
hBID	129	28	46	12
mBID	65	21	42	20
CED9	96	18	43	3
KSHV BCL-2	78	35	47	7
BHRF1	58	26	41	1

Hidden Markov models (HMM) analysis was used to investigate the similarities of individual secondary structural elements in each structure. HMM analysis yields a HMM score and a percent identity for each sequence analyzed. BCL-XL and BCL-W had the best homology to BAX helices, with five helices showing HMM scores (Table 12). These helices were #2, #4, #5, #6 and #8m which had HMM scores as high as 36.99 at 40% identity for BCL-XL and 35.78 (40% identity) for BCL-W. BCL-2, which had a moderate global (BLAST) alignment with BAX, only showed three helices (#5,#6, and #8) with HMM scores of 36.57 (33% identity), 17.74 (21% identity) and 11.76 (25% identity). This demonstrated that the moderate homology between many BCL-2 family members is found in the loop regions and not within those amino acids that form helices. Additionally, I found no correlation between the HMM scores (and percent identity) and the stability of the individual helices in each structure. These homologous regions represent BH domain of the proteins, are similar in sequence, but vary in their respective stabilization of the structure. Interestingly, helices #1 and #9 from BAX have no homology (based on the HMM analysis) and represent two of the four helices within the BAX structure

with negative (favorable) IE. Given that these helices are at the termini of BAX, and the helix-9 is known to facilitate localization of BAX to mitochondria, indicate that these helices may be unique in their transitional roles compared to other BCL-2 family members.

Table 13a-c Analysis of hidden Markov Models homology of the BCL-2 family members.
All listed BCL-2 family members were compared with BAX. Helix number and interaction energy (IE) is listed for each protein. Analysis of hidden Markov model homology (HMM) analysis is provided next to each helix and corresponds only to this specific helix. If no HHM score is listed, the homology (for that specific helix) is below the statistical homology level for the HMM server.

a)

Helix Number	BAX (1F16)	IE (kcal/mol)	BCL-2 (1G5M)	IE (kcal/mol)	HMM score (% identity)
1	15-36	-58.66	10-25	-168.85	
2	53-72	-132.36	92-109	-98.40	
3	73-81	31.02	113-118	149.96	
4	87-100	55.02	122-138	27.85	
5	107-128	-405.14	143-164	10.10	36.57 (33%)
6	129-147	27.07	166-184	158.81	17.74 (21%)
7	149-155	104.78	184-193	68.78	
8	158-165	89.82	194-203	227.33	11.76 (25%)
9	170-189	-76.71			
AVE		-40.57		46.95	
SD		158.09		133.93	
|SD/AVE|		3.90		2.85	

b)

Helix Number	BCL-W (1MK3)	IE (kcal/mol)	HMM score (% identity)	hBID (2BID)	IE (kcal/mol)	HMM score (% identity)
1	8-23	-65.22		16-31	416.53	
2	40-56	132.80	19.54 (20%)	35-43	269.45	
3	58-70	32.24		81-101	58.92	
4	74-87	124.11	9.43 (29%)	107-116	84.50	
5	92-112	-71.19	35.78 (40%)	121-138	116.45	
6	114-132	30.47	19.85 (21%)	147-164	-40.76	
7	133-141	-15.26		169-182	200.88	
8	142-148	6.25	11.01 (13%)	185-194	-160.94	
9	154-168	52.19				
AVE		25.15			100.14	
SD		72.14			259.49	
|SD/AVE|		2.87			2.59	

c)

Helix Number	mBID (1DDB)	IE (kcal/mol)	HMM score (% identity)	CED9 (1OHU)	IE (kcal/mol)	HMM score (% identity)
1	15-27	416.53		75-78	-93.60	
2	32-39	293.92		79-95	-223.38	
3	83-100	148.88		110-139	-395.92	
4	106-113	379.87		145-154	39.50	
5	125-138	140.63		167-186	-289.80	33.32 (26%)
6	142-162	-40.76		191-212	-383.65	16.57 (21%)
7	167-180	200.88		213-218	36.98	
8	185-192	-160.94		220-240	50.05	
9						
AVE		119.13			-157.47	
SD		179.90			190.35	
|SD/AVE|		1.52			1.21	

d)

Helix Number	KSHV BCL-2 (1K3K)	IE (kcal/mol)	HMM score (% identity)	BHRF1 (1Q59)	IE (kcal/mol)	HMM score (% identity)
1	10-19	51.83		7-19	137.76	
2	34-55	-49.39		44-61	372.44	
3	61-71	31.90		61-73	193.53	
4	71-77	8.78		80-90	485.57	
5	83-101	-138.25	37.48 (41%)	98-118	-319.07	
6	105-114	32.15		121-138	360.99	
7	114-124	58.84	10.25 (14%)	139-146	134.31	
8	124-131	-165.27	13.16 (57%)	152-157	320.33	
9	134-144	-91.53				
AVE		-28.99			210.74	
SD		85.12			247.39	
|SD/AVE|		2.94			1.17	

4.3.3 Peptide Binding Changes Helical IE Distribution

The pro-apoptotic proteins BCL-XL and CED9 are deposited in the PDB database in two forms – free and peptide bound. This gave me the opportunity to explore how the helical stability and packing change upon peptide binding. CED9 and BCL-XL, free and with bound peptide, are depicted in Figure 21.
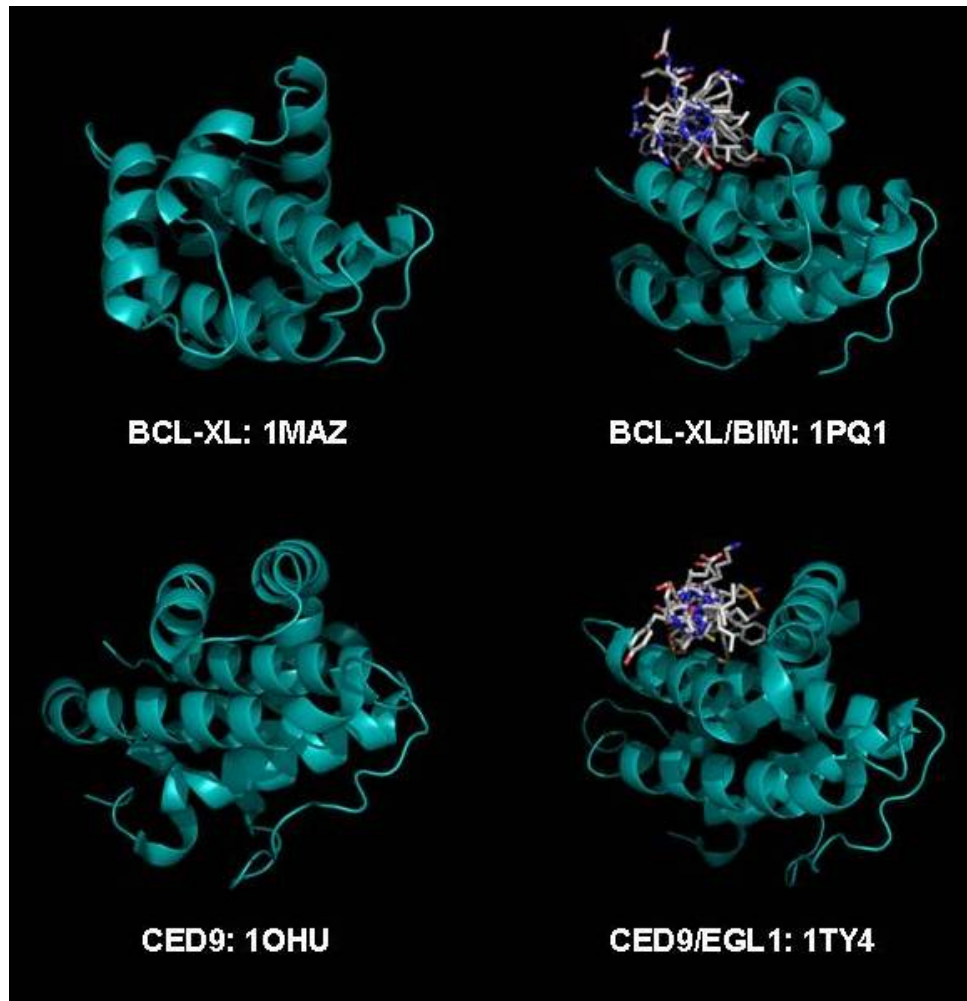
Figure 21: The BH3 only peptide binds into the hydrophobic groove of BCL-XL.
Ribbon diagrams of BCL-XL and CED9 bound to the BIM peptide and the peptide from EGL-1. Each peptide binds to the hydrophobic groove in both the BCL-XL and CED9 structure in a position that spans the most unstable (based on helical IE values) regions of both structures (represented in the Tables 14-17). BCL-XL, CED9 protein – teal, BIM, EGL-1 peptide – sticks.

The structural analysis demonstrated changes in the secondary structure upon peptide binding. To resolve this issue and to obtain comparable values, I performed two sets of calculations. The first set used the same residues for both the free and bound forms, irrespective of any change in the secondary structure. The second set of calculations includes the values of the binding energy from free and bound protein as they are designated in their PDB headers. This approach enabled us to compare any changes in helical interaction energy relative to the resulting changes in secondary structure caused by ligand (peptide) binding. Both set of calculations yielded similar pattern of helical stability and packing. I discuss in the detail only data sets with the same residues for both free and bound protein.

Computational calculations of helical stability were performed with the peptide removed. The peptide was treated as a ligand and the energy of the binding was calculated. The ratio |SD/AVE| decreased upon ligand binding in BCL-XL (Tables 14-16) and also in CED9 (Table 17). Free BCL-XL had a |SD/AVE| ratio of 4.38 in the complex with BIM 2.75, BAD 0.92 and BAK 0.95. The interaction energy between BCL-XL and BAD peptide was the strongest (-428.93 kcal/mol; Table 16) and the lowest was between BCL-XL and BAK (-114.90 kcal/mol; Table 15) and BCL-XL and BIM (-132.76; Table 14). It is important to mention that the peptides differ in the length by 33 amino acids in the BIM peptide, 16 amino acids in the BAK and 25 amino acids in BAD. Despite the differences in the peptide length, BAD and BAK peptides displayed different effects on the structural changes in BCL-XL compared to the BIM peptide. The BAD and BAK peptide seemed to significantly destabilize all the helices in the protein; the average energy values of the helices changed from -46.7 kcal/mol to 198.43 kcal/mol for BAD (Table 16).

Table 14: Helical stability of unbound BCL-XL and BCL-XL/BIM complex.
Bcl-XL is shown in the table with calculations using the same atoms (not only helical regions) due to changes in secondary structure. Changes in secondary structure (due to peptide binding) are shown in the second row. The average interaction energies (AVE), standard deviations (SD), and SD/AVE values are shown for all structures. As shown, peptide binding results in a significant decrease in SD/AVE values for Bcl-XL.

Helix Number	BCL-XL Sequence	(1MAZ) Helix Energy (kcal/mol)	BCL-XL/BIM Sequence	(1PQ1) Helix Energy (kcal/mol)	BCL-XL/BIM Sequence	(1PQ1) Helix Energy (kcal/mol)
1	2-19	-277.61	3-19	-269.25	2-19	-227.68
2	84-100	-342.32	82-102	-223.13	84-100	-322.04
3	106-112	98.15	103-106	75.03	106-112	88.54
4	120-131	104.33	107-112	113.62	120-131	63.42
5	137-156	-238.75	118-131	39.71	137-156	-326.84
6	160-177	23.75	136-158	-248.49	160-177	-383.01
7	179-184	79.06	159-185	-0.82	179-184	185.12
8	187-194	179.43	186-196	123.52	187-194	201.32
Peptide			83-115	-132.76	83-115	-132.76
AVE		-46.74		-48.73		-90.15
SD		204.69		169.20		248.05
|SD/AVE|		4.38		3.47		2.75

BIM peptide, on the other hand, caused significant stabilization of the helices in BCL-XL; the average energy of the helices changes from -46.74 kcal/mol to -90.15. Despite the different effects of the bound peptides on the structure of BCL-XL, the most dramatic energy changes involved helices $\alpha1$, $\alpha2$, $\alpha7$ and $\alpha8$ in all cases of BIM, BAK and BAD peptide binding. Furthermore, the ratio |SD/AVE| dropped below my cutoff for transitional proteins, and the energy values for helical stability were more evenly distributed.

Table 15: Helical stability of unbound BCL-XL and BCL-XL/BAK complex.

Bcl-XL is shown in the table with calculations using the same atoms (not only helical regions) due to changes in secondary structure. Changes in secondary structure (due to peptide binding) are shown in the second row. The average interaction energies (AVE), standard deviations (SD), and SD/AVE values are shown for all structures. As shown, peptide binding results in a significant decrease in SD/AVE values for Bcl-XL.

Helix Number	BCL-XL Sequence	(1MAZ) Helix Energy (kcal/mol)	BCL-XL/BAK Sequence	(1BXL)) Helix Energy (kcal/mol)	BCL-XL/BAK Sequence	(1BXL) Helix Energy (kcal/mol)
1	2-19	-277.61	3-20	-148.96	2-19	-3.96
2	84-100	-342.32	25-27	152.58	84-100	114.14
3	106-112	98.15	42-104	301.80	106-112	261.44
4	120-131	104.33	119-130	285.24	120-131	284.91
5	137-156	-238.75	139-157	-24.07	137-156	6.44
6	160-177	23.75	160-176	182.11	160-177	174.31
7	179-184	79.06	179-185	433.45	179-184	427.25
8	187-194	179.43	187-194	411.06	187-94	411.06
9			199-204	206.21		
Peptide			572-587	-114.90	572-587	-114.90
AVE		-46.74		199.93		209.45
SD		204.69		190.81		166.29
|SD/AVE|		4.38		0.95		0.79

The final conclusion of the comparison among BIM, BAK and BAD binding to BCL-XL were: (1) the |SD/AVE| ratio significantly decreased in all cases; (2) there were significant changes in the interaction energy values from many of the helices; and (3) the bound peptide interacted with the protein at regions that have some of the highest interaction energy values when the protein was in the unbound form. This indicates that one can differentiate not only the transitional proteins from others, but also enable the prediction of the regions within the protein where the ligand will most likely bind.

Table 16: Helical stability of unbound BCL-XL and BCL-XL/BAD complex.

Bcl-XL is shown in the table with calculations using the same atoms (not only helical regions) due to changes in secondary structure. Changes in secondary structure (due to peptide binding) are shown in the second row. The average interaction energies (AVE), standard deviations (SD), and SD/AVE values are shown for all structures. As shown, peptide binding results in a significant decrease in SD/AVE values for Bcl-XL.

Helix Number	BCL-XL Sequence	(1MAZ) Helix Energy (kcal/mol)	BCL-XL/BAD Sequence	(1G5J) Helix Energy (kcal/mol)	BCL-XL/BAD Sequence	(1G5J) Helix Energy (kcal/mol)
1	2-19	-277.61	2-25	-71.21	2-19	53.86
2	84-100	-342.32	27-31	185.25	84-100	-14.41
3	106-112	98.15	45-105	328.18	106-112	254.60
4	120-131	104.33	106-110	-43.49	120-131	285.00
5	137-156	-238.75	122-136	298.20	137-156	26.70
6	160-177	23.75	139-161	460.95	160-177	186.74
7	179-184	79.06	164-181	190.22	179-184	383.22
8	187-194	179.43	183-212	519.87	187-194	411.75
Peptide			301-325	-428.94	301-325	-428.94
AVE		-46.74		233.50		198.43
SD		204.69		214.03		163.07
|SD/AVE|		4.38		0.92		0.82

Table 17: Helical stability of unbound CED9and CED9/EGL1 complex.

CED9 is shown in the table with calculations using the same atoms (not only helical regions) due to changes in secondary structure. Changes in secondary structure (due to peptide binding) are shown in the second row. The average interaction energies (AVE), standard deviations (SD), and SD/AVE values are shown for all structures. As shown, peptide binding results in a minor decrease in SD/AVE values for CED9.

Helix Number	CED9 Sequence	(1OHU) Helix Energy (kcal/mol)	CED9/EGL1 Sequence	(1TY4) Helix Energy (kcal/mol)	CED9/EGL1 Sequence	(1TY4) Helix Energy (kcal/mol)
1	75-78	-93.60	75-78	1.87	75-78	6.33
2	79-95	-223.38	79-95	-180.92	79-95	-180.92
3	110-139	-395.92	110-140	-241.03	110-139	-262.34
4	145-154	39.50	141-145	30.87	145-154	-29.58
5	167-186	-289.80	146-159	-33.44	167-186	-240.55
6	191-212	-383.65	167-187	-155.06	191-212	-340.39
7	213-218	36.98	191-211	-387.51	213-218	51.00
8	220-240	50.05	220-236	-23.00	220-240	-23.00
Peptide				-246.85		-246.85
AVE		-157.48				-127.43
SD		190.35				146.10
|SD/AVE|		1.21				1.15

4.4 DISCUSSION

The BCL-2 family proteins are crucial regulators of mitochondrial apoptotic pathway. Their activity is thought to be regulated by significant changes in their 3D structure. The analysis of helical stability expressed as helical interaction energy (IE) revealed significant trends in their IE distribution. These transitional proteins displayed regions of high helical stability accompanied by regions that were relatively unstable.

The BCL-2 family members were partitioned in subgroups according to the distribution of the helical stability. BAX, BCL-XL, BCL-2, BCL-W and the BCL-2 homolog from KSHV displayed stable core helix surrounded by rather unstable outer helices. BCL-2 and BCL-XL formed separate subgroups by displaying higher stability of $\alpha 1$ and $\alpha 2$ than their core helices. The differences in the distribution of helical stability and packing could be related to the structural and functional differences among BCL-2 family members. BAX, BCL-XL, BCL-2, BCL-W and the BCL-2 homolog from KSHV have pronounced hydrophobic pockets which modulate the activity of the proteins. Depending on the binding partner of the hydrophobic pocket, the occupancy of the pocket inhibits or facilitates the activity of the apoptotic protein. BCL-2 and BCL-XL also have a very long flexible loop between helices $\alpha 1$ and $\alpha 2$, which play a significant role in the regulation of the activity of BCL-XL and BCL-2 (Borner 2003;Petros et al. 2004). The BH3-only protein BID and the BCL-2 homolog from EBV did not group with the other members of BCL-2 family, indicating that varied helical stability mediates structural transitions specific to the function of the protein.

The occupancy of the hydrophobic pocket is predicted to regulate the intracellular distribution of these proteins and consequently their activity (Denisov et al. 2003;Petros et al.

2004;Petros et al. 2000;Tschammer et al. 2007b). Latent BAX is a cytosolic protein in healthy cells, with the α9 helix sequestered within a hydrophobic pocket (Suzuki et al. 2000). During apoptosis, BAX may undergo a conformational change that exposes transmembrane domains, helix α9 and possibly helix α5 and α6, to promote mitochondrial membrane binding (Annis et al. 2005). Similarly, BCL-W has its C-terminal helix folded into its hydrophobic pocket when localized in the cytosol. In response to apoptotic stimuli, helix α9 is exposed and inserts into the mitochondrial membranes (Denisov et al. 2003). The activity of the BCL-2 family proteins thus seems to be regulated by the occupancy of the hydrophobic pocket. It is possible that the also the helical stability of these proteins is regulated by the occupancy of the hydrophobic pocket. I predict that the more stable structures, with hydrophobic pockets occupied by their C-terminal helices, such as BAX or BCL-W, will not undergo structural transitions unless their C-terminal helix is released or displaced from the pocket. This C-terminal α9 helix is one of the helices that stabilize the 3D structure of the protein. These data support the role of the α9 helix as a type of transitional switch that allows translocation of BAX from the cytosol to the mitochondria upon apoptotic stimuli(Tschammer et al. 2007b).

BCL-XL, whose structure was determined with both an unoccupied pocket (displaying the most flexible helices) and with peptides bound, demonstrated that the structural stabilization occur upon binding of the BH3 peptides (BIM, BAD and BAK), but the extent of structural changes depends on the binding partner. These data corroborate binding studies that were done with BH3 peptides measured by plasmon resonance (Kuwana et al. 2005). In this study, the BIM peptide had a dissociation constant of 9.2 ± 5.3 nM, and the BAD peptide had a binding constant of 2.05 ± 0.8 nM. These data correlate well to my calculated binding energies for the peptides

and demonstrates that the increase in (shown through my calculations and the dissociation constants) affinity may regulate how much of a structural transition BCL-XL undergoes during binding to different partners.

This may be a direct link to the functional role that each BCL-2 family member has in the presence of various BH3 containing proteins. My findings indicate that the function of the BCL-2 family members may be dependent on which BH-3 containing proteins interact with. The current dogma states that the BH3-only proteins can be functionally subdivided into activators, like BID and BIM, which induce the oligomerization of BAX and BAK, and sensitizers, like BAD, NOXA or PUMA, which directly bind anti-apoptotic proteins (Certo et al. 2006). I propose hat these activators or sensitizers both bind anti-apoptotic proteins, but may have different consequences upon the stability of the anti-apoptotic proteins and its ability to transition during apoptosis. The binding of BH3-peptides (or the entire BH3-only proteins) like that of BAD to the hydrophobic groove may "lock" BCL-2 family protein into a structural state that is resistant to conformational transitions, thereby negating its pro- or anti- apoptotic function, while binding BIM may favor a degree of transitioning. By understanding how the interaction energy (in the reference to the *in vitro* binding data) correlates with the level of structural transition, a potential link between the various functions of BCL-2 family member with the respect to their BH3 protein binding partners can be established.

The analysis of the helical stability contributes certain degree of knowledge to the understanding how BCL-2 regulators of apoptosis undergo transitions, but additional studies are required that better represent the biological conditions *in vivo*. Many of BCL-2 family proteins are involved in membrane binding that allows the insertion into various organelles, most noticeably mitochondria. These types of structural transitions cannot be accurately represented

by the analysis where the proteins are considered static structures. The nature of these transitional mechanisms, which are not amendable to current methods for high resolution structure determination (because of the membrane binding and sample heterogeneity), represents the dynamic nature of polypeptides and give insight into their mechanism of action. In the absence of such high resolution data, our analysis of the static stability of the individual helices gives insight into the protein's mechanism of action, as well as enabling classification and identifying peptide binding location.

5 CONCLUSIONS

Apoptosis is essential for the development and the maintenance of cellular homeostasis. Proteins of the BCL-2 family are key modulators of this process. In response to diverse apoptotic stimuli, the pro-apoptotic member of BCL-2 family BAX redistributes from the cytosol to the mitochondria or endoplasmic reticulum and primes cells for death. The activation of this lethal protein is poorly understood.

My study is comprised of three parts. First part was governed by the hypothesis that the C-terminal α9 helix of BAX crucially regulates the intracellular distribution and activation of BAX, not as putative membrane domain, but as "molecular switch" that triggers conformational changes of BAX needed for the redistribution from the cytosol to mitochondrial membrane. Computational analysis using molecular mechanics and computational docking using web based server GRAMM-X indicated that the C-terminal α9 helix of BAX can dock into the hydrophobic pocket of BAX in two directions – in forward orientation that occurs during self-association and reverse orientation that might occur during dimerization. Co-immunoprecipitation and crosslinking demonstrated that an EGFP tagged α9 helix of BAX associated with BAX lacking its C-terminal. Peptide encoding last 20 amino acids of BAX efficiently induced the translocation of wild type and C-terminally truncated BAX into the mitochondria, further confirming that the C-terminal α9 helix of BAX serves as a "molecular switch", triggering conformational changes in BAX which are needed for the redistribution from cytosol to mitochondria. This is novel discovery, which is not important only to reach a fuller understanding of how BAX is regulated, but will enable the design of novel therapeutics which could modulate the activity of BAX. Studies using peptides encoding BH3 domain sequences or small-molecule BCL-2 antagonists,

which bound to the hydrophobic groove of BCL-2 with high affinity, showed that these substances can act as competitive inhibitors of BCL-2 function, inducing the selective death of cancer cells. We propose that similar peptides or small molecules derived from the sequence of C-terminal α9 of BAX could in the same fashion inhibit or activate the function of BAX. As example a small molecule could cause a displacement of self-associated C-terminus of BAX, triggering conformational changes in BAX that lead to association with mitochondrial outer membrane and induction of apoptosis. Specific targeting of such a compound to tumors or cancer cells could trigger the apoptosis of these pathogenic cells. On the other hand, the design of a peptide that would "lock" the C-terminal α9 of BAX and prevent its release could protect cells from apoptosis in e.g. neurodegenerative, myocardic and ischemic diseases.

The second part of the study was computational and focused on examining the helical stability of proteins. As a result my study, it became evident that BAX has a broad variation in the distribution of the helical interaction energy, ranging from stable core helix to destabilized helices on the periphery. This led to hypothesis that proteins which undergo 3D structural transitions during execution of their function have broad variation in the distribution of the helical interaction energy compared to the proteins which do not undergo such transitions. Computational analysis of a random set of all-alpha proteins from the Protein Data Bank demonstrated that the analysis of the helical interaction energy within the proteins yields a measure of the propensity of the protein to undergo transitions and can be used to predict the likelihood that the protein analyzed will undergo transitions. No measure of the propensity for such transitions is currently available for stable proteins that are involved in signaling. Hence, I developed a novel computational method for the prediction of the propensity for transition. With an increasing number of protein structures being determined by structural genomics, parameters,

such as the propensity for transition, will provide needed information about the areas of least stability within a protein's 3D structure and possibly identify novel region(s) of contacts for the biological molecules that are involved in the interaction(s). This information may aid in the design of experiments to elucidate a protein's function in the context of its interaction with the surfaces with other protein or ligands.

The third part of the study was a computational analysis of the BCL-2 family, using the computational method developed in the second part of the study. I used this method to estimate the propensity of individual BCL-2 family members to undergo transitions in relation to changes in the distribution of the helical interaction energy upon ligand binding. The analysis resulted in a strong correlation between the computational results and published experimental findings, confirming the ability of the computational method to predict transitional proteins. Most importantly, the computational method revealed that the binding of the ligand, such as a peptide, to a protein can have stabilizing or destabilizing effect, carrying important consequences for the activation or repression of the protein. One example of this is the previously described dual function of the C-terminal $\alpha 9$ of BAX that is dependent upon the orientation of its binding to the hydrophobic groove. A similar trend was observed for the anti-apoptotic protein, BCL-XL, in that binding of a BH3 peptide from BIM, stabilized the protein, while binding of a BH3 peptide from BAD within the same groove destabilized the protein. Furthermore, the distribution of IE values decreased in the specific regions of the proteins which displayed the least structural stability, indicating a potential application for the identification of the binding site for the ligand. This computational analysis thus contributes to the better understanding of the function and regulation of the BCL-2 family members.

REFERENCES

1. Allinger,N.L., Geise,H.J., Pyckhout,W., Paquette,L.A., and Gallucci,J.C. 1989a. Structures of Norbornane and Dodecahedrane by Molecular Mechanics Calculations (Mm3), X-Ray Crystallography, and Electron-Diffraction. *Journal of the American Chemical Society* **111**:1106-1114.

2. Allinger,N.L., Yuh,Y.H., and Lii,J.H. 1989b. Molecular Mechanics - the Mm3 Force-Field for Hydrocarbons .1. *Journal of the American Chemical Society* **111**:8551-8566.

3. Allinger,N. 1976. Calculation of molecular structure and energy by force-field methods. *Adv. Phys. Org. Chem.* **13**:1-85.

4. Annis,M.G., Soucie,E.L., Dlugosz,P.J., Cruz-Aguado,J.A., Penn,L.Z., Leber,B., and Andrews,D.W. 2005. Bax forms multispanning monomers that oligomerize to permeabilize membranes during apoptosis. *EMBO J* **24**:2096-2103.

5. Antonsson,B., Montessuit,S., Lauper,S., Eskes,R., and Martinou,J.C. 2000. Bax oligomerization is required for channel-forming activity in liposomes and to trigger cytochrome c release from mitochondria. *Biochem J* **345 Pt 2**:271-278.

6. Antonsson,B., Montessuit,S., Sanchez,B., and Martinou,J.C. 2001. Bax Is Present as a High Molecular Weight Oligomer/Complex in the Mitochondrial Membrane of Apoptotic Cells. *J. Biol. Chem.* **276**:11615-11623.

7. Arokium,H., Camougrand,N., Vallette,F.M., and Manon,S. 2004. Studies of the Interaction of Substituted Mutants of BAX with Yeast Mitochondria Reveal That the C-terminal Hydrophobic {alpha}-Helix Is a Second ART Sequence and Plays a Role in the Interaction with Anti-apoptotic BCL-xL. *J. Biol. Chem.* **279**:52566-52573.

8. Bartels,C., Widmer,A., and Ehrhardt,C. 2005. Absolute free energies of binding of peptide analogs to the HIV-1 protease from molecular dynamics simulations. *J Comput Chem* **26**:1294-1305.

9. Belaud-Rotureau,M.A., Leducq,N., Macouillard,P., Diolez,P., Lacoste,L., Lacombe,F., Bernard,P., and Belloc,F. 2000. Early transitory rise in intracellular pH leads to Bax conformation change during ceramide-induced apoptosis. *Apoptosis* **5**:551-560.

10. Berjanskii,M.V. and Wishart,D.S. 2005. A simple method to predict protein flexibility using secondary chemical shifts. *J Am Chem Soc* **127**:14970-14971.

11. Berman,H.M., Westbrook,J., Feng,Z., Gilliland,G., Bhat,T.N., Weissig,H., Shindyalov,I.N., and Bourne,P.E. 2000. The Protein Data Bank. *Nucleic Acids Res.* **28**:235-242.

12. Borner,C. 2003. The Bcl-2 protein family: sensors and checkpoints for life-or-death decisions. *Mol Immunol* **39**:615-647.

13. Bouillet,P. and Strasser,A. 2002. BH3-only proteins -- evolutionarily conserved proapoptotic Bcl-2 family members essential for initiating programmed cell death. *J. Cell Sci.* **115**:1567-1574.

14. Brooks,B.R., Bruccoleri,R.E., Olafson,B.D., Swaminathan,S., States,D.J., and Karplus,M. 1983. A Program for Marcomolecular Energy, Minimization, and Dynamics Calculations. *J Comput Chem* **4**:187-217.

15. Brusca,J.S. and Radolf,J.D. 1994. Isolation of integral membrane proteins by phase partitioning with Triton X-114. *Methods Enzymol* **228**:182-193.

16. Cartron,P.F., Oliver,L., Mayat,E., Meflah,K., and Vallette,F.M. 2004. Impact of pH on Bax alpha conformation, oligomerisation and mitochondrial integration. *FEBS Lett* **578**:41-46.

17. Case,D.A., Cheatham,T.E., Darden,T., Gohlke,H., Luo,R., Merz,K.M., Onufriev,A., Simmerling,C., Wang,B., and Woods,R.J. 2005. The Amber biomolecular simulation programs. *J Comput Chem* **26**:1668-1688.

18. Certo,M., Del Gaizo Moore,V., Nishino,M., Wei,G., Korsmeyer,S., Armstrong,S.A., and Letai,A. 2006. Mitochondria primed by death signals determine cellular addiction to antiapoptotic BCL-2 family members. *Cancer Cell* **9**:351-365.

19. Cheng,Y., Zhang,Y., and McCammon,J.A. 2005. How does the cAMP-dependent protein kinase catalyze the phosphorylation reaction: an ab initio QM/MM study. *J Am Chem Soc* **127**:1553-1562.

20. Chipuk,J.E., Kuwana,T., Bouchier-Hayes,L., Droin,N.M., Newmeyer,D.D., Schuler,M., and Green,D.R. 2004. Direct Activation of Bax by p53 Mediates Mitochondrial Membrane Permeabilization and Apoptosis. *Science* **303**:1010-1014.

21. Chou,J.J., Li,H., Salvesen,G.S., Yuan,J., and Wagner,G. 1999. Solution structure of BID, an intracellular amplifier of apoptotic signaling. *Cell* **96**:615-624.

22. Cory,S., Huang,D.C., and Adams,J.M. 2003. The Bcl-2 family: roles in cell survival and oncogenesis. *Oncogene* **22**:8590-8607.

23. Cosulich,S.C., Worrall,V., Hedge,P.J., Green,S., and Clarke,P.R. 1997. Regulation of apoptosis by BH3 domains in a cell-free system. *Curr Biol* **7**:913-920.

24. Das,A.K., Cohen,P.W., and Barford,D. 1998. The structure of the tetratricopeptide repeats of protein phosphatase 5: implications for TPR-mediated protein-protein interactions. *EMBO J* **17**:1192-1199.

25. Degenhardt,K., Sundararajan,R., Lindsten,T., Thompson,C., and White,E. 2002. Bax and Bak Independently Promote Cytochrome c Release from Mitochondria. *J. Biol. Chem.* **277**:14127-14134.

26. del Mar,M., Corbalan-Garcia,S., and Gomez-Fernandez,J.C. 2001. Conformation of the C-terminal domain of the pro-apoptotic protein Bax and mutants and its interaction with membranes. *Biochemistry* **40**:9983-9992.

27. Demarest,S.J., Martinez-Yamout,M., Chung,J., Chen,H., Xu,W., Dyson,H.J., Evans,R.M., and Wright,P.E. 2002. Mutual synergistic folding in recruitment of CBP/p300 by p160 nuclear receptor coactivators. *Nature* **415**:549-553.

28. Demaurex,N. 2002. pH Homeostasis of Cellular Organelles. *News Physiol Sci* **17**:1-5.

29. Denisov,A.Y., Madiraju,M.S.R., Chen,G., Khadir,A., Beauparlant,P., Attardo,G., Shore,G.C., and Gehring,K. 2003. Solution Structure of Human BCL-w: MODULATION OF LIGAND BINDING BY THE C-TERMINAL HELIX. *J. Biol. Chem.* **278**:21124-21128.

30. Dharap,S.S., Qiu,B., Williams,G.C., Sinko,P., Stein,S., and Minko,T. 2003. Molecular targeting of drug delivery systems to ovarian cancer by BH3 and LHRH peptides. *J Control Release* **91**:61-73.

31. Dijkers,P.F., Medema,R.H., Lammers,J.W., Koenderman,L., and Coffer,P.J. 2000. Expression of the pro-apoptotic Bcl-2 family member Bim is regulated by the forkhead transcription factor FKHR-L1. *Curr Biol* **10**:1201-1204.

32. Dosztanyi,Z., Csizmok,V., Tompa,P., and Simon,I. 2005. IUPred: web server for the prediction of intrinsically unstructured regions of proteins based on estimated energy content. *Bioinformatics* **21**:3433-3434.

33. Dumont,M.E. and Richards,F.M. 1988. The pH-dependent conformational change of diphtheria toxin. *J. Biol. Chem.* **263**:2087-2097.

34. Earnshaw,W.C., Martins,L.M., and Kaufmann,S.H. 1999. Mammalian caspases: structure, activation, substrates, and functions during apoptosis. *Annu Rev Biochem* **68**:383-424.

35. Eddy,S.R. 1996. Hidden Markov models. *Curr Opin Struct Biol* **6**:361-365.

36. Ekert,P.G., Jabbour,A.M., Manoharan,A., Heraud,J.E., Yu,J., Pakusch,M., Michalak,E.M., Kelly,P.N., Callus,B., Kiefer,T., Verhagen,A., Silke,J., Strasser,A.,

Borner,C., and Vaux,D.L. 2006. Cell death provoked by loss of interleukin-3 signaling is independent of Bad, Bim, and PI3 kinase, but depends in part on Puma. *Blood* **108**:1461-1468.

37. Epand,R.F., Martinou,J.C., Montessuit,S., and Epand,R.M. 2003. Transbilayer lipid diffusion promoted by Bax: implications for apoptosis. *Biochemistry* **42**:14576-14582.

38. Galkin,A., Sarikaya,E., Lehmann,C., Howard,A., and Herzberg,O. 2004. X-ray structure of HI0817 from Haemophilus influenzae: protein of unknown function with a novel fold. *Proteins* **57**:874-877.

39. Garcia-Saez,A.J., Coraiola,M., la Serra,M., Mingarro,I., Menestrina,G., and Salgado,J. 2005. Peptides Derived from Apoptotic Bax and Bid Reproduce the Poration Activity of the Parent Full-Length Proteins. *Biophys. J.* **88**:3976-3990.

40. Garcia-Saez,A.J., Coraiola,M., Serra,M.D., Mingarro,I., Muller,P., and Salgado,J. 2006. Peptides corresponding to helices 5 and 6 of Bax can independently form large lipid pores. *FEBS J.* **273**:971-981.

41. Gardai,S.J., Hildeman,D.A., Frankel,S.K., Whitlock,B.B., Frasch,S.C., Borregaard,N., Marrack,P., Bratton,D.L., and Henson,P.M. 2004. xPhosphorylation of Bax Ser184 by Akt Regulates Its Activity and Apoptosis in Neutrophils. *J. Biol. Chem.* **279**:21085-21095.

42. Graham,F.L., Smiley,J., Russell,W.C., and Nairn,R. 1977. Characteristics of a human cell line transformed by DNA from human adenovirus type 5. *J. Gen. Virol.* **36**:59-74.

43. Gross,A., McDonnell,J.M., and Korsmeyer,S.J. 1999. BCL-2 family members and the mitochondria in apoptosis. *Genes & Dev.* **13**:1899-1911.

44. Hanson,G.T., McAnaney,T.B., Park,E.S., Rendell,M.E., Yarbrough,D.K., Chu,S., Xi,L., Boxer,S.G., Montrose,M.H., and Remington,S.J. 2002. Green fluorescent protein variants as ratiometric dual emission pH sensors. 1. Structural characterization and preliminary application. *Biochemistry* **41**:15477-15488.

45. Hinchliffe,A. 2006. *Molecular Modeling for Beginners*. Wiley: West Suusex.

46. Hinds,M.G., Lackmann,M., Skea,G.L., Harrison,P.J., Huang,D.C.S., and Day,C.L. 2003. The structure of Bcl-w reveals a role for the C-terminal residues in modulating biological activity. *EMBO J.* **22**:1497-1507.

47. Hope,M.J. and Cullis,P.R. 1987. Lipid asymmetry induced by transmembrane pH gradients in large unilamellar vesicles. *J. Biol. Chem.* **262**:4360-4366.

48. Hough,E., Hansen,L.K., Birknes,B., Jynge,K., Hansen,S., Hordvik,A., Little,C., Dodson,E., and Derewenda,Z. 1989. High-resolution (1.5 A) crystal structure of phospholipase C from Bacillus cereus. *Nature* **338**:357-360.

49. Hsu,Y.T., Wolter,K.G., and Youle,R.J. 1997. Cytosol-to-membrane redistribution of Bax and Bcl-XL duringáapoptosis. *PNAS* **94**:3668-3672.

50. Hsu,Y.T. and Youle,R.J. 1998. Bax in Murine Thymus Is a Soluble Monomeric Protein That Displays Differential Detergent-induced Conformations. *J. Biol. Chem.* **273**:10777-10783.

51. Hsu,Y.T. and Youle,R.J. 1997. Nonionic Detergents Induce Dimerization among Members of the Bcl-2 Family. *J. Biol. Chem.* **272**:13829-13834.

52. Huang,Q., Petros,A.M., Virgin,H.W., Fesik,S.W., and Olejniczak,E.T. 2003. Solution structure of the BHRF1 protein from Epstein-Barr virus, a homolog of human Bcl-2. *J Mol Biol* **332**:1123-1130.

53. Huang,Q., Petros,A.M., Virgin,H.W., Fesik,S.W., and Olejniczak,E.T. 2002. Solution structure of a Bcl-2 homolog from Kaposi sarcoma virus. *PNAS* **99**:3428-3433.

54. Jeong,S.Y., Gaume,B., Lee,Y.J., Hsu,Y.T., Ryu,S.W., Yoon,S.H., and Youle,R.J. 2004. Bcl-xL sequesters its C-terminal membrane anchor in soluble, cytosolic homodimers. *EMBO J.* **23**:2146-2155.

55. Karbowski,M., Norris,K.L., Cleland,M.M., Jeong,S.Y., and Youle,R.J. 2006. Role of Bax and Bak in mitochondrial morphogenesis. *Nature* **443**:658-662.

56. Karbowski,M., Lee,Y.J., Gaume,B., Jeong,S.Y., Frank,S., Nechushtan,A., Santel,A., Fuller,M., Smith,C.L., and Youle,R.J. 2002. Spatial and temporal association of Bax with mitochondrial fission sites, Drp1, and Mfn2 during apoptosis. *J. Cell Biol.* **159**:931-938.

57. Karplus,K., Barrett,C., and Hughey,R. 1998. Hidden Markov models for detecting remote protein homologies. *Bioinformatics* **14**:846-856.

58. Kelley,L.A., Gardner,S.P., and Sutcliffe,M.J. 1996a. An automated approach for clustering an ensemble of NMR-derived protein structures into conformationally related subfamilies. *Protein Eng* **9**:1063-1065.

59. Kelley,L.A., Gardner,S.P., and Sutcliffe,M.J. 1997. An automated approach for defining core atoms and domains in an ensemble of NMR-derived protein structures. *Protein Eng* **10**:737-741.

60. Kelley,L.A., Gardner,S.P., and Sutcliffe,M.J. 1996b. An automated approach for clustering an ensemble of NMR-derived protein structures into conformationally related subfamilies. *Protein Eng.* **9**:1063-1065.

61. Keough,D.T., Brereton,I.M., de Jersey,J., and Guddat,L.W. 2005. The crystal structure of free human hypoxanthine-guanine phosphoribosyltransferase reveals extensive conformational plasticity throughout the catalytic cycle. *J Mol Biol* **351**:170-181.

62. Khaled,A.R., Kim,K., Hofmeister,R., Muegge,K., and Durum,S.K. 1999. From the Cover: Withdrawal of IL-7 induces Bax translocation from cytosol to mitochondria through a rise in intracellular pH. *PNAS* **96**:14476-14481.

63. Kim,H.Y. and Cho,Y. 1997. Structural similarity between the pocket region of retinoblastoma tumour suppressor and the cyclin-box. *Nat Struct Biol* **4**:390-395.

64. Kim,J.M., Bae,H.R., Park,B.S., Lee,J.M., Ahn,H.B., Rho,J.H., Yoo,K.W., Park,W.C., Rho,S.H., Yoon,H.S., and Yoo,Y.H. 2003. Early Mitochondrial Hyperpolarization and Intracellular Alkalinization in Lactacystin-Induced Apoptosis of Retinal Pigment Epithelial Cells. *J. Pharmacol. Exp. Ther.* **305**:474-481.

65. Krammer,P.H. 2000. CD95's deadly mission in the immune system. *Nature* **407**:789-795.

66. Kuwana,T., Bouchier-Hayes,L., Chipuk,J.E., Bonzon,C., Sullivan,B.A., Green,D.R., and Newmeyer,D.D. 2005. BH3 domains of BH3-only proteins differentially regulate Bax-mediated mitochondrial membrane permeabilization both directly and indirectly. *Mol Cell* **17**:525-535.

67. Lagadic-Gossmann,D., Huc,L., and Lecureur,V. 2004. Alterations of intracellular pH homeostasis in apoptosis: origins and roles. *Cell Death Differ* **11**:953-961.

68. Letai,A. 2005. Pharmacological manipulation of Bcl-2 family members to control cell death. *J. Clin. Invest.* **115**:2648-2655.

69. Lii,J.H. and Allinger,N.L. 1989. Molecular Mechanics - the Mm3 Force-Field for Hydrocarbons .2. Vibrational Frequencies and Thermodynamics. *Journal of the American Chemical Society* **111**:8566-8575.

70. Lii,J.H. and Allinger,N.L. 1994. Directional Hydrogen-Bonding in the Mm3 Force-Field .1. *Journal of Physical Organic Chemistry* **7**:591-609.

71. Lii,J.H. and Allinger,N.L. 1998a. Directional hydrogen bonding in the MM3 force field: II. *Journal of Computational Chemistry* **19**:1001-1016.

72. Lii,J. and Allinger,N. 1998b. Directional hydrogen bonding in the MM3 force field:II. *Computational Chemistry* **19**:1001-1016.

73. Lin,K., Simossis,V.A., Taylor,W.R., and Heringa,J. 2005. A simple and fast secondary structure prediction method using hidden neural networks. *Bioinformatics* **21**:152-159.

74. Linseman,D.A., Butts,B.D., Precht,T.A., Phelps,R.A., Le,S.S., Laessig,T.A., Bouchard,R.J., Florez-McClure,M.L., and Heidenreich,K.A. 2004. Glycogen Synthase

Kinase-3{beta} Phosphorylates Bax and Promotes Its Mitochondrial Localization during Neuronal Apoptosis. *J. Neurosci.* **24**:9993-10002.

75. Lipford,E., Wright,J.J., Urba,W., Whang-Peng,J., Kirsch,I.R., Raffeld,M., Cossman,J., Longo,D.L., Bakhshi,A., and Korsmeyer,S.J. 1987. Refinement of lymphoma cytogenetics by the chromosome 18q21 major breakpoint region. *Blood* **70**:1816-1823.

76. Liu,X., Dai,S., Zhu,Y., Marrack,P., and Kappler,J.W. 2003. The structure of a Bcl-xL/Bim fragment complex: implications for Bim function. *Immunity* **19**:341-352.

77. Llopis,J., McCaffery,J.M., Miyawaki,A., Farquhar,M.G., and Tsien,R.Y. 1998. Measurement of cytosolic, mitochondrial, and Golgi pH in single living cells with green fluorescent proteins. *PNAS* **95**:6803-6808.

78. Locksley,R.M., Killeen,N., and Lenardo,M.J. 2001. The TNF and TNF receptor superfamilies: integrating mammalian biology. *Cell* **104**:487-501.

79. Lu,L., Arakaki,A.K., Lu,H., and Skolnick,J. 2003. Multimeric Threading-Based Prediction of Protein-Protein Interactions on a Genomic Scale: Application to the Saccharomyces cerevisiae Proteome. *Genome Res.* **13**:1146-1154.

80. Machida,K. 2007. *Principles of Molecular Mechanics*. Wiley.

81. Marani,M., Tenev,T., Hancock,D., Downward,J., and Lemoine,N.R. 2002. Identification of Novel Isoforms of the BH3 Domain Protein Bim Which Directly Activate Bax To Trigger Apoptosis. *Mol. Cell. Biol.* **22**:3577-3589.

82. Matsuyama,S., Llopis,J., Deveraux,Q.L., Tsien,R.Y., and Reed,J.C. 2000. Changes in intramitochondrial and cytosolic pH: early events that modulate caspase activation during apoptosis. *Nat Cell Biol* **2**:318-325.

83. McDonnell,J.M., Fushman,D., Milliman,C.L., Korsmeyer,S.J., and Cowburn,D. 1999. Solution structure of the proapoptotic molecule BID: a structural basis for apoptotic agonists and antagonists. *Cell* **96**:625-634.

84. McGuffin,L.J. and Jones,D.T. 2003. Improvement of the GenTHREADER method for genomic fold recognition. *Bioinformatics* **19**:874-881.

85. Meiler,J. and Baker,D. 2006. ROSETTALIGAND: protein-small molecule docking with full side-chain flexibility. *Proteins* **65**:538-548.

86. Minko,T., Dharap,S.S., and Fabbricatore,A.T. 2003. Enhancing the efficacy of chemotherapeutic drugs by the suppression of antiapoptotic cellular defense. *Cancer Detect Prev* **27**:193-202.

87. Muchmore,S.W., Sattler,M., Liang,H., Meadows,R.P., Harlan,J.E., Yoon,H.S., Nettesheim,D., Chang,B.S., Thompson,C.B., Wong,S.L., Ng,S.L., and Fesik,S.W. 1996.

X-ray and NMR structure of human Bcl-xL, an inhibitor of programmed cell death. *Nature* **381**:335-341.

88. Nechushtan,A., Smith,C.L., Hsu,Y.T., and Youle,R.J. 1999. Conformation of the Bax C-terminus regulates subcellular location and cell death. *EMBO J.* **18**:2330-2341.

89. Nechushtan,A., Smith,C.L., Lamensdorf,I., Yoon,S.H., and Youle,R.J. 2001. Bax and Bak Coalesce into Novel Mitochondria-associated Clusters during Apoptosis. *J. Cell Biol.* **153**:1265-1276.

90. Nelson,D.A. and White,E. 2004. Exploiting different ways to die. *Genes & Dev.* **18**:1223-1226.

91. Nomura,M., Shimizu,S., Sugiyama,T., Narita,M., Ito,T., Matsuda,H., and Tsujimoto,Y. 2003. 14-3-3 Interacts Directly with and Negatively Regulates Pro-apoptotic Bax. *J. Biol. Chem.* **278**:2058-2065.

92. Ohtsuka,T., Ryu,H., Minamishima,Y.A., Macip,S., Sagara,J., Nakayama,K.I., Aaronson,S.A., and Lee,S.W. 2004. ASC is a Bax adaptor and regulates the p53-Bax mitochondrial apoptosis pathway. *Nat Cell Biol* **6**:121-128.

93. Orth,P., Saenger,W., and Hinrichs,W. 1999. Tetracycline-chelated Mg2+ ion initiates helix unwinding in Tet repressor induction. *Biochemistry* **38**:191-198.

94. Patel,L., Abate,C., and Curran,T. 1990. Altered protein conformation on DNA binding by Fos and Jun. *Nature* **347**:572-575.

95. Petros,A.M., Nettesheim,D.G., Wang,Y., Olejniczak,E.T., Meadows,R.P., Mack,J., Swift,K., Matayoshi,E.D., Zhang,H., Thompson,C.B., and Fesik,S.W. 2000. Rationale for Bcl-xL/Bad peptide complex formation from structure, mutagenesis, and biophysical studies. *Protein Sci.* **9**:2528-2534.

96. Petros,A.M., Olejniczak,E.T., and Fesik,S.W. 2004. Structural biology of the Bcl-2 family of proteins. *Biochim Biophys Acta* **1644**:83-94.

97. Petros,A.M., Medek,A., Nettesheim,D.G., Kim,D.H., Yoon,H.S., Swift,K., Matayoshi,E.D., Oltersdorf,T., and Fesik,S.W. 2001. Solution structure of the antiapoptotic protein bcl-2. *PNAS* **98**:3012-3017.

98. Pryde,J.G. 1998. Partitioning of proteins in Triton X-114. *Methods Mol Biol* **88**:23-33.

99. Putcha,G.V., Moulder,K.L., Golden,J.P., Bouillet,P., Adams,J.A., Strasser,A., and Johnson,E.M. 2001. Induction of BIM, a proapoptotic BH3-only BCL-2 family member, is critical for neuronal apoptosis. *Neuron* **29**:615-628.

100. Puthalakath,H., Huang,D.C., O'Reilly,L.A., King,S.M., and Strasser,A. 1999. The proapoptotic activity of the Bcl-2 family member Bim is regulated by interaction with the dynein motor complex. *Mol Cell* **3**:287-296.

101. Qin,H., Srinivasula,S.M., Wu,G., Fernandes-Alnemri,T., Alnemri,E.S., and Shi,Y. 1999. Structural basis of procaspase-9 recruitment by the apoptotic protease-activating factor 1. *Nature* **399**:549-557.

102. Rodriguez,R., Chinea,G., Lopez,N., Pons,T., and Vriend,G. 1998. Homology modeling, model and software evaluation: three related resources. *Bioinformatics* **14**:523-528.

103. Ruffolo,S.C., Breckenridge,D.G., Nguyen,M., Goping,I.S., Gross,A., Korsmeyer,S.J., Li,H., Yuan,J., and Shore,G.C. 2000. BID-dependent and BID-independent pathways for BAX insertion into mitochondria. *Cell Death Differ* **7**:1101-1108.

104. Sattler,M., Liang,H., Nettesheim,D., Meadows,R.P., Harlan,J.E., Eberstadt,M., Yoon,H.S., Shuker,S.B., Chang,B.S., Minn,A.J., Thompson,C.B., and Fesik,S.W. 1997. Structure of Bcl-xL-Bak Peptide Complex: Recognition Between Regulators of Apoptosis. *Science* **275**:983-986.

105. Schinzel,A., Kaufmann,T., Schuler,M., Martinalbo,J., Grubb,D., and Borner,C. 2004. Conformational control of Bax localization and apoptotic activity by Pro168. *J. Cell Biol.* **164**:1021-1032.

106. Schlesinger,P.H., Gross,A., Yin,X.M., Yamamoto,K., Saito,M., Waksman,G., and Korsmeyer,S.J. 1997. Comparison of the ion channel characteristics of proapoptotic BAX and antiapoptoticáBCL-2. *PNAS* **94**:11357-11362.

107. Schlick,T. 2006. *Molecular Modeling and Simulation; An Interdisciplinary Guide*. Springer: New York.

108. Shangary,S. and Johnson,D.E. 2002. Peptides derived from BH3 domains of Bcl-2 family members: a comparative analysis of inhibition of Bcl-2, Bcl-x(L) and Bax oligomerization, induction of cytochrome c release, and activation of cell death. *Biochemistry* **41**:9485-9495.

109. Sharma,A., Sharma,I., Kogkasuriyachai,D., and Kumar,N. 2003. Structure of a gametocyte protein essential for sexual development in Plasmodium falciparum. *Nat Struct Biol* **10**:197-203.

110. Simonen,M., Keller,H., and Heim,J. 1997. The BH3 domain of Bax is sufficient for interaction of Bax with itself and with other family members and it is required for induction of apoptosis. *Eur. J. Biochem.* **249**:85-91.

111. Soding,J., Biegert,A., and Lupas,A.N. 2005. The HHpred interactive server for protein homology detection and structure prediction. *Nucleic Acids Res.* **33**:W244-W248.

112. Steed,P.M. and Wanner,B.L. 1993. Use of the rep technique for allele replacement to construct mutants with deletions of the pstSCAB-phoU operon: evidence of a new role for the PhoU protein in the phosphate regulon. *J. Bacteriol.* **175**:6797-6809.

113. Stevens,R.C., Yokoyama,S., and Wilson,I.A. 2001. Global Efforts in Structural Genomics. *Science* **294**:89-92.

114. Suzuki,M., Youle,R.J., and Tjandra,N. 2000. Structure of Bax: coregulation of dimer formation and intracellular localization. *Cell* **103**:645-654.

115. Tafani,M., Cohn,J.A., Karpinich,N.O., Rothman,R.J., Russo,M.A., and Farber,J.L. 2002. Regulation of Intracellular pH Mediates Bax Activation in HeLa Cells Treated with Staurosporine or Tumor Necrosis Factor-alpha. *J. Biol. Chem.* **277**:49569-49576.

116. Tovchigrechko,A. and Vakser,I.A. 2005a. Development and testing of an automated approach to protein docking. *Proteins* **60**:296-301.

117. Tovchigrechko,A. and Vakser,I.A. 2006a. GRAMM-X public web server for protein-protein docking. *Nucleic Acids Res.* **34**:W310-W314.

118. Tovchigrechko,A. and Vakser,I.A. 2005b. Development and testing of an automated approach to protein docking. *Proteins* **60**:296-301.

119. Tovchigrechko,A. and Vakser,I.A. 2006b. GRAMM-X public web server for protein-protein docking. *Nucleic Acids Res.* **34**:W310-W314.

120. Tremblais,K., Oliver,L., Juin,P., Le Cabellec,T.M., Meflah,K., and Vallette,F.M. 1999. The C-terminus of bax is not a membrane addressing/anchoring signal. *Biochem Biophys Res Commun* **260**:582-591.

121. Tschammer,N., Khaled,A.R., and Selby,T.S. 2007a. Analysis of helix packing energies to probe the stability and mechanism of structural transitions in proteins. *submitted*.

122. Tschammer,N., Selby,T.S., and Khaled,A.R. 2007b. Structural transitions that regulate the apoptotic activity of BAX are dependant on its C-terminal alpha-9 helix. *submitted*.

123. Tsuruta,F., Sunayama,J., Mori,Y., Hattori,S., Shimizu,S., Tsujimoto,Y., Yoshioka,K., Masuyama,N., and Gotoh,Y. 2004. JNK promotes Bax translocation to mitochondria through phosphorylation of 14-3-3 proteins. *EMBO J* **23**:1889-1899.

124. Utz,P.J. and Anderson,P. 2000. Life and death decisions: regulation of apoptosis by proteolysis of signaling molecules. *Cell Death Differ* **7**:589-602.

125. Wachter,R.M., Elsliger,M.A., Kallio,K., Hanson,G.T., and Remington,S.J. 1998. Structural basis of spectral shifts in the yellow-emission variants of green fluorescent protein. *Structure* **6**:1267-1277.

126. Wei,M.C., Lindsten,T., Mootha,V.K., Weiler,S., Gross,A., Ashiya,M., Thompson,C.B., and Korsmeyer,S.J. 2000. tBID, a membrane-targeted death ligand, oligomerizes BAK to release cytochrome c. *Genes & Dev.* **14**:2060-2071.

127. Woo,J.S., Jung,J.S., Ha,N.C., Shin,J., Kim,K.H., Lee,W., and Oh,B.H. 2003. Unique structural features of a BCL-2 family protein CED-9 and biophysical characterization of CED-9/EGL-1 interactions. *Cell Death Differ* **10**:1310-1319.

128. Yan,N., Gu,L., Kokel,D., Chai,J., Li,W., Han,A., Chen,L., Xue,D., and Shi,Y. 2004. Structural, biochemical, and functional analyses of CED-9 recognition by the proapoptotic proteins EGL-1 and CED-4. *Mol Cell* **15**:999-1006.

129. Yethon,J.A., Epand,R.F., Leber,B., Epand,R.M., and Andrews,D.W. 2003. Interaction with a Membrane Surface Triggers a Reversible Conformational Change in Bax Normally Associated with Induction of Apoptosis. *J. Biol. Chem.* **278**:48935-48941.

130. Yoshida,T., Tomioka,I., Nagahara,T., Holyst,T., Sawada,M., Hayes,P., Gama,V., Okuno,M., Chen,Y., Abe,Y., Kanouchi,T., Sasada,H., Wang,D., Yokota,T., Sato,E., and Matsuyama,S. 2004. Bax-inhibiting peptide derived from mouse and rat Ku70. *Biochem Biophys Res Commun* **321**:961-966.

131. Zhang,H., Kim,J.K., Edwards,C.A., Xu,Z., Taichman,R., and Wang,C.Y. 2005. Clusterin inhibits apoptosis by interacting with activated Bax. *Nat Cell Biol* **7**:909-915.

132. Zhang,Z., Lapolla,S.M., Annis,M.G., Truscott,M., Roberts,G.J., Miao,Y., Shao,Y., Tan,C., Peng,J., Johnson,A.E., Zhang,X.C., Andrews,D.W., and Lin,J. 2004. Bcl-2 Homodimerization Involves Two Distinct Binding Surfaces, a Topographic Arrangement That Provides an Effective Mechanism for Bcl-2 to Capture Activated Bax. *J. Biol. Chem.* **279**:43920-43928.

133. Zhou,P., Chou,J., Olea,R.S., Yuan,J., and Wagner,G. 1999. Solution structure of Apaf-1 CARD and its interaction with caspase-9 CARD: A structural basis for specific adaptor/caspase interaction. *PNAS* **96**:11265-11270.

134. Zhu,Y., Swanson,B.J., Wang,M., Hildeman,D.A., Schaefer,B.C., Liu,X., Suzuki,H., Mihara,K., Kappler,J., and Marrack,P. 2004. Constitutive association of the proapoptotic protein Bim with Bcl-2-related proteins on mitochondria in T cells. *PNAS* **101**:7681-7686.